Moduli spaces and brane constructions of $5d$ $\mathcal{N} = 1$ theories

by

Carl C. M. F. B. Bouchard

and supervised by

Prof. Amihay Hanany

September 2025

Submitted in partial fulfilment of the requirements for the degree of Master of Science of Imperial College London

Abstract

Supersymmetric theories with 8 supercharges provide a unique playground for studying non-perturbative effects in quantum field theories, balancing control with rich physical phenomena. When studying their moduli spaces, one can make use of a duality between the Coulomb branch of a $3d$ magnetic theory and the Higgs branch of a 3, 4, 5 and $6d$ electric theory via the tool of magnetic quivers. While finding a magnetic quiver for a single theory is straightforward in most cases, identifying them for entire families of theories is a significant challenge. This work provides a pedagogical introduction to theories with 8 supercharges and systematically extends the magnetic quiver analysis to a wider range of families. We find a pattern for balanced A_n type quivers, with flavour nodes only on the outside gauge nodes of the electric quiver, where different coupling phases correspond to integer partitions of $n+1$, which in turn define the magnetic quiver and its global symmetry. We also analyse a subset of general A_2 quivers at finite coupling. Finally, to handle more complex cases, we introduce a Python library that automates the computation of magnetic quivers from brane webs. We apply this to make progress on A_2 quivers, whose toric diagram is convex, at infinite coupling.

Acknowledgments

I would like to thank Prof. Amihay Hanany, not only for supervising this dissertation, but also for sparking my interest in supersymmetric gauge theories and string theory.

I would also like to thank Elias Van den Driessche and Guhesh Kumaran for answering many of my questions.

Contents

0. Introduction

"The mathematician plays a game in which he himself invents the rules while the physicist plays a game in which the rules are provided by nature, but as time goes on it becomes increasingly evident that the rules which the mathematician finds interesting are the same as those which nature has chosen."

— Paul A. M. Dirac

Quantum field theory has been remarkably successful over the past century, but its strongly coupled regimes are still poorly understood as conventional perturbative methods falter. This necessitates the development of a new set of tools to tackle these complex problems. One powerful approach is to include supersymmetry. This gives us a tight handle on the strongly coupled dynamics; however, too much supersymmetry renders our theories too rigid, not allowing for the necessary field contents that give rise to interesting phenomena.

A particularly fruitful area of study is the set of theories with 8 supercharges – $3d$ $\mathcal{N} = 4$, $4d$ $\mathcal{N} = 2$, $5d$ $\mathcal{N} = 1$, and $6d$ $\mathcal{N} = (1, 0)$. These offer a unique balance between being sufficiently constrained and yet still dynamic enough to be interesting, a feature first demonstrated in the work of Seiberg and Witten on $4d$ $\mathcal{N} = 2$ theories [1, 2]. This richness is most evident in the structure of their moduli spaces. While in the standard model, the Higgs boson's vacuum expectation value (vev) parameterises a simple circle, in theories with 8 supercharges, we have a remarkable landscape of sophisticated geometries, including symplectic singularities, closures of nilpotent orbits, and hyper-Kähler manifolds. The presence of singular spaces is not merely a mathematical curiosity, but it also allows for novel phenomena, such as partial-Higgsing [3], where gauge symmetries can break in intricate ways. We will generally view the moduli spaces as algebraic varieties; this perspective creates a strong synergy between physics and mathematics as the vast and rigorous toolkit of algebraic geometry becomes available to us.

In general, the moduli space splits into two branches: the Coulomb branch parameterised by vevs of the vector multiplets, and the Higgs branch parameterised by vevs of the hypermultiplets. The Higgs branch is, in most cases, protected from quantum corrections and can be, when a Lagrangian description exists, constructed as a hyper-Kähler quotient. On the other hand, the Coulomb branch is not protected and thus more complex to deal with. There are various tools to study the Coulomb branch. For $4d$ $\mathcal{N} = 2$ theories, we have the Seiberg-Witten curves [2], and for $3d$ $\mathcal{N} = 4$ theories, we have the monopole formula [4].

In studying many of these supersymmetric theories, particularly for strong coupling regimes, we will have to depart from the usual approach of writing down a Lagrangian, as such a description might not even exist. Instead, we will use a quiver diagram which conveniently encodes the gauge and flavour symmetries as well as the field content and its representations under the relevant symmetries [5].

Another crucial aspect of these theories is their connection to string theory, which provides elegant constructions for many of them. They can be engineered either as the compactification of a higher-dimensional framework (see, for example, [6]), or as the worldvolume theory on a system of intersecting branes (for $3d$, see [7]; for $4d$, see [8]; for $5d$, see [9, 10]; and for $6d$, see [11]). A lot of emphasis is put on the brane construction point of view - mostly for $3d$ and $5d$ - as it offers a remarkably powerful and intuitive picture. For example, there are various dualities which find a natural explanation in terms of brane dynamics. One of these is $3d$ mirror symmetry, where the Coulomb branch of one theory is the same as the Higgs branch of another, and vice versa. This phenomenon has a straightforward interpretation as deformations of brane systems via Hanany-Witten transitions [7]. Furthermore, the brane systems can often quickly be translated into a quiver diagram, giving us a comprehensive set of tools to investigate them.

A particularly important theme of this dissertation will be the set of $5d$ $\mathcal{N} = 1$ theories. These have the peculiar property that naively they are non-renormalisable, as the coupling constant has a negative mass dimension. But, as shown by Seiberg and collaborators in [12, 13, 14], there exist non-trivial UV fixed points where the theory flows to a superconformal field theory. At this fixed point, instanton states become massless and contribute to the Higgs branch of the theory, leading to global symmetry enhancement.

Due to this effect, we are especially interested in the Higgs branch of 5-dimensional theories. At finite coupling, the Higgs branch is simply a hyper-Kähler quotient, if a Lagrangian description exists, but at infinite coupling, we require the technology of magnetic quivers [15]. They are based on the conjecture that the Higgs branch for any electric theory in $d = 3, 4, 5, 6$ is equivalent to the Coulomb branch of a magnetic theory in $d = 3$. And, as it turns out, this method is not only good for the infinite coupling case, but also holds for finite coupling. This is useful when the Lagrangian description does not exist, but also means we have one tool which we can freely use for all cases. Additionally, since the scalars parameterising the Higgs branch, upon acquiring a vev, induce the Higgs mechanism, the structure of the Higgs branch gives us physical insight into the pattern of gauge symmetry breaking. This pattern can be computed using the quiver subtraction algorithm, where we can subtract certain quivers called elementary slices from the magnetic quiver to identify the pattern of partial-Higgsing [3].

Aim: The goal of this dissertation is twofold:

(i) We provide a thorough introduction to theories with 8 supercharges, and in particular the $5d$ $\mathcal{N} = 1$ case.

(ii) We extend the magnetic quiver analysis to new types of $5d$ $\mathcal{N} = 1$ families.

Organisation: In accordance with the overall aims, this dissertation is split into two parts. Part I gives a pedagogical introduction to theories with 8 supercharges. This includes:

(i) Mathematical discussions about representation theory and algebraic geometry in chapters 1 and 2. This is to set a language and formalism that permeates throughout the entire dissertation.

(ii) The basics of supersymmetric theories with 8 supercharges, such as their field content and moduli space structure in chapter 3.

(iii) Brane system constructions of theories with 8 supercharges in $d = 3, 5$ in chapters 4 and 5.

(iv) More contemporary tools in the analysis of quiver gauge theories in chapter 6.

Applying the methods covered in part I, part II examines the magnetic quiver analysis for certain families of quivers. This includes:

(i) A pattern of balanced quivers of type A_n with flavour nodes only on the outside gauge nodes in chapter 7.

(ii) An analysis of various cases for general quivers of type A_2 at finite coupling in chapter 8.

(iii) Magnetic quivers for theories of type A_2, whose toric diagram is convex, at infinite coupling in chapter 10. Enabling this analysis is a Python library we created to algorithmically compute magnetic quivers from brane webs; this is discussed in chapter 9.

Part I

Preliminaries and Methods

1. Representation theory

Let us begin by briefly examining some of the most fundamental concepts that underlie much of this dissertation. We will assume some familiarity with highest weights and how they correspond to different irreducible representations (irreps) of a group.

For a slightly more thorough exposition of these concepts, see [16]. As well as the standard references [17, 18] for a more general discussion.

1.1 Notation and basic tools

Recall that any highest weight μ, and therefore any irreducible representation, can be written in terms of fundamental weights λ_i as

$$\mu = \sum_i n_i \lambda_i \,, \tag{1.1}$$

where $n_i = 0, 1, 2, \ldots$. Hence, we may denote any irrep by a vector formed out of the different n_i

$$[n_1 n_2 \cdots n_r] \,, \tag{1.2}$$

where r is the rank of the group. These are the so-called **Dynkin labels** and they are a neat tool when discussing representations as they simplify many calculations.

We can often very quickly compute tensor products by making use of the following straightforward rules

(i) the dimensions on both sides of the equal sign have to match,

(ii) the tensor product of two representations $[n_1 \cdots n_r]$ and $[m_1 \cdots m_r]$ includes a term of the form $[n_1 + m_1, \cdots, n_r + m_r]$,

(iii) the charge under the centre of the group is preserved.

For example, consider the irreps [10] and [01] of A_2, then we clearly have

$$\underbrace{[10][01]}_{3\times 3} = \underbrace{[11]}_{8} + \underbrace{[00]}_{1} \,, \tag{1.3}$$

where we can always calculate the dimension of a representation using the Weyl dimension formula.

For representations of $SO(n)$, the relevant centres which are preserved are[1]

$$SO(2n+1) : \mathbb{Z}_2\,, \quad SO(0 \bmod 4) : \mathbb{Z}_2 \times \mathbb{Z}_2\,, \quad SO(2 \bmod 4) : \mathbb{Z}_4\,. \tag{1.4}$$

There are two more operations that we are frequently interested in, they are the **symmetric** and **anti-symmetric products**. The symmetric product is the subspace of the tensor product which stays invariant under the exchange of two components. Similarly, the anti-symmetric product is the subspace that acquires a minus sign under the exchange of two components. We can write a general tensor product as

$$[n_1 \dots n_r][n_1 \dots n_r] = \mathrm{Sym}^2[n_1 \dots n_r] + \Lambda^2[n_1 \dots n_r]\,. \tag{1.5}$$

Lastly, we may construct a generating function for the symmetric and anti-symmetric products, but we will postpone this discussion until section 2.2.

1.2 $SO(n)$ representations

A useful way to think about irreducible representations is in terms of Dynkin diagram nodes. Since the fundamental weights are defined to be dual to the roots, and the roots correspond to a node in the Dynkin diagram, we can equally associate a fundamental weight with each node. This is illustrated in figure 1.1. For B_n and D_n, some of the relevant irreps are called

- $[0 \dots 0]$: scalar representation
- $[10 \dots 0]$: vector representation
- $[010 \dots 0]$: adjoint representation
- $[0 \dots 01]$: spinor representation (for B_n)
- $[0 \dots 10]$ and $[0 \dots 01]$: spinor representations (for D_n)

The supersymmetry algebra depends on the Lorentz spinors, whose properties vary in different dimensions. In table 1.1 we summarise some of these properties. From the table, we can already deduce that, to have a theory with 8 supercharges, we require that $d \leq 6$. Additionally, if we are in for example $4d$, we will require two sets of supercharges, that is $\mathcal{N} = 2$.

[1] These are technically the centres of the spin group, but at the level of representations, the statements above are still valid.

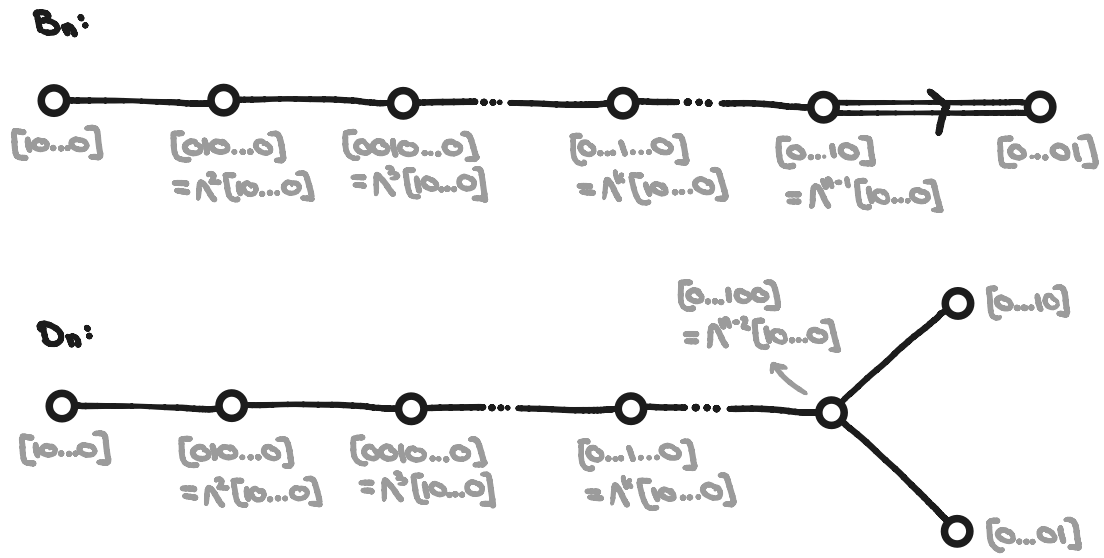

Figure 1.1: Dynkin diagrams for B_n and D_n algebras with corresponding irreps labelled.

$SO(1, d-1)$	Spinor Type	Spinor Dimension	Supercharges	R-Symmetry Rep.
2 (mod 8)	Majorana Weyl	1	1	$\mathfrak{so}(\mathcal{N}_L)$, $\mathfrak{so}(\mathcal{N}_R)$
3 (mod 8)	Majorana	2	2	$\mathfrak{so}(\mathcal{N})$
4 (mod 8)	Complex Weyl	2	4	$\mathfrak{u}(\mathcal{N})$
5 (mod 8)	Symplectic Majorana	4	8	$\mathfrak{sp}(\mathcal{N})$
6 (mod 8)	Symplectic Majorana Weyl	4	8	$\mathfrak{sp}(\mathcal{N}_L)$, $\mathfrak{sp}(\mathcal{N}_R)$
7 (mod 8)	Symplectic Majorana	8	16	$\mathfrak{sp}(\mathcal{N})$
8 (mod 8)	Complex Weyl	8	16	$\mathfrak{u}(\mathcal{N})$
9 (mod 8)	Majorana	16	16	$\mathfrak{so}(\mathcal{N})$
10 (mod 8)	Majorana Weyl	16	16	$\mathfrak{so}(\mathcal{N}_L)$, $\mathfrak{so}(\mathcal{N}_R)$
11 (mod 8)	Majorana	32	32	$\mathfrak{so}(\mathcal{N})$

Table 1.1: Properties of Lorentz spinors in various dimensions. The spinor type and R-symmetry follow a mod 8 relation. For even dimensions, the spinor dimension is $2^{\frac{d}{2}-1}$ and for odd dimensions $2^{\frac{d-1}{2}}$. This can be seen from the fact that the D_n algebra has two spinors and the B_n algebra only one. Also see [19].

2. Algebraic geometry

As many of our studies are concerned with moduli spaces of vacua, we will need some machinery to describe their geometries. The methods relevant for us fall under the study of algebraic geometry, and as such, we will present them in the pseudo-formal manner that a theoretical physicist tends to approach rigorous mathematics with.

Again, some of the standard references for algebraic geometry are [20, 21] and more specific references will be made in the sections.

2.1 Hilbert series

An algebraic variety is, at its heart, a geometric object defined by polynomial equations.

Definition 1. An **affine algebraic set** is the set of solutions $a_1, \ldots, a_m$ of a system of polynomial equations $f_1, \ldots, f_n$ in $\mathbb{C}$ (or more generally some algebraically closed field K)

$$\mathcal{V}(f_1, \ldots, f_m) = \{(a_1, \ldots, a_n) \in \mathbb{C}^n : f_1(a_i) = \cdots = f_m(a_i) = 0\} \ . \tag{2.1}$$

An **affine variety** is an affine algebraic set that is irreducible. That is, it is not the union of two proper algebraic sets.

Every affine algebraic variety $\mathcal{V}$ has an associated algebraic object called its **coordinate ring**, denoted $\mathbb{C}[\mathcal{V}]$. To define it, we begin with the polynomial ring $\mathbb{C}[x_1, \ldots, x_n]$. This ring contains all possible polynomials in the ambient space $\mathbb{C}^n$. Then, consider the polynomials that vanish at every point on $\mathcal{V} \subseteq \mathbb{C}^n$. This set is the **ideal** of the variety. Or more formally, we have

$$I(\mathcal{V}) = \{f \in \mathbb{C}[x_1, \ldots, x_n] : f(p) = 0 \,, \quad \forall p \in \mathcal{V}\} \ . \tag{2.2}$$

Using this, we can give the definition of the coordinate ring of a variety:

Definition 2. The **coordinate ring** of an affine variety $\mathbb{C}[\mathcal{V}]$ is defined to be

$$\mathbb{C}[\mathcal{V}] = \frac{\mathbb{C}[x_1, \ldots, x_n]}{I(\mathcal{V})} \,, \tag{2.3}$$

i.e. two functions in $\mathbb{C}[x_1, \ldots, x_n]$ are equivalent if their difference vanishes on $\mathcal{V}$.

Every polynomial ring $\mathbb{C}[x_1, \ldots, x_n]$ naturally can be graded by polynomial degree. In general, we can write a **graded ring** as

$$R = \bigoplus_{d \geq 0} R_d \,. \tag{2.4}$$

With this in hand, we are ready to meet one of the most important tools that we have at our disposal.

Definition 3. The **Hilbert series** of a graded ring R is

$$\mathrm{HS}(t) = \sum_{d=0}^{\infty} \dim(R_d) t^d \,. \tag{2.5}$$

When the base field is $\mathbb{C}$, the Hilbert series counts holomorphic functions on the variety. Since the Hilbert series will be so ubiquitous throughout this work, we shall dedicate some time to its properties.

The Hilbert series is a generating function encoding many geometric properties. In general, it may be written in the form

$$\mathrm{HS}(t) = \frac{P(t)}{Q(t)} \,, \tag{2.6}$$

where $P(t)$ is some polynomial with integer coefficients and $Q(1) = 0$. One of its most crucial properties is:

Theorem 1. *The dimension of an algebraic variety is equal to the order of the pole of its Hilbert series at t=1.*

A special set of varieties is called **complete intersections**. A variety of co-dimension c is a complete intersection if there exist exactly c equations that define the variety. For example, S^2 embedded in $\mathbb{R}^3$ has codimension 1 and is defined by a single equation $x^2 + y^2 + z^2 = 1$. For a complete intersection, the Hilbert series takes on a particularly nice form.

Theorem 2. *If an algebraic variety is a complete intersection, the Hilbert series is of the form*

$$HS(t) = \frac{\prod_j (1 - t^{b_j})^{r_j}}{\prod_i (1 - t^{a_i})^{g_i}} \,, \tag{2.7}$$

where a_i is the degree of the ith generator and g_i is the number of generators at that degree. Similarly, b_j is the degree of the jth relation and r_j is the number of relations at that degree.

Not all is lost when the variety fails to be a complete intersection. In this case, the denominator can still be brought into this form, but the numerator fails to factorise in this particular manner. This reflects the fact that, in addition to the relations between generators, we will now also have relations between relations. These are known as **syzygies**.

If there is some global symmetry under which the polynomials are charged, we can include an additional counting variable - or fugacity - in the Hilbert series to keep track of this. We call this

the **refined Hilbert series**, and it is of the form

$$\mathrm{HS}(t,x) = \sum_{d=0}^{\infty} \mathcal{R}(d) t^d \,, \tag{2.8}$$

where $\mathcal{R}_d$ is the character of some representation, possibly reducible, of the symmetry group which depends on the value of d. An interesting feature of this is that the t^2 term in the Hilbert series is always the character of the adjoint representation of the symmetry group (after a possible fugacity mapping).

Closely related to the Hilbert series is the highest weight generating function [22], where instead of keeping track of the whole character, we only keep the highest weight.

Definition 4. Consider a refined Hilbert series of the form

$$\mathrm{HS}(t,x_i) = \sum_{d=0}^{\infty} [n_{1,d} \dots n_{r,d}] t^d \,. \tag{2.9}$$

The **highest weight generating function** for this Hilbert series is

$$\mathrm{HS}(t,x_i) = \sum_{d=0}^{\infty} \mu_1^{n_{1,d}} \dots \mu_r^{n_{r,d}} t^d \,, \tag{2.10}$$

where we have introduced the fugacities $\mu_1, \dots, \mu_r$ which are raised to the power of the highest weight.

Consider, for example, the representation [10020] of $SU(6)$ then the corresponding term in μ-fugacities is $\mu_1^1 \mu_4^2$. Lastly, we would be remiss if we did not mention the following neat fact about the Hilbert series of Calabi-Yau varieties.

Theorem 3. *An affine algebraic variety is Calabi-Yau if and only if the numerator of the rational form of the Hilbert series is palindromic.*

Example 1. Starting with a simple example, consider the space $\mathbb{C}^2$ with coordinate ring $\mathbb{C}[z_1, z_2]$. We can now make a table counting the monomials at different orders. Monomials can very much be seen as the functional equivalent of vector basis elements.

Degree	Monomials	Number
0	1	1
1	z_1, z_2	2
2	$z_1^2, z_1 z_2, z_2^2$	3
	...	
n	$z_1^n, z_1^{n-1} z_2, \ldots, z_2^n$	$n+1$
	...	

Thus, the Hilbert series is

$$\mathrm{HS}(t) = \sum_{n=0}^{\infty} (n+1) t^n = \frac{1}{(1-t)^2} \,. \tag{2.11}$$

Since there are no relations between the generators, we also say that the space is freely generated. But we can do more. Suppose we sum over the generators (tracked by fugacities), then

$$\sum_{m,n} t_1^n t_2^m = \frac{1}{(1-t_1)(1-t_2)} \,. \tag{2.12}$$

This is essentially a refined Hilbert series. Making the remapping[a] $t_1 \mapsto tx$ and $t_2 \mapsto t/x$, we obtain

$$\begin{aligned} \mathrm{HS}(t,x) = \frac{1}{(1-tx)(1-t/x)} &= 1 + (x + \frac{1}{x})t + (x^2 + 1 + \frac{1}{x^2})t^2 + \cdots \\ &= 1 + [1]t + [2]t + \cdots \,, \end{aligned} \tag{2.13}$$

where we have recognised the characters as belonging to $SU(2)$.

[a] The map is determined by the charges of each generator under the global symmetry; here the charges are $+1$ and -1 under $SU(2)$.

2.2 Plethystics

Let us now return to a point of discussion from section 1.1. We want to construct a function that produces symmetric products of functions. We will not go through all the details, but instead just outline the construction. The tools in this section were introduced in [23, 24], and for a review see [16].

Suppose we want to generate all possible symmetric rank-k tensors $a_{i_1 \ldots i_k}$ consisting of rank-1 tensors x_i where $i = 1, \ldots, n$ for all $k = 0, 1, 2, \ldots$. One can verify that the following function does exactly that

$$\prod_{i=1}^{n} \frac{1}{1-x_i} = 1 + \sum_i x_i + \sum_{i \leq j} x_i x_j + \cdots \,. \tag{2.14}$$

This can be manipulated into the form

$$\prod_{i=1}^{n} \frac{1}{1-x_i} = \exp\left(\sum_{k=1}^{\infty} \frac{f(x_i^k)}{k}\right) , \tag{2.15}$$

where $f(x_i^k) = \sum_i x_i^k$. Using this, we can define a function which generates symmetric products of some function $f(x_i)$.

Definition 5. The **plethystic exponential** of some function $f(x_1, \ldots, x_n)$, where $f(0, \ldots, 0) = 0$, is

$$\mathrm{PE}[f(x_1, \ldots, x_n)] = \exp\left(\sum_{k=1}^{\infty} \frac{f(x_1^k, \ldots, x_n^k)}{k}\right) . \tag{2.16}$$

In particular, if we include an additional fugacity t in the argument of the plethystic exponential, we get

$$\mathrm{PE}[f(x_i)t] = \sum_{k=0}^{\infty} \mathrm{Sym}^k[f]t^k . \tag{2.17}$$

There are some useful identities which are not terribly difficult to prove

$$\mathrm{PE}[f+g] = \mathrm{PE}[f]\mathrm{PE}[g] \tag{2.18}$$

and

$$\mathrm{PE}\left[\sum_i g_i t^{a_i} - \sum_j r_j t^{b_j}\right] = \frac{\prod_j (1-t^{b_j})^{r_j}}{\prod_i (1-t^{a_i})^{g_i}} . \tag{2.19}$$

The latter should remind one of the expression for the Hilbert series of a complete intersection. The interpretation is hence straightforward, if we have g_i generators at degree a_i and r_j relations between generators at degree b_j, the Hilbert series of that variety is given by the left-hand side of (2.19).

In addition to the plethystic exponential, as the name suggests, there also exists an inverse operation.

Definition 6. The **plethystic logarithm** is defined to be the inverse of the plethystic exponential, and it takes the form

$$\mathrm{PL}[f(x_1, \ldots, x_n)] = \sum_{k=1}^{\infty} \frac{\mu(k)}{k} \log\left(f(x_1^k, \ldots, x_n^k)\right) , \tag{2.20}$$

where $\mu(k)$ is the Möbius function.

Similar to the identities for the plethystic exponential, for the plethystic logarithm, we have

$$\mathrm{PL}[fg] = \mathrm{PL}[f] + \mathrm{PL}[g] \tag{2.21}$$

and

$$\mathrm{PL}\left[\frac{\prod_j (1-t^{b_j})^{r_j}}{\prod_i (1-t^{a_i})^{g_i}}\right] = \sum_i g_i t^{a_i} - \sum_j r_j t^{b_j} . \tag{2.22}$$

Thus, we may use the PL as a method to extract information about the generators and relations of a variety from its Hilbert series. If the PL turns out to have an infinite number of terms, then we do not have a complete intersection, and we have syzygies.

Example 2. Let us explicitly construct the variety $\mathbb{C}^2/\mathbb{Z}_n$, where $\mathbb{Z}_n$ acts on the coordinates $(z_1, z_2) \in \mathbb{C}^2$ as

$$(z_1, z_2) \sim (e^{2\pi i/n} z_1, e^{-2\pi i/n} z_2)\,. \tag{2.23}$$

We can easily see that the space of $\mathbb{Z}_n$ invariant monomials is generated by

$$a = z_1^n\,, \quad b = z_2^n \quad \text{and} \quad c = z_1 z_2\,, \tag{2.24}$$

where a and b are at degree n and c is at degree 2. They are related via a relation at degree $2n$

$$ab = c^n\,. \tag{2.25}$$

Additionally, $\mathbb{C}^2/\mathbb{Z}_n$ has a global $SU(2)$ symmetry under which the generators a and b form a doublet and c a singlet.

Keeping track of all this information, we can now construct the Hilbert series of the variety using the plethystic exponential

$$\begin{aligned} \mathrm{HS}(t,x) &= \mathrm{PE}\left([0]t^2 + [1]t^n - t^{2n}\right) \\ &= \frac{1-t^{2n}}{(1-t^n x)(1-t^2)(1-t^n/x)}\,, \end{aligned} \tag{2.26}$$

where the Dynkin labels denote the usual $SU(2)$ irreps, $[n] = x^n + x^{n-2} + \cdots + x^{-n}$. In the next chapter, we will see that this turns out to be the Hilbert series for the Coulomb branch of SQED with n flavours.

2.3 Symplectic singularities

This section may be omitted until chapter 6, and will not be necessary before. Yet, due to its nature, it is much more fitting here.

Symplectic singularities are at the very centre of everything we study. Most moduli spaces we will encounter are symplectic singularities, or unions thereof. For theories with 8 supercharges, these include the Higgs branch in dimensions 3 to 6 and the 3-dimensional Coulomb branch.

For a brilliant introductory lecture, which we will broadly follow here, see [25]. Additionally, see [26, 27].

Definition 7. A **symplectic manifold** is a pair (M, ω), where M is a manifold and $\omega \in \Omega^2(M)$ is a non-degenerate closed 2-form. That is

(i) $d\omega = 0$,

(ii) For $X, Y \in \mathfrak{X}(M)$, if $\omega(X, Y) = 0$ for all Y, then $X = 0$.

Definition 8 (Beauville [28])**.** A normal variety X is said to have a **symplectic singularity** if:

(i) the smooth part X_{reg} of X is a symplectic manifold,

(ii) for any resolution $\pi : Y \to X$, where Y is a smooth variety, the pullback $\pi^*\omega$ is closed but possibly degenerate.

In general, we will refer to the whole variety X as the symplectic singularity, which is technically not correct, but makes talking about it much easier.

Theorem 4 (Kaledin [29])**.** *If we have a symplectic singularity X, then we can decompose this space into a disjoint union of open and smooth symplectic varieties, called* ***symplectic leaves*** *$\mathcal{L}_i$, that is*

$$X = \bigsqcup_i \mathcal{L}_i \,. \tag{2.27}$$

Furthermore, the exists a stratification between the leaves given by a partial ordering

$$\mathcal{L}_i < \mathcal{L}_j \quad \text{if} \quad \mathcal{L}_i \subset \overline{\mathcal{L}}_j \,, \tag{2.28}$$

where $\overline{\mathcal{L}}_j$ is the closure of $\mathcal{L}_j$.

Theorem 5 (Kaledin [29])**.** *Locally, around some point $p \in \mathcal{L}_i$ the space looks like*

$$X_{locally} = \mathcal{L}_i \times \mathcal{T}_i \,, \tag{2.29}$$

where $\mathcal{T}_i$ is another symplectic singularity, called the ***transverse slice****. We sketch this in figure 2.1.*

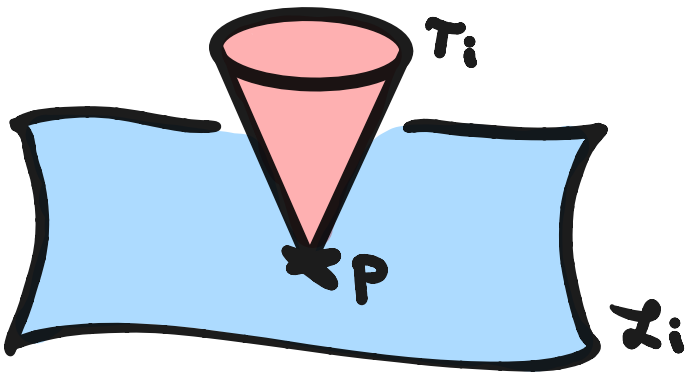

Figure 2.1: Local picture for a point $p \in \mathcal{L}_i$.

Another thing we can do, which will become relevant again later on, is to consider a transverse slice not within all of X but rather a subspace given by the closure of a symplectic leaf $\overline{\mathcal{L}_j}$. This transverse slice is given by

$$\mathcal{T}_i^j = \mathcal{T}_i \cap \overline{\mathcal{L}}_j \,. \tag{2.30}$$

Example 3. Suppose we have a symplectic singularity X, where we have two singular loci, a $0d$ and $1d$ locus, one living within the other (left-hand side of figure 2.2). Then we can decompose this space as is shown in figure 2.2. And clearly we have the stratification $\mathcal{L}_0 < \mathcal{L}_1 < \mathcal{L}_2 = X_{\text{reg}}$.

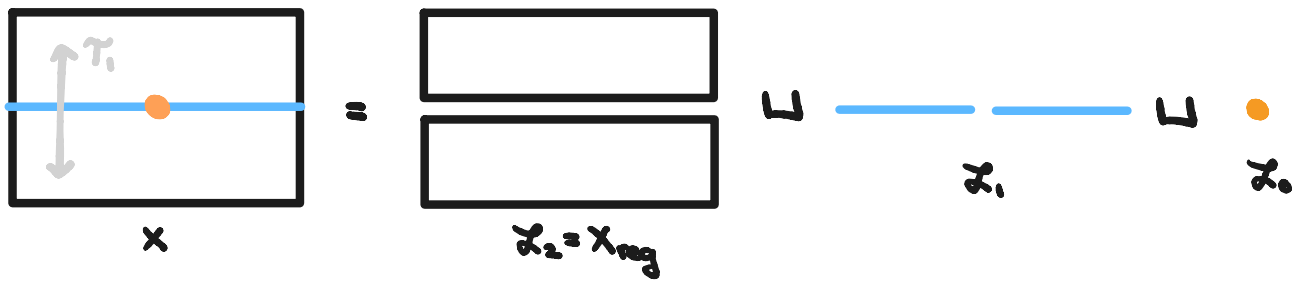

Figure 2.2: Decomposition of symplectic singularity.

2.4 Nilpotent orbits and their closures

This discussion broadly follows [30]; a more formal introduction to nilpotent orbits can be found in [31].

A large subclass of symplectic singularities are closures of nilpotent orbits. This is due to an important theorem by Namikawa [32]:

Theorem 6 (Namikawa)**.** *A symplectic singularity is the closure of a nilpotent orbit of algebra* $\mathfrak{g}(\mathbb{C})$*, where* $\mathfrak{g}(\mathbb{C})$ *is the algebra of the global symmetry of the variety, if all of its generators are of spin 1 only under* $SU(2)_R$*.*

We can illustrate this with two examples. Consider first the space $\mathbb{C}^2$, the generators are z_1 and z_2, which belong to the multiplets $(z_1, \bar{z}_2)$ and $(z_2, \bar{z}_1)$ both in the [1] representation under $SU(2)_R$. And, as such, they have spin 1/2, meaning that $\mathbb{C}^2$ is not a closure of a nilpotent orbit.

Next, consider the space $\mathbb{C}^2/\mathbb{Z}_2$. We now have the generators z_1^2, z_2^2, and $z_1 z_2$. The first two live in multiplets $\text{Sym}^2[1] = [2]$, and the last one in the [2] irrep of the product $[1][1] = [2] + [0]$. Therefore, all the generators do have spin 1, and $\mathbb{C}^2/\mathbb{Z}_2$ is isomorphic to the closure of a nilpotent orbit. In this case, the closure of the nilpotent orbits can be written as $\mathbb{C}^2/\mathbb{Z}_2 = \overline{min.A_1}$.

The algebra of type A_n

Definition 9. Let X be an element of a complex semisimple Lie algebra $\mathfrak{g}$. X is **nilpotent** if

$$(\text{ad}\, X)^m = 0\,, \tag{2.31}$$

where $m > 0$ and $\text{ad} : \mathfrak{g} \to \text{End}(\mathfrak{g})$ is the adjoing representation.

To construct nilpotent orbits, we will make use of a classification theorem.

Theorem 7 (Type A_n)**.** *Nilpotent orbits in $\mathfrak{sl}(n)$ are in one-to-one correspondence with the set of partitions $\mathcal{P}(n)$ of n.*

A **partition** of n is an ordered set of numbers $(\lambda_1, \ldots, \lambda_r)$ such that $\sum_i \lambda_i = n$, $\lambda_1 \geq \cdots \geq \lambda_r$, and $\lambda_i \in \mathbb{N}$. For example, the set of partitions of 4 would be

$$\mathcal{P}(4) = \{(4), (3,1), (2^2), (2,1^2), (1^4)\}\,, \tag{2.32}$$

where we use the superscript to denote multiples of a number, e.g. $(1^2) = (1,1)$.

We will also need to define the **elementary Jordan block** J_i, which is an $i \times i$ matrix of the form

$$J_i = \begin{pmatrix} 0 & 1 & 0 & \cdots & 0 & 0 \\ 0 & 0 & 1 & \cdots & 0 & 0 \\ \vdots & \vdots & \vdots & \ddots & \vdots & \vdots \\ 0 & 0 & 0 & \cdots & 0 & 1 \\ 0 & 0 & 0 & \cdots & 0 & 0 \end{pmatrix}. \tag{2.33}$$

A nilpotent endomorphism of $\mathbb{C}^n$ can be built from a partition $\lambda = (\lambda_1, \ldots, \lambda_r)$ and elementary Jordan blocks as

$$X_\lambda = \begin{pmatrix} J_{\lambda_1} & 0 & \cdots & 0 \\ 0 & J_{\lambda_2} & \cdots & 0 \\ \vdots & \vdots & \ddots & \vdots \\ 0 & 0 & \cdots & J_{\lambda_r} \end{pmatrix}. \tag{2.34}$$

X_λ is a nilpotent element of $\mathfrak{sl}(n, \mathbb{C})$, and its **nilpotent orbit** is defined as

$$\mathcal{O}_\lambda = PSL(n) \cdot X_\lambda\,. \tag{2.35}$$

Two different partitions correspond to two disjoint orbits, that is, for $\lambda, \lambda' \in \mathcal{P}(n)$

$$\mathcal{O}_\lambda \cap \mathcal{O}_{\lambda'} = \emptyset \quad \Longleftrightarrow \quad \lambda \neq \lambda'\,. \tag{2.36}$$

A note on the nomenclature of nilpotent orbits. Starting from the bottom, the orbits are called: trivial, minimal, next-to-minimal, next-to-next-to-minimal, etc.. Conversely, starting from the top: regular, sub-regular, sub-sub-regular, etc.. And we write them as

$$\overline{min.A_n}\,, \quad \overline{n.min.A_n}\,, \quad \ldots \quad \text{and} \quad \overline{reg.A_n}\,, \quad \overline{s.reg.A_n}\,, \quad \ldots\,. \tag{2.37}$$

Example 4. Consider the case of $\mathfrak{sl}(2,\mathbb{C})$. The set of partitions is $\mathcal{P}(2) = \{(2),(1^2)\}$. For the trivial partition (1^2), we have the Jordan normal matrix

$$X_{(1^2)} = \begin{pmatrix} 0 & 0 \\ 0 & 0 \end{pmatrix} . \tag{2.38}$$

And the orbit corresponding to this element is trivially

$$\begin{aligned} \mathcal{O}_{(1^2)} &= \left\{ M = S \cdot \begin{pmatrix} 0 & 0 \\ 0 & 0 \end{pmatrix} \cdot S^{-1} : S \in SL(2,\mathbb{C}) \right\} \\ &= \left\{ \begin{pmatrix} 0 & 0 \\ 0 & 0 \end{pmatrix} \right\} . \end{aligned} \tag{2.39}$$

Since the centre of $SL(2,\mathbb{C})$ is $\mathbb{Z}_2$, in the operation in the first line of (2.39), it does not matter whether $S \in SL(2,\mathbb{C})$ or $S \in PSL(2,\mathbb{C})$, as they will both give the same element.

The second orbit turns out to be more interesting. For the parition (2), we have the Jordan normal matrix

$$X_{(2)} = \begin{pmatrix} 0 & 1 \\ 0 & 0 \end{pmatrix} . \tag{2.40}$$

And, therefore, the orbit becomes

$$\begin{aligned} \mathcal{O}_{(2)} &= \left\{ M = S \cdot X_{(2)} \cdot S^{-1} : S \in SL(2,\mathbb{C}) \right\} \\ &= \left\{ \begin{pmatrix} -ac & a^2 \\ -c^2 & ac \end{pmatrix} \right\} . \end{aligned} \tag{2.41}$$

One can explicitly check that $M^2 = 0$. Crucially, $\mathcal{O}_{(2)}$ is disjoint from $\mathcal{O}_{(1^2)}$ as the condition $ad - bc = 1$ would be violated otherwise. The closure of $\mathcal{O}_{(2)}$ is given by

$$\overline{\mathcal{O}}_{(2)} = \mathcal{O}_{(2)} \cup \mathcal{O}_{(1^2)} . \tag{2.42}$$

The set $\overline{\mathcal{O}}_{(2)}$ is now an algebraic variety with three generators a^2, c^2, and ac. This we recognise as the Kleinian surface singularity $\mathbb{C}^2/\mathbb{Z}_2$. The orbit just above the trivial orbit is called the minimal orbit, thus in our notation from earlier: $\mathbb{C}^2/\mathbb{Z}_2 = \overline{min.A_1}$.

The other classical algebras of type B_n, C_n, and D_n

We will not construct the nilpotent orbits for the other algebras explicitly, but they follow the same pattern, with the exception that we have additional rules for the partitions. These are characterised in the following theorems (see [31] for more detail):

Theorem 8 (Type B_n)**.** *Nilpotent orbits in $\mathfrak{so}(2n+1,\mathbb{C})$ are in one-to-one correspondence with the set of partitions of $2n+1$ in which even parts occur with even multiplicity.*

For example, in $\mathfrak{so}(7,\mathbb{C})$ there are 7 nilpotent orbits:

$$\mathcal{O}_{(7)}, \mathcal{O}_{(5,1^2)}, \mathcal{O}_{(3,1^4)}, \mathcal{O}_{(3,2^2)}, \mathcal{O}_{(3^2,1)}, \mathcal{O}_{(2^2,1^3)}, \mathcal{O}_{(1^7)}\,. \tag{2.43}$$

Theorem 9 (Type C_n)**.** *Nilpotent orbits in $\mathfrak{sp}(2n,\mathbb{C})$ are in one-to-one correspondence with the set of partitions of $2n$ in which odd parts occur with even multiplicity.*

For example, in $\mathfrak{sp}(6,\mathbb{C})$ there are 8 nilpotent orbits:

$$\mathcal{O}_{(6)}, \mathcal{O}_{(4,2)}, \mathcal{O}_{(4,1^2)}, \mathcal{O}_{(3^2)}, \mathcal{O}_{(2^3)}, \mathcal{O}_{(2^2,1^2)}, \mathcal{O}_{(2,1^4)}, \mathcal{O}_{(1^6)}\,. \tag{2.44}$$

Theorem 10 (Type D_n)**.** *Nilpotent orbits in $\mathfrak{so}(2n,\mathbb{C})$ are in one-to-one correspondence with the set of partitions of $2n$ in which even parts occur with even multiplicity, except that partitions consisting only of even parts with even multiplicities correspond to two orbits denoted $\mathcal{O}^I$ and $\mathcal{O}^{II}$.*

For example, in $\mathfrak{so}(8,\mathbb{C})$ there are 12 nilpotent orbits:

$$\mathcal{O}_{(7,1)}, \mathcal{O}_{(5,3)}, \mathcal{O}^I_{(4^2)}, \mathcal{O}^{II}_{(4^2)}, \mathcal{O}_{(5,1^3)}, \mathcal{O}_{(3^2,1^2)}, \mathcal{O}_{(3,2^2,1)}, \mathcal{O}^I_{(2^4)}, \mathcal{O}^{II}_{(2^4)}, \mathcal{O}_{(3,1^5)}, \mathcal{O}_{(2^2,1^4)}, \mathcal{O}_{(1^8)}\,. \tag{2.45}$$

3. Supersymmetric gauge theories

We are now ready to tackle the main character of this dissertation: supersymmetric gauge theories, particularly quiver gauge theories with 8 supercharges. These theories have proven to be a particularly fertile area of research, yielding significant insights into quantum field theory, non-perturbative effects, and geometric structures.

It is assumed that the reader has some prior exposure to supersymmetry; otherwise, some classics to brush up on are [33, 34].

3.1 Supermultiplets in $3d$, $4d$ and $5d$

The massless particles in a theory can be classified by their representations under the (super)Poincaré algebra. This is obtained in the usual way using Wigner's little group construction. One of the major benefits of supersymmetry is that all particles fall into so-called **supermultiplets**, which heavily restrict the number and type of allowed particles.

We will use the constraints of supersymmetry to construct the relevant multiplets here; for a more bottom-up and traditional approach, a great explanation can be found in [33].

If we have n supercharges, then the minimal number of degrees of freedom that a multiplet can have, with this amount of supersymmetry, is $2^{n/4}$. And, as we will be interested in theories with 8 supercharges, the minimal number of degrees of freedom is four. We will refer to the multiplet with this number of degrees of freedom as the **half-hypermultiplet**. Its specific form depends on the little and R-symmetry group.

$5d$ $\mathcal{N} = 1$

The little group is $SO(3)$ and the R-symmetry is $Sp(1)$. Since we will have to split four degrees of freedom evenly across bosonic and fermionic states, the only possibility is

$$\begin{aligned} h &= 2[0] + [1] \\ &= [0][1]_R + [1][0]_R \,, \end{aligned} \tag{3.1}$$

where we omit the label for the representation under the little group, and the representation under the R-symmetry is labelled by a subscript R. From the half-hypermultiplet, we can construct further

multiplets with the same amount of supersymmetry. One of them is the **hypermultiplet**,

$$\begin{aligned} H_5 = 2h &= 4[0] + 2[1] \\ &= \underbrace{2[0][1]_R}_{\varphi_{1,2}} + \underbrace{2[1][0]_R}_{\psi_{1,2}}, \end{aligned} \tag{3.2}$$

where we have two complex scalars $\varphi_{1,2}$ and two spinors $\psi_{1,2}$. The **vector multiplet** is

$$\begin{aligned} V_5 = h[1] &= [2] + 2[1] + [0] \\ &= \underbrace{[2][0]_R}_{A_\mu} + \underbrace{[0][0]_R}_{\phi} + \underbrace{[1][1]_R}_{\psi_{1,2}}, \end{aligned} \tag{3.3}$$

where we have one gauge boson A_μ, one real scalar ϕ and two spinors $\psi_{1,2}$.

$4d$ $\mathcal{N} = 2$

The reason we started with analysing the 5-dimensional case is that we now merely need to dimensionally reduce the already existing multiplets. In 4 dimensions, the little group is $SO(2) \simeq U(1)$ and as such irreps are simply labelled by their charge under $U(1)$, we will use the fugacity q to keep track of this. The R-symmetry is $U(2) \simeq U(1) \times SU(2)$. The hypermultiplet becomes

$$\begin{aligned} H_4 &= 4q^0 + 2(q^1 + q^{-1}) \\ &= \underbrace{2q^0 \times [1]^0_R}_{\varphi_{1,2}} + \underbrace{(q^1 + q^{-1}) \times ([0]^{+1}_R + [0]^{-1}_R)}_{\psi_{1,2}}, \end{aligned} \tag{3.4}$$

where attached the $U(1)$ R-symmetry charge to the Dynkin label. The particle content stays the same as before. The vector multiplet, on the other hand, becomes

$$\begin{aligned} V_4 &= (q^2 + q^{-2}) + 2q^0 + 2(q^1 + q^{-1}) \\ &= \underbrace{(q^2 + q^{-2}) \times [0]^0_R}_{A_\mu} + \underbrace{q^0 \times ([0]^{+2}_R + [0]^{-2}_R)}_{\varphi} + \underbrace{q^1 \times [1]^{+1}_R + q^{-1} \times [1]^{-1}_R}_{\psi_{1,2}}, \end{aligned} \tag{3.5}$$

where the real scalar in 5 dimensions has turned into a complex scalar in 4 dimensions.

$3d$ $\mathcal{N} = 4$

In three dimensions, the little group is trivial, and we can only use the $SO(4)_R \simeq SU(2)_\mathcal{C} \times SU(2)_\mathcal{H}$ R-symmetry to label states. The hypermultiplet consists of two complex scalars which form a doublet under $SU(2)_\mathcal{H}$, i.e.

$$H_3 = \underbrace{2[1]_\mathcal{H}[0]_\mathcal{C}}_{\varphi_{1,2}} + \text{fermions}\,. \tag{3.6}$$

When we reduce the gauge field in the 4d vector multiplet, we get a vector as well as an additional scalar. The gauge field now has one degree of freedom, and we can dualise the gauge field A to an S^1-valued scalar α via $*dA = d\alpha$, where α is called the dual photon. This has another implication, because the quantity $J = d\alpha$ is conserved, Noether's theorem implies that we have $U(1)_J$ symmetry. This symmetry is not seen by the Lagrangian, and so we refer to it as a hidden or topological symmetry. The vector multiplet can be written as

$$V_3 = \underbrace{[0]_{\mathcal{H}}[0]_{\mathcal{C}}}_{A_\mu} + \underbrace{[0]_{\mathcal{H}}[2]_{\mathcal{C}}}_{\phi_{1,2,3}} + \text{fermions}\,. \tag{3.7}$$

One final point to note is that the multiplets with 8 supercharges can be expressed in terms of multiplets with 4 supercharges. For example, the vector multiplet splits into a vector multiplet and a chiral multiplet, and the hypermultiplet splits into a chiral and anti-chiral multiplet.

3.2 Quivers

Rather than writing down the Lagrangian of a theory, we can encode all the relevant information in a **quiver diagram**, initially introduced in [5]. There are different ways of drawing a quiver for different numbers of supercharges. In theories with 8 supercharges, we have vector and hypermultiplets that can transform in various ways under gauge and global symmetries. All this information can be written in the following way:

- A vector multiplet transforming in the adjoint representation of a gauge group G is denoted by a circular node

- A hypermultiplet in the bifundamental representation of two groups G and G' is drawn as a line between two nodes

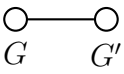

  If instead the hypermultiplet transforms under some flavour symmetry F, we can draw a square node to mark that no vector multiplet is associated with this group

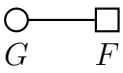

If we are instead in a theory with 4 supercharges, such as $4d$ $\mathcal{N} = 1$ or $3d$ $\mathcal{N} = 2$, we have chiral and vector multiplets. They are represented by:

- For a vector multiplet transforming in the adjoint representation, we again have a circular node

- For a chiral multiplet transforming in the fundamental representation of G and anti-fundamental representation of G', we draw an arrow between the two nodes

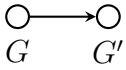

  Similarly to before, if we have some flavour symmetry F, we can simply replace the circular gauge node with a square flavour node.

Example 5. Suppose we have a theory with gauge group $U(1)$ and flavour symmetry $SU(n)$. This theory is also called **SQED with n flavours**. If we have 8 supercharges, we can write this as

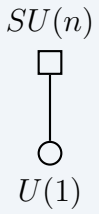

Alternatively, since the 8 supercharge multiplets decompose into 4 supercharge multiplets, we can express the same theory as

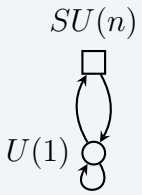

3.3 Moduli spaces - an overview

A moduli space of vacuum expectation values (vevs) is the space of values that the scalar fields can take on such that the potential is minimised. In the standard model, the Higgs boson's moduli space is a simple circle S^1. Much of the fascination with supersymmetric theories comes from the fact that their moduli spaces have an incredibly rich geometric structure. These spaces can be viewed as affine algebraic varieties, which is of course the whole reason we bothered introducing them in chapter 2.

For theories with 8 supercharges, we have scalars in both the vector and hypermultiplet. The moduli space now splits into different branches. The **Higgs branch** is parameterised by the vevs in the hypermultiplet, with the vevs in the vector multiplet being set to zero. The **Coulomb branch**, on the other hand, is parameterised by vevs in the vector multiplet, with the vevs in the hypermultiplet turned off. More compactly, if q are the scalars in the hypermultiplet and ϕ are the scalars in the vector multiplet, we have, on a generic point

$$\begin{aligned} \mathcal{H}: &\quad \langle q \rangle \neq 0 \quad \text{and} \quad \langle \phi \rangle = 0 \\ \mathcal{C}: &\quad \langle q \rangle = 0 \quad \text{and} \quad \langle \phi \rangle \neq 0\,. \end{aligned} \tag{3.8}$$

We can turn on different vevs from both multiplets; in this case, we are on a **mixed branch**.

For theories in dimensions 3, 4, and 5, the Higgs branch is a symplectic singularity, or hyperKähler variety, whereas the same is only true for the Coulomb branch in 3 dimensions.

3.4 Higgs branch

Let us now explore these different branches in more detail, as well as consider concrete examples to explain some of the main computational methods at our disposal. Beginning with the Higgs branch.

Definition 10. The **classical Higgs branch** is defined as

$$\mathcal{H}_{\text{classical}} = \mathbb{H}^n /\!/\!/ G = \frac{\{(q, \bar{q}) : \text{F- and D-terms}\}}{G}\,, \tag{3.9}$$

where $(q, \bar{q})$ are the scalars in the hypermultiplets, n is the number of hypermultiplets, and G is the gauge group. This is a hyperKähler quotient, denoted by $/\!/\!/$.

As it turns out, imposing D-terms and quotienting over the gauge group is equivalent to simply quotienting over the complexified gauge group. Another simple consequence of the definition is that the dimension of the Higgs branch is

$$\dim_{\mathbb{H}}(\mathcal{H}) = n_{\text{hypers}} - n_{\text{vectors}}\,, \tag{3.10}$$

where n_{hypers} is the number of hypermultiplets and n_{vectors} is the number of vector multiplets, which is the same as the dimension of the gauge group G.

Let us consider now SQED with n flavours in $3d$ $\mathcal{N} = 4$. In the 4 supercharge notation, we have the following quiver

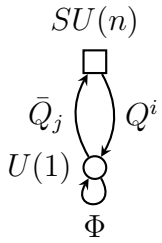

The corresponding fields and their transformations are

	$U(1)$	$SU(n)$
Q^i	-1	$[10\ldots0]$
$\bar{Q}_j$	1	$[0\ldots01]$
Φ	0	$[0\ldots0]$

where Q^i is an $n \times 1$ matrix, $\bar{Q}_j$ is a $1 \times n$ matrix and Φ is a 1×1 matrix. We will denote the scalar fields in these chiral multiplets as q^i, $\bar{q}_j$, and ϕ, respectively. The dimension of the Higgs branch will be

$$\dim_{\mathbb{H}}(\mathcal{H}) = n - 1\,. \tag{3.11}$$

To explicitly construct the Higgs branch, we need to solve the F-terms. To this end, the superpotential can be read off the quiver by going around the loop

$$\mathcal{W} = \mathrm{Tr}(\bar{Q}\Phi Q)\,, \tag{3.12}$$

and thus the scalar potential, given by the F-terms, is

$$V(q^i, \bar{q}_j) = \frac{\partial \mathcal{W}(q, \bar{q}, \phi)}{\partial \phi} = q^i \bar{q}_i\,, \tag{3.13}$$

where we exchanged the chiral multiplets for their scalar fields. We then find that the restriction on the scalars is that $q^i \bar{q}_i = 0$.

A gauge invariant combination of our operators q^i and $\bar{q}_j$ would be $M^i{}_j = q^i \bar{q}_j$, which is an $n \times n$ matrix with $\mathrm{rank}(M) \leq 1$. The latter follows from

$$\mathrm{rank}(M) \leq \min\{\mathrm{rank}(q), \mathrm{rank}(\bar{q})\} = 1\,. \tag{3.14}$$

Imposing our vacuum condition on this operator, we can see that

$$M^2 = M^i{}_j M^j{}_k = q^i \bar{q}_j q^j \bar{q}_k = 0 \quad \text{and} \quad \mathrm{Tr}(M) = q^i \bar{q}_i = 0\,. \tag{3.15}$$

We therefore have that the Higgs branch is

$$\mathcal{H}\Big(\begin{array}{c} n \\ \square \\ | \\ \circ \\ 1 \end{array} \Big) = \{M \in SU(n,\mathbb{C}) : \text{rank}(M) \leq 1, \text{Tr}(M) = 0, M^2 = 0\} \\ = \overline{min.A_{n-1}}\,. \tag{3.16}$$

This we recognise as the closure of the minimal nilpotent orbit of A_{n-1}. In the case of 3-dimensional theories, the Higgs branch receives no quantum corrections and stays classical

$$\mathcal{H}_{\text{quantum}} = \mathcal{H}_{\text{classical}}\,. \tag{3.17}$$

If we are simply interested in the Hilbert series, we do not need to explicitly construct the variety as we did above. Recall that the Hilbert series counts gauge-invariant quantities at different orders. To get all the contributions from the generators and relations, we compute the plethystic exponential. This will not be gauge-invariant, as such we need to get rid of all the gauge-variant contributions. For more details, see [35]. To this end, we introduce:

Definition 11. The **Molien-Weyl formula** projects representations of a group G onto the trivial representation, and as such, every non-invariant contribution cancels, leaving only the gauge invariant part. In general, it takes the form

$$\int_G d\mu_G \,\text{PE}\Big[\chi_G^R(z_a)t\Big]\,, \tag{3.18}$$

where χ_G^R is the character of the representation R and the measure is the Haar measure given by

$$\int_G d\mu_G = \frac{1}{(2\pi i)^r}\oint_{|z_1|=1}\cdots\oint_{|z_r|=1}\frac{dz_1}{z_1}\cdots\frac{dz_r}{z_r}\prod_{\alpha^+}\left(1-\prod_{l=1}^{r} z_l^{\alpha_l^+}\right), \tag{3.19}$$

where α^+ are the positive roots and r is the rank.

Some common examples of the Haar measure are

$$\begin{aligned}\int_{SU(2)} d\mu_{SU(2)} &= \frac{1}{2\pi i}\oint_{|z|=1}\frac{dz}{z}(1-z^2)\,,\\ \int_{SU(3)} d\mu_{SU(3)} &= \frac{1}{(2\pi i)^2}\oint_{|z_1|=1}\oint_{|z_2|=1}\frac{dz_1}{z_1}\frac{dz_2}{z_2}(1-z_1z_2)\left(1-\frac{z_1^2}{z_2}\right)\left(1-\frac{z_2^2}{z_1}\right).\end{aligned} \tag{3.20}$$

Example 6. Let us take a specific example, the Higgs branch of $U(1)$ with two flavours. To compute the Hilbert series, we include the number and fugacity under the gauge group of q^i and

$\bar{q}_i$ as well as a term for their relation at second order

$$\begin{aligned} \mathrm{HS}(t) &= \frac{1}{2\pi i}\oint_{|z|=1}\frac{dz}{z}\,\mathrm{PE}\left[2z^{-1}t + 2z^{1}t - t^2\right] \\ &= \frac{1}{2\pi i}\oint_{|z|=1}\frac{dz}{z}\frac{(1-t^2)}{(1-zt)^2(1-t/z)^2}\,. \end{aligned} \tag{3.21}$$

Because $|t| < 1$, the only pole inside the circle $|z| = 1$ is the second-order pole at $z = t$. After a simple application of the Residue theorem, one finds that

$$\mathrm{HS}(t) = \frac{1-t^4}{(1-t^2)^3}\,. \tag{3.22}$$

This matches the Hilbert series of the space $\mathbb{C}^2/\mathbb{Z}_2$.

Example 7. Consider the following quiver:

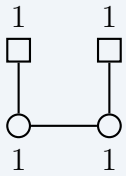

We associate each gauge group with a fugacity a and b, respectively. The bifundamental representations of the chiral multiplets can then be written as

$$(a + \frac{1}{a})\,, \quad (b + \frac{1}{b})\,, \quad \text{and} \quad (\frac{a}{b} + \frac{b}{a})\,. \tag{3.23}$$

For each gauge node, we also have a chiral multiplet transforming trivially and imposing a constraint. Thus, the Hilbert series is

$$\begin{aligned} \mathrm{HS}(t) &= \frac{1}{(2\pi i)^2}\oint_{|a|=1}\oint_{|b|=1}\frac{da}{a}\frac{db}{b}\,\mathrm{PE}\left[(a+\frac{1}{a})t + (b+\frac{1}{b})t + (\frac{a}{b}+\frac{b}{a})t - 2t^2\right] \\ &= \frac{1-t^6}{(1-t^3)^2(1-t^2)}\,, \end{aligned} \tag{3.24}$$

which corresponds to the variety $\mathbb{C}^2/\mathbb{Z}_3$.

3.5 Coulomb branch

The Coulomb branch is parameterised by the scalars in the vector multiplet, which transform in the adjoint representation of the gauge group.

Definition 12. The **Coulomb branch** is defined as

$$\mathcal{C} = \{\phi_i : V(\phi_i) = 0\} \,, \tag{3.25}$$

where the potential for the scalars in the vector multiplet takes the form

$$V \sim \sum_{i<j} \mathrm{Tr}[\phi_i, \phi_j]^2 \,. \tag{3.26}$$

To minimise this potential, the scalars ϕ_i take values in the Cartan subalgebra $\mathfrak{h}$ of the gauge group such that $V(\phi_i) = 0$. On a generic point, the gauge group G breaks to its maximal torus $U(1)^r$, where r is the rank.

In the case of $3d$ $\mathcal{N} = 4$ theories, we have three real scalars and an S^1-valued scalar (the dual photon). Classically, the Coulomb branch is thus

$$\mathcal{C}_{\text{classical}} = \frac{(\mathbb{R}^3 \times S^1)^r}{\mathcal{W}_G} \,, \tag{3.27}$$

where r is again the rank and $\mathcal{W}_G$ is the Weyl group. The dimension of this space is

$$\dim_{\mathbb{H}}(\mathcal{C}) = \mathrm{rank}(G) \,, \tag{3.28}$$

where G is the gauge group. The Coulomb branch receives quantum corrections that change many of its properties, but its dimension will be preserved.

The Coulomb branch as a space of dressed monopole operators

The 3-dimensional case is special, as we can define a conserved current $J^{(1)} = *_3 F^{(2)}$, where F is the field strength of the gauge field A. The equations of motion and the Bianchi identity can be reexpressed in terms of this current

$$\begin{aligned} dF^{(2)} &= 0 \qquad & d *_3 F^{(2)} &= 0 \\ d *_3 J^{(1)} &= 0 \qquad & dJ^{(1)} &= 0 \,, \end{aligned} \tag{3.29}$$

where the bottom-right equation indicates that the current is conserved and we have some $U(1)_J$ topological symmetry.

If we now source the Bianchi identiy for F, we get the existence of some monopole operator $V_m(x)$

$$d *_3 J^{(1)} = dF^{(2)} = m\delta^{(3)} \,. \tag{3.30}$$

For a vector multiplet with 4 supercharges, consisting of a gauge field A and a real scalar field σ

together with fermions, the singular boundary conditions become

$$\begin{aligned} A_{\pm} &\sim \frac{m}{2}(\pm 1 - \cos\theta)d\varphi \\ \sigma &\sim \frac{m}{2r}\,, \end{aligned} \tag{3.31}$$

as $r \to 0$ in spherical coordinates (r, θ, φ). The magnetic charge m lives in the coweight lattice $\hat{\Lambda}$ of the gauge group G.

As we are dealing with a theory with 8 supercharges, and so far we have neglected the two remaining scalars (or one complex scalar), which are in the chiral multiplet in the decomposition of the 8 supercharges vector multiplet. This complex scalar Φ can be used to dress the monopole operator by multiplication of a gauge-invariant polynomial of Φ

$$\mathcal{O}_{m,P} = V_m \times P_m(\Phi)\,. \tag{3.32}$$

All together, we get a so-called **bare monopole operator** V_m from the vector multiplet with 4 supercharges, and **dressing factors** from the chiral multiplet with 4 supercharges, thus forming a space of **dressed monopole operators** for the full vector multiplet with 8 supercharges.

Next, we want a way to count the dressed monopole operators graded under the R-symmetry and the global symmetry of the Coulomb branch. This method goes under the name of monopole formula and was first developed in [4].

Theorem 11. *The **monopole formula** gives us the Hilbert series for a space of dressed monopole operators. It is given by*

$$HS(t,z) = \sum_{m \in \hat{\Lambda}/\mathcal{W}} \left(\prod_i z_i^{J_i(m)} \right) P_G(t,m)\, t^{2\Delta(m)}\,, \tag{3.33}$$

where m are the magnetic charges in the coweight lattice $\hat{\Lambda}$ quotiented by the Weyl group $\mathcal{W}$ of the gauge group G, z_i are the fugacities counting the topological charges under $U(1)_J$, $P_H(t,m)$ is the dressing factor, and t is the fugacity counting the R-charge / conformal dimension.

Let us unpack this in some more detail. We should be very familiar with the weight lattice Λ of a Lie algebra from any course on representation theory. This lattice is also sometimes called the weight lattice of electric charges. To get elements in the dominant chamber only, one quotients by the Weyl group $\mathcal{W}$. Then, since we are counting magnetic elements, we need to sum over the dual weight lattice $\hat{\Lambda}$. Again, we quotient by the corresponding Weyl group to restrict to charges in the dominant chamber only.

The fugacity t counts the R-charge $r(m)$ of the bare monopole operators and is given by

$$r(m) = \underbrace{\frac{1}{2}\sum_{i=1}^{N_f}\sum_{\rho\in R_i}|\rho(m)|}_{\text{hplet contribution}} - \underbrace{\sum_{\alpha\in\Phi^+}|\alpha(m)|}_{\text{vplet contribution}} \tag{3.34}$$

where N_F are the number of flavours, ρ are the weights of the representation R_i, and α are the positive roots of the Lie algebra of the gauge group. There are three types of theories, see [19, 36]:

(i) If $r(m) > 1/2$ for any $m \neq 0$, then the theory is called **good**. The Coulomb branch will be a cone, at the tip of which the theory flows to an interacting SCFT in the IR. In the UV, the R-charge matches the conformal dimension $r(m) = \Delta(m)$.

(ii) If $r(m) \geq 1/2$ with some m saturating the bound, the theory is called **ugly**. The Coulomb branch will be a cone times $\mathbb{H}^n$ for some $n \in \mathbb{N}$. At the tip of the cone, the theory flows to an interacting SCFT as well as a free part. The conformal dimension again matches the R-charge.

(iii) If $r(m) < 1/2$ for some $m \neq 0$, the theory is called **bad**. In this case, the Coulomb branch is some more complicated space, the conformal dimension is not equal to the R-charge, and the Hilbert series diverges.

Since t is only counting the bare monopole operators, we still need to account for the dressing. This is done via the dressing factor

$$P_G(t,m) = \prod_{i=1}^{r}\frac{1}{1-t^{2d_i(m)}}\,, \tag{3.35}$$

where d_i is the degree of the independent Casimir operators.

The fugacities z_i count the topological charges under the $U(1)_J$ symmetries, and after a fugacity mapping, will give us the characters of the global symmetry of the Coulomb branch. The fugacity mapping is given Cartan matrix of the global symmetry. We can get the unrefined Hilbert series in the normal way by simply setting $z_i = 1$.

Crucially, even though we may seem to limit ourselves to the very specific case of $3d$ $\mathcal{N} = 4$, it turns out that there is a very powerful conjecture which underlies much of what is to follow.

Conjecture 1. *For a cone of the Higgs branch $\mathcal{H}$ - in any of the dimensions $3, 4, 5, 6$ - of some theory (called the **electric quiver**), there exists a theory in 3 dimensions (**magnetic quiver**) whose Coulomb branch is equal to the cone of the Higgs branch. That is:*

$$\mathcal{H}^{d=3,4,5,6}(\textit{electric quiver}) = \bigcup_i \mathcal{C}^{d=3}(\textit{ith magnetic quiver})\,. \tag{3.36}$$

Example 8. Let us compute the Hilbert series for the Coulomb branch of $U(1)$ with n flavours. The R-charge is

$$\Delta(m) = \frac{n}{2}|m|\,, \tag{3.37}$$

where m is the magnetic charge of $U(1)$, which lives in the magnetic lattice $\mathbb{Z}$. The dressing factor takes the form

$$P(t) = \frac{1}{1-t^2}\,. \tag{3.38}$$

And thus, the Hilbert series becomes

$$\begin{aligned} \mathrm{HS}(t,z) &= \frac{1}{1-t^2}\sum_{m\in\mathbb{Z}} z^m t^{n|m|} \\ &= \frac{1-t^{2n}}{(1-zt^n)(1-t^2)(1-t^n/z)}\,. \end{aligned} \tag{3.39}$$

One may immediately recognise this from our discussion in section 2.2 as $\mathbb{C}^2/\mathbb{Z}_n$. Hence, we see that by quantising our moduli space changes drastically:

$$\mathcal{C}_{\text{classical}} = \underbrace{\mathbb{R}^3 \times S^1}_{\text{smooth}} \quad \to \quad \mathcal{C}_{\text{quantum}} = \underbrace{\mathbb{C}^2/\mathbb{Z}_n}_{\text{singular}}\,. \tag{3.40}$$

Example 9. Let us now look at another quiver and compute its Coulomb branch Hilbert series:

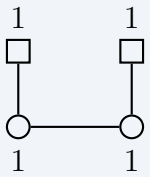

We will give the two gauge nodes magnetic charges a and b, respectively. Thus, the R-charge is given by

$$\Delta(a,b) = \frac{1}{2}(|a| + |a-b| + |b|) - 0\,, \tag{3.41}$$

and we will have a dressing factor for each $U(1)$ gauge group. The Hilbert series then becomes, again via the monopole formula,

$$\begin{aligned} \mathrm{HS}(t) &= \frac{1}{(1-t^2)^2}\sum_{a,b\in\mathbb{Z}} t^{|a|+|a-b|+|b|} \\ &= \frac{1+4t^2+t^4}{(1-t^2)^4} \\ &= 1 + 8t^2 + 27t^4 + \mathcal{O}(t^6)\,. \end{aligned} \tag{3.42}$$

And if one computes the refined Hilbert series

$$\mathrm{HS}(t, x_1, x_2) = 1 + [1,1]t^2 + [2,2]t^4 + \mathcal{O}(t^6)\,, \tag{3.43}$$

where after a mapping one recognises the $SU(3)$ characters. The dimension of this space is 4, due to the order of the pole at $t = 1$. This matches the dimension of $\overline{min.A_2}$.

3.6 Field theory in $5d$ theories

As we will primarily focus on 5-dimensional theories in the latter parts of this dissertation, we should spend some time investigating their field-theoretic properties.

Consider some arbitrary non-abelian gauge theory, its action in 5 dimensions

$$S = \frac{1}{g^2}\int d^5x\,\mathrm{Tr}\Big(- F_{\mu\nu}F^{\mu\nu} + \cdots \Big)\,, \tag{3.44}$$

where g is the gauge coupling, and F is the field strength of the gauge field A_μ. Crucially, we can show that the mass dimension of g is $[g] = -1/2$. This means that - naively - the theory is non-renormalisable and thus solely a low-energy effective field theory. But, as Seiberg found in [12], there exist non-trivial fixed points in the UV where the theory flows to some superconformal field theory (SCFT).

The key to this picture is understanding the non-perturbative effects of instanton states. Instantons have a mass that is inversely proportional to the gauge coupling,

$$m_I \propto \frac{1}{g^2}\,. \tag{3.45}$$

As we move towards strongly coupled regimes, the instantons become massless and will contribute to the Higgs branch of the theory. And because they are charged under a topological symmetry

$$J^{(1)} = *\,\mathrm{Tr}(F \wedge F)\,, \tag{3.46}$$

they will enhance the global symmetry. This enhancement is not always possible, i.e. for some $5d$ $\mathcal{N} = 1$ theory, there does not necessarily exist a fixed point. Later, when discussing the brane picture, we will see that certain arrangements of branes can prevent us from reaching a fixed point.

Prepotential

The exact form of the low-energy effective action of our theory is determined by the **prepotential**. See [37] for a review. Intriligator, Morrison, and Seiberg (IMS) proposed a one-loop exact prepotential in [13]. More recently, there have been successful efforts to construct a **complete prepotential** capturing non-perturbative effects and global symmetries over the whole parameter region [38].

As we have seen, the Coulomb branch is parameterised by a single scalar $\phi \in \mathbb{R}$. On a generic point on the Coulomb branch, the gauge group breaks to its maximal torus $U(1)^r \subset G$. For this low-energy Abelian theory, the IMS prepotential is

$$\mathcal{F}(\phi) = \frac{1}{2} m_0 h_{ij} \phi_i \phi_j + \frac{\kappa}{6} d_{ijk} \phi_i \phi_j \phi_k + \frac{1}{12} \left(\sum_{\alpha \in \text{roots}} |\alpha \cdot \phi|^3 - \sum_f \sum_{\omega \in R_f} |\omega \cdot \phi + m_f|^3 \right), \tag{3.47}$$

where $m_0 = 1/g_0^2$, κ is the classical Chern-Simons level, $h_{ij} = \text{Tr}(T_i T_j)$, and $d_{ijk} = \frac{1}{2}\text{Tr}(T_i \{T_j, T_k\})$ with T_i being the Cartan generators. Also, α are roots in the Lie algebra associated to the gauge group, m_f is the mass of hypermultiplet matter f, where we sum over weights ω in the corresponding representation of the matter R_f. The first two terms are classical results, and the term in brackets is the one-loop correction.

The power of the prepotential comes from the fact that, using it, we can easily compute various quantities, such as the monopole string tension

$$T_i = \frac{\partial \mathcal{F}}{\partial \phi_i}, \tag{3.48}$$

and the effective coupling/metric on the Coulomb branch

$$(\tau_{\text{eff}})_{ij} = \frac{\partial^2 \mathcal{F}}{\partial \phi_i \partial \phi_j}. \tag{3.49}$$

In general, the BPS spectrum of our theories includes electrically charged objects such as W-bosons, instantons which are charged under the topological symmetry, and magnetically charged monopoles.

Chern-Simons terms

In a non-Abelian theory in 5-dimensions, we can include the following Chern-Simons terms

$$\frac{\kappa}{24\pi^2} \int \text{Tr} \left(A \wedge F \wedge F - \frac{1}{2} A \wedge A \wedge A \wedge F + \frac{1}{10} A \wedge A \wedge A \wedge A \wedge A \right). \tag{3.50}$$

where κ is the Chern-Simons level. The Chern-Simons level is not gauge invariant, and hence we need a consistency condition such that it does not contribute to the path integral non-trivially. For $G = SU(N_c)$ with n_+ massive flavours with $m > 0$ and n_- massive flavours with $m < 0$, the low-energy effective Chern-Simons level is

$$\kappa_{\text{eff}} = \kappa - \frac{n_+ - n_-}{2}, \tag{3.51}$$

and for consistency we require $\kappa_{\text{eff}} \in \mathbb{Z}$.

4. Brane constructions for $3d$ theories

The true beauty of supersymmetric gauge theories comes from their realisations via brane configurations in type IIA or IIB string theory. These brane constructions allow us to encode much of the information of the gauge theory and give detailed insight into non-perturbative effects. In particular, they allow us to get an intuitive picture of the moduli spaces of supersymmetric theories.

We will begin with the seminal work by Hanany and Witten [7] on $3d$ $\mathcal{N} = 4$ gauge theories, realised on the worldvolume of intersecting D3, D5, and NS5 branes. This is to provide a more pedagogical introduction to brane constructions, which is somewhat more straightforward than the 5-dimensional case we will examine afterwards.

For readers less familiar with branes in string theory, in particular with branes ending on branes and branes as algebraic objects, the lecture notes [16] offer an accessible introduction.

4.1 General setup

We can construct a 3-dimensional theory with 8 supercharges by placing a D3 brane between two D5 or NS5 branes such that they share a $(2+1)$-dimensional worldvolume and the remaining dimensions are allocated as in table 4.1. This can be depicted as in figure 4.1, where the directions corresponding to the D5 and NS5 branes extend to infinity, whereas the x^6 direction of the D3 brane is bound between the D5 and NS5 branes.

	x^0	x^1	x^2	x^3	x^4	x^5	x^6	x^7	x^8	x^9
NS5	×	×	×	×	×	×				
D3	×	×	×				×			
D5	×	×	×					×	×	×

Table 4.1: Brane setup for a 3-dimensional theory breaking 1/4 of the 32 supercharges in type IIB, where the x^6 direction will be spatially restricted between either D5 or NS5 branes.

By inspecting the brane system in table 4.1, we can see that our initial $SO(1,9)$ Lorentz symmetry breaks into

$$SO(1,2) \times SO(3)_{\mathcal{C}} \times SO(3)_{\mathcal{H}} \subset SO(1,9)\,. \tag{4.1}$$

Since these symmetries have to represent spinors as well, we can infer that the R-symmetry becomes

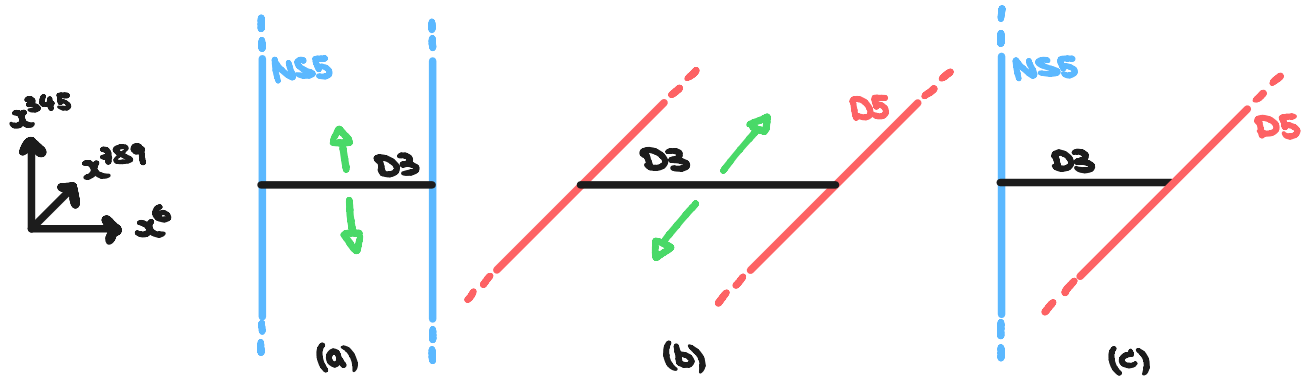

Figure 4.1: Different cases of the brane setup for the D3-D5-NS5 system. The D3 brane is suspended between: (a) Two NS5 branes, (b) two D5 branes, and (c) one NS5 and one D5 brane. The green arrows indicate directions in which the D3 brane is free to move. Using these building blocks, one can construct more complex brane systems.

$SU(2)_{\mathcal{C}} \times SU(2)_{\mathcal{H}}$.

Suppose we have a single D3 brane; it will have a vector multiplet in 16 supercharges living on its world volume. If the 3-brane ends on a 5-brane, the total supersymmetry halves and as such, the vector multiplet decomposes into a vector multiplet and a hypermultiplet

$$V_{3d,\mathcal{N}=8} = V_{3d,\mathcal{N}=4} + H_{3d,\mathcal{N}=4}\,. \tag{4.2}$$

Depending on the type of boundary condition, Dirichlet or Neumann, that the 5-brane imposes, half of the massless fields are set to zero. The analysis in [7] shows that:

- A D3 brane ending on an NS5 brane results in a vector multiplet on the world volume of the 3-brane. This will be parameterised by the three directions along the NS5 brane (x^3, x^4, x^5) and a massless gauge field a_μ with $\mu = 0, 1, 2$. Making a total of 4 degrees of freedom.
- A D3 brane ending on a D5 brane results in a hypermultiplet, parameterised by the three directions along the D5 brane (x^7, x^8, x^9) and a scalar b that comes from dimensionally reducing a 4-dimensional gauge field to 3 dimensions. Again, giving us the necessary 4 degrees of freedom.

As a consequence, if we have both Dirichlet and Neumann boundary conditions (corresponding to case (c) in figure 4.1), we do not have any moduli.

With this in hand, we can construct $3d$ $\mathcal{N} = 4$ pure SYM theories with $U(n)$ gauge group, see (a) in figure 4.2. If we include D5 branes in between the NS5 branes, we will have additional strings stretching between the D3 branes and the D5 branes, resulting in hypermultiplets. This is shown in figure 4.2 (b). This can be extended even further to other algebras by including orientifold planes, see for example [39].

There is another important concept coming out of [7], namely that of the **Hanany-Witten transition**. If you move a D5 brane through an NS5 brane, it creates a D3 brane connecting the two, and crucially leaves the moduli space unchanged. Schematically, we can illustrate it as shown

in figure 4.3.

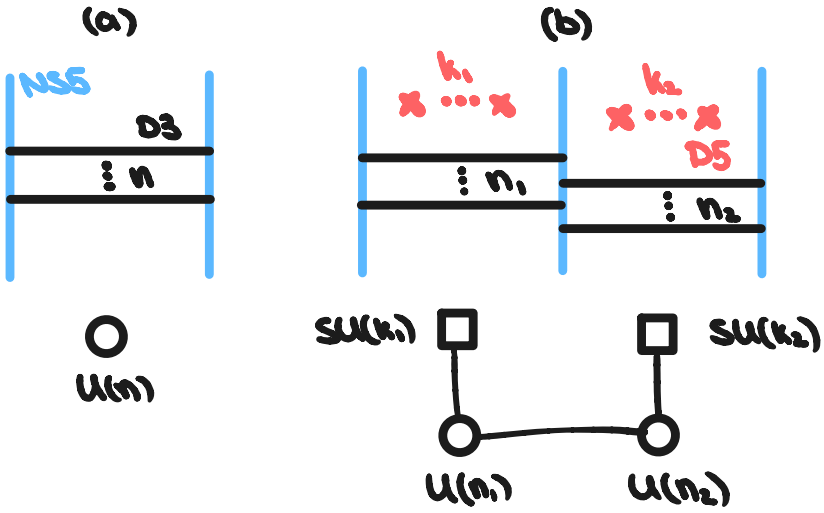

Figure 4.2: Brane construction for: (a) a pure $U(n)$ SYM theory, (b) a theory with gauge group $U(n_1) \times U(n_2)$ and additional flavours. The red crosses represent D5 branes going into the page, and should be thought of as being on top of the D3 branes to give massless hypermultiplets.

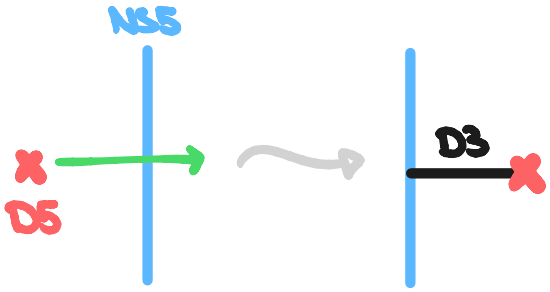

Figure 4.3: Hanany-Witten transition. Moving a D5 brane through an NS5 brane creates a D3 brane which connects the D5 to the NS5 brane.

4.2 3*d* Mirror symmetry

With the Hanany-Witten transitions at our disposal, we can finally explain an intricacy which the reader might have already noticed. From our computations of Hilbert series' in sections 3.4 and 3.5, we found

$$\mathcal{H}\left(\begin{array}{c} n \\ \square \\ | \\ \circ \\ 1 \end{array}\right) = \overline{min.A_{n-1}} = \mathcal{C}\left(\begin{array}{ccccc} 1 & & & & 1 \\ \square & & & & \square \\ | & & & & | \\ \circ & - & \cdots & - & \circ \\ \underbrace{1 \qquad\qquad 1}_{n-1} & & & & \end{array}\right), \tag{4.3}$$

and similarly

$$\mathcal{C}\Big(\begin{array}{c}n\\ \square\\ \circ\\ 1\end{array}\Big) = \mathbb{C}^2/\mathbb{Z}_n = \mathcal{H}\Big(\begin{array}{ccccc}1 & & & & 1\\ \square & & & & \square\\ \circ & - & \cdots & - & \circ\\ \underbrace{1 \qquad\qquad 1}_{n-1} & & & & \end{array}\Big)\,. \tag{4.4}$$

Where some of these we had found explicitly, and others we only saw examples of.

This is, of course, no coincidence, but due to a duality called $3d$ mirror symmetry [40, 7]. Different theories in the UV can flow to the same theory in the IR. The characteristic relations of $3d$ mirror symmetry are

$$\begin{aligned} \text{Quiver } A &\leftrightarrow \text{Quiver } B\\ \mathcal{H}_A &\leftrightarrow \mathcal{C}_B\\ \mathcal{C}_A &\leftrightarrow \mathcal{H}_B\\ SU(2)_{\mathcal{C}/\mathcal{H}} &\leftrightarrow SU(2)_{\mathcal{H}/\mathcal{C}}\\ \text{FI/mass} &\leftrightarrow \text{mass/FI}\,. \end{aligned} \tag{4.5}$$

To see why this is the case, we can utilise the Hanany-Witten transitions. Consider the brane system for $U(1)$ with n flavours as in figure 4.4. By moving two of the D5 branes out of the NS5 branes on opposite ends, performing an S-duality (NS5 $\leftrightarrow$ D5, D3 $\leftrightarrow$ D3), and rotating the coordinates that go into the page up, such that they align with the upwards direction, we arrive at the other quiver.

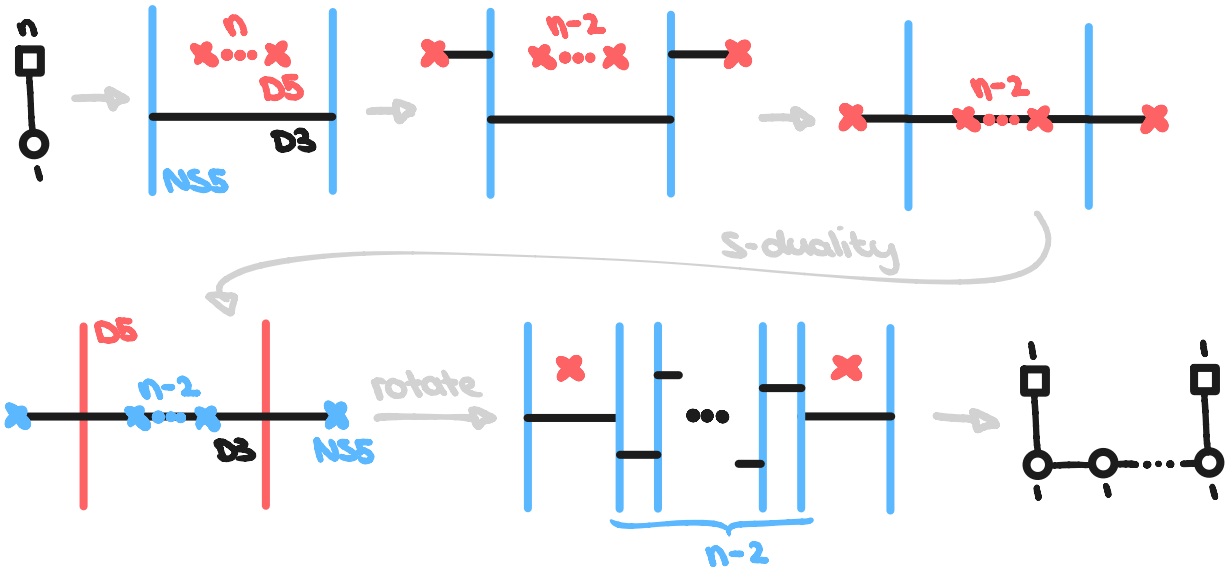

Figure 4.4: Mirror symmetry of two quivers via Hanany-Witten transitions and S-duality.

4.3 Branches of the moduli space - a brane perspective

A major advantage of the brane picture is the way the moduli spaces are encoded in the relative positions of the branes. In figure 4.1, we saw that we are free to move the D3 brane along the NS5

or D5 branes. We also know that this encodes four moduli, three directions, plus either a massless gauge field or the scalar from dimensional reduction. So it is clear that the position of the D3 brane along the 5-branes corresponds to a position on the moduli space.

Let us begin with the simple example of $U(1)$ with one flavour, as there is only a Coulomb branch and no Higgs branch. The Coulomb branch is parameterised by the D3 brane moving along the NS5 branes and has a singular point when it overlaps with the D5 brane, see figure 4.5.

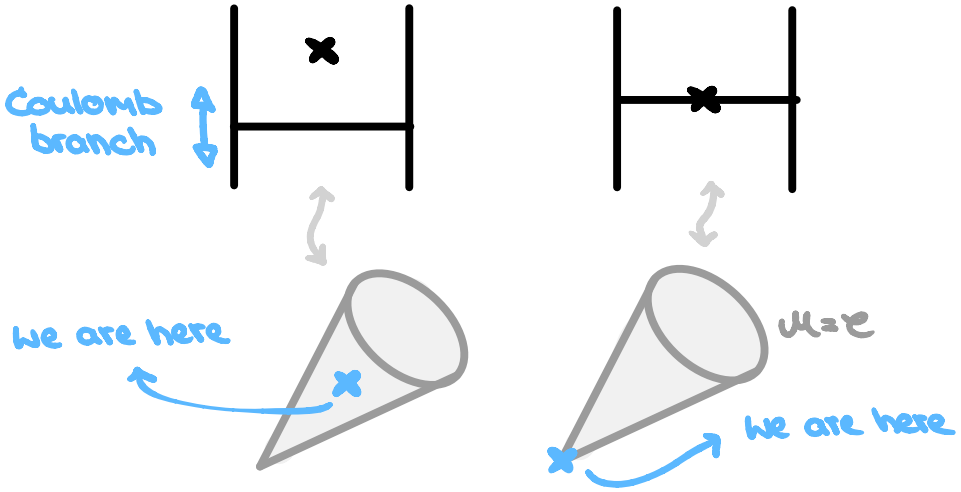

Figure 4.5: Brane realisation of the moduli space of $U(1)$ with one flavour. Coulomb branch $\mathcal{C}$ is parameterised by the position of the D3 brane along NS5 branes.

Building up in complexity, we can look at $U(1)$ with two flavours, see figure 4.6. The novelty in this case comes from the fact that, once the D3 brane lies on top of the D5 branes, the part of the D3 brane which is between the D5 branes is free to move inside and out of the page along the D5 branes. This movement parameterises the Higgs branch.

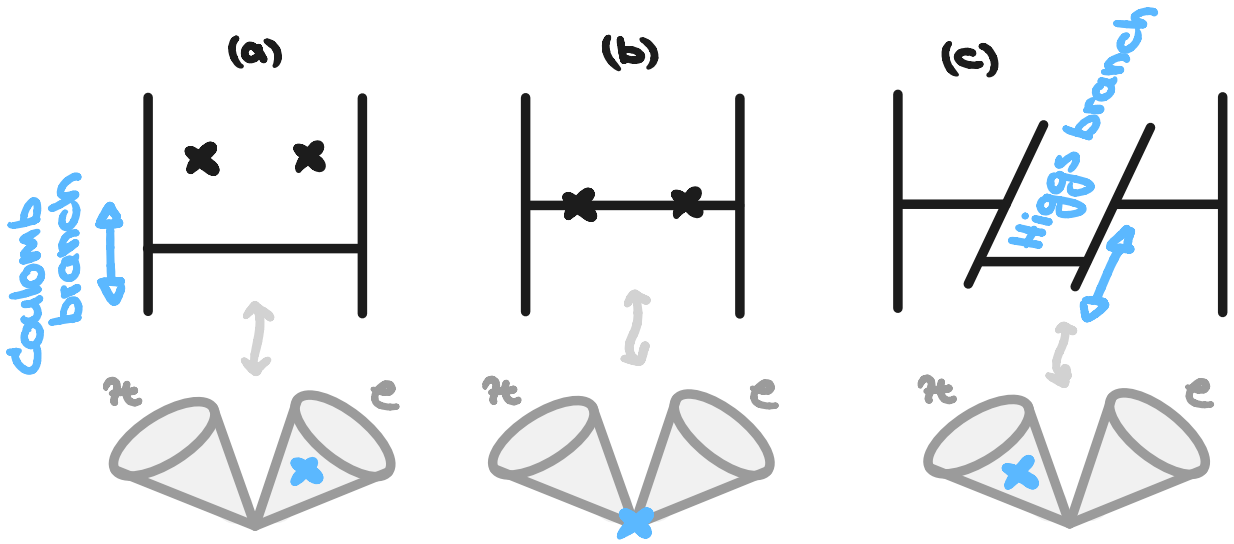

Figure 4.6: Brane realisation of the moduli space of $U(1)$ with two flavour. In (a) we are on a generic point on the Coulomb branch $\mathcal{C}$, in (b) we are at the origin of both branches, and in (c) we are on a generic point on the Higgs branch $\mathcal{H}$. In (c), we have drawn in the third dimension, which before was going perpendicularly into the page.

There are two more things that we can do. One is to offset the height of the D5 branes, and the other is to offset the depth of the NS5 branes, see figure 4.7. This is equivalent to introducing a mass term and an FI term, respectively. And as a result, for case (a) in figure 4.7, the Higgs branch gets lifted and the singularity at the origin of the Coulomb branch gets resolved. Similarly, for case (b) in figure 4.7, the Coulomb branch gets lifted and the singularity at the origin on the Higgs branch gets resolved.

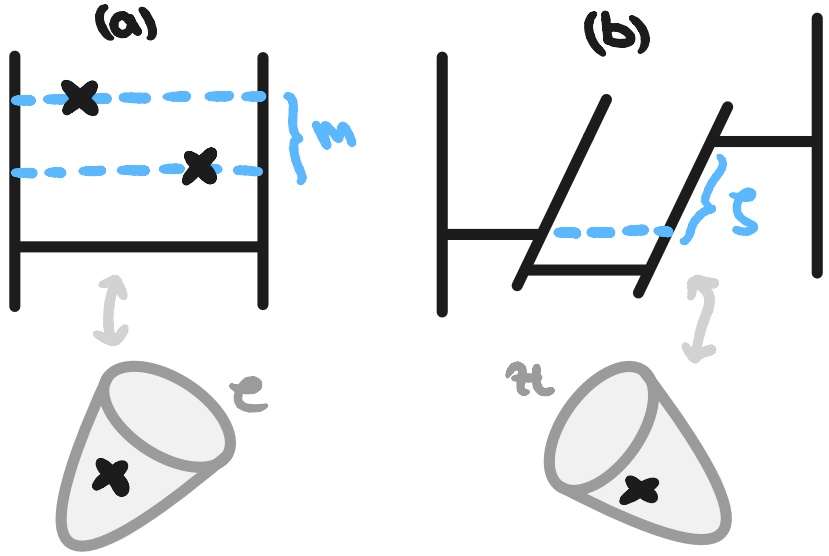

Figure 4.7: Mass and FI terms via offsets of branes. (a) The Higgs branch gets lifted, and the singularity gets resolved. (b) The Coulomb branch gets lifted, and the singularity gets resolved.

5. Brane constructions for $5d$ theories

Having gained some experience with brane systems in chapter 4, we will turn to the case of $5d$ $\mathcal{N}=1$ theories engineered on **brane webs** consisting of (p,q) 5 and 7-branes. They were first introduced in the works [9, 10, 41].

5.1 The brane web

Consider the brane configuration in table 5.1, which generalises the Hanany–Witten setup via T-dualities. The novelty of this construction is that when a D5 brane ends on an NS5 brane in the (x^5, x^6)-plane, conservation of the overall R-R and NS-NS charges requires them to form a bound state. Since the D5 and NS5 branes have charges $(1,0)$ and $(0,1)$, respectively, the overall bound state is a $(1,1)$ brane.

	x^0	x^1	x^2	x^3	x^4	x^5	x^6	x^7	x^8	x^9
NS5	×	×	×	×	×	×				
D5	×	×	×	×	×		×			
(p,q) 5-brane	×	×	×	×	×	α				
$[p,q]$ 7-brane	×	×	×	×	×			×	×	×

Table 5.1: Brane setup for a 5-dimensional theory breaking 1/4 of the 32 supercharges in type IIB.

As Aharony and Hanany found in [9], the resulting bound state will be at an angle α corresponding to its charges. The angle α is given by $\tan(\alpha) = q\tau_2/(p+q\tau_1)$, where $\tau = \tau_1 + i\tau_2$ is the axiodilaton. For illustrative purposes, when drawing brane webs, we choose $\tau = i$, resulting in the relation

$$\tan(\alpha) = \frac{q}{p}\,. \tag{5.1}$$

We can see this in action in figure 5.1.

We can also note that because there is an $SO(3)$ symmetry rotating the remaining 3 coordinates x^7, x^8, and x^9, we will have an overall $SU(2)_R$ R-symmetry.

To construct a gauge theory in the usual manner by stacking D-branes, we will inadvertently end up with external branes (otherwise, we are not restricting the x^6 direction, and we will have a $6d$ theory). Fixing the position of the external branes in space means that we are freezing an overall

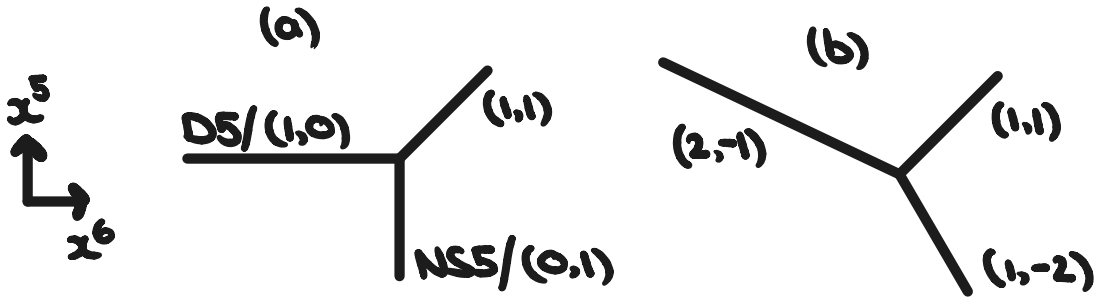

Figure 5.1: (a) A D5 brane combining with NS5 brane to form bound state of a $(1,1)$ 5-brane. (b) A $(2,-1)$, $(1,1)$, and $(1,-2)$ brane web vertex. The overall charge going into the vertices is conserved.

$U(1)$ degree of freedom. This turns our $U(n)$ theories into $SU(n)$ theories. To add hypermultiplets to our theory, we can include semi-infinite D5 branes. Some examples are shown in figure 5.2.

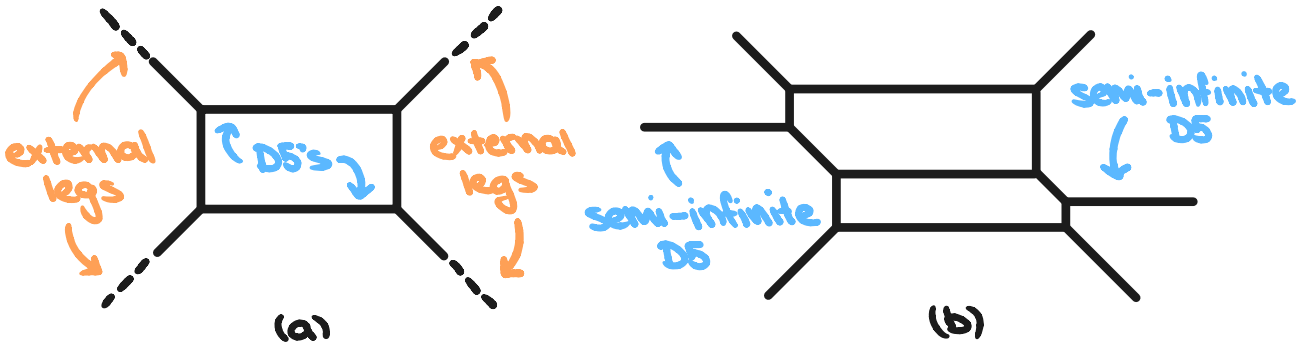

Figure 5.2: (a) Pure $SU(2)$ SYM theory. (b) $SU(3)$ with 2 flavours.

Beyond capturing non-perturbative physics, the brane web also encodes the complete information of the field theory itself. This can simply be deduced from what types of branes can exist between the D5 and NS5 branes in the brane web. In particular, we have W-bosons, monopoles, and instantons arising from F1, D3, and D1 branes, respectively. This is shown in more detail in figure 5.3.

Another important aspect is that the mass of the hypermultiplet m_h can be increased arbitrarily by moving the semi-infinite D5 brane up along the other branes. Once it reaches the top D5 brane, a **flop transition** happens where the brane web adjusts to conserve charge. This is shown in figure 5.4.

Coulomb branch

In general, we can distinguish between two types of deformations: local deformations, where the external legs are fixed, and global deformations, where they are not, see figure 5.5. Recall that the dimension of the Coulomb branch is the rank of the gauge group, and since in 5-dimensions we only have a single real scalar in the vector multiplet, the Coulomb branch of, say, $SU(2)$ pure SYM will be parameterised by this single real scalar. In the brane picture, the scalar corresponds to the size

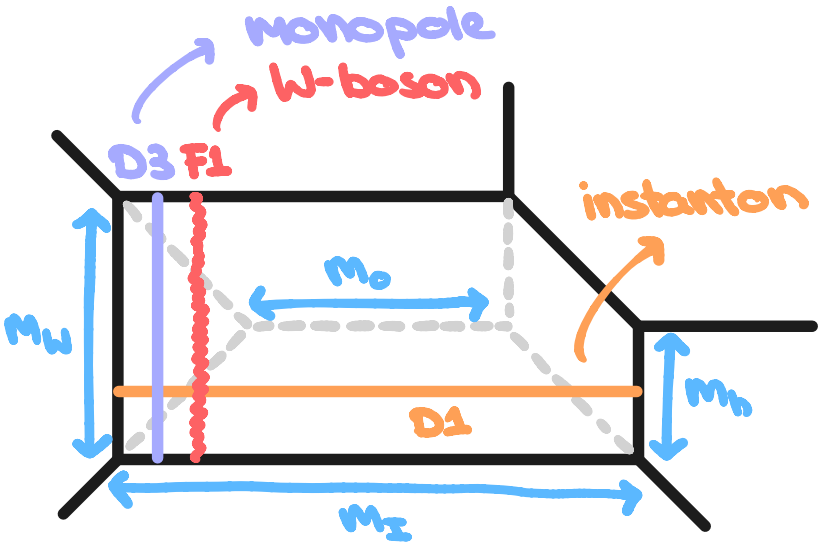

Figure 5.3: BPS states from brane web. The bare coupling strength is given by $m_0 = 1/g_0^2$, and the masses of hypermultiplets, instantons, and W-bosons are m_h, m_I, and m_W, respectively. The red line is an F1 string corresponding to a W-boson, the purple line is a D3 brane corresponding to a monopole, and the orange line is a D1 string corresponding to an instanton.

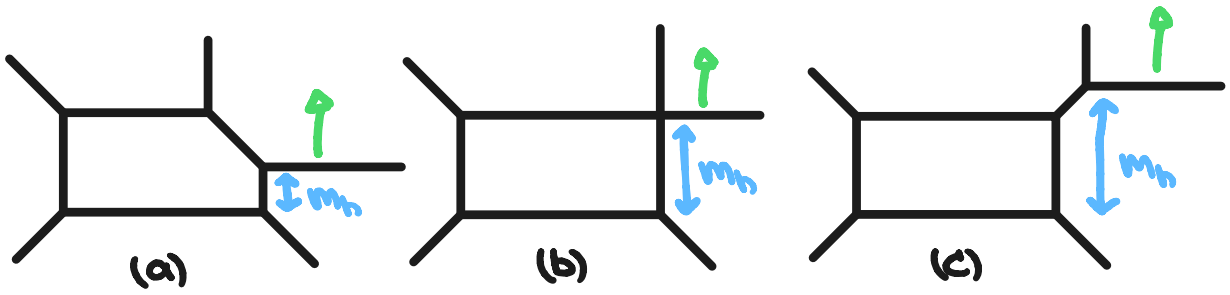

Figure 5.4: Flop transition for $SU(2)$ theory with 1 flavour. In all stages of the transition (a) - (c), the charge at the vertices is conserved.

of the face, and thus, in general

$$\begin{aligned}\text{rank}(G_{\text{gauge}}) = \text{number of local deformations} &= E_{\text{internal}} - V + 1 \\ &= F_{\text{internal}}\,,\end{aligned} \tag{5.2}$$

where E_{internal} are non-external branes, V are vertices, and F_{internal} are the faces. A similar relationship holds for the global symmetry

$$\text{rank}(G_{\text{global}}) = \text{number of global deformations} = E_{\text{external}} - 3\,, \tag{5.3}$$

where E_{external} are the external legs.

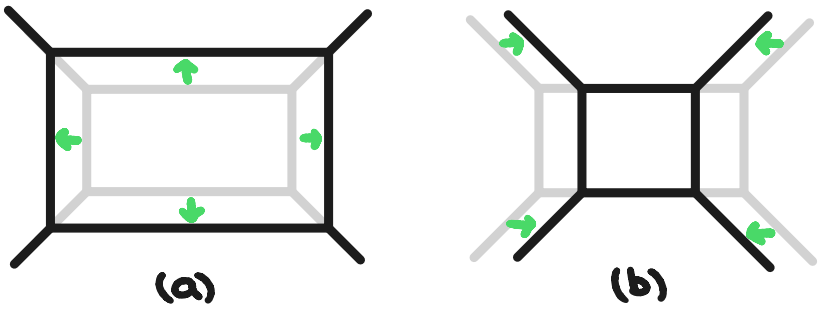

Figure 5.5: Deformations for $SU(2)$ pure SYM theory: (a) local transformation, and (b) global transformation. Local deformations parameterise the Coulomb branch.

7-branes and the S-rule

Up to this point, we have allowed the external 5-branes to extend to infinity. For analysing the Higgs branch, however, it will be crucial to restrict these legs by letting each of the (p, q) 5-branes end on a $[p, q]$ 7-brane. A $[p, q]$ 7-brane is a co-dimension 2 object and thus sources an $SL(2, \mathbb{Z})$ monodromy. Choosing a monodromy cut emanating from the 7-brane, the axio-dilaton τ jumps by this $SL(2, \mathbb{Z})$ element across the cut, as well as any (p, q) 5-brane crossing the cut must have its charge adjusted accordingly. The monodromy of a $[p, q]$ 7-brane is given by

$$M_{[p,q]} = \begin{pmatrix} 1 - pq & p^2 \\ -q^2 & 1 + pq \end{pmatrix}\,. \tag{5.4}$$

If a (p, q) 5-brane crosses the monodromy cut of a $[P, Q]$ 7-brane, its charge vector transforms, over the cut, as

$$\begin{pmatrix} r \\ s \end{pmatrix} = M_{[P,Q]} \begin{pmatrix} p \\ q \end{pmatrix}\,. \tag{5.5}$$

Additionally, this allows us to generalise the Hanany-Witten transition to moving a 7-brane through a 5-brane. For example, in figure 5.6, we can move a 7-brane, which has a 5-brane ending

on it, past the vertex. The 5-brane that connected the 7-brane to the vertex vanishes, but due to the monodromy cut the other 5-branes remain as they were.

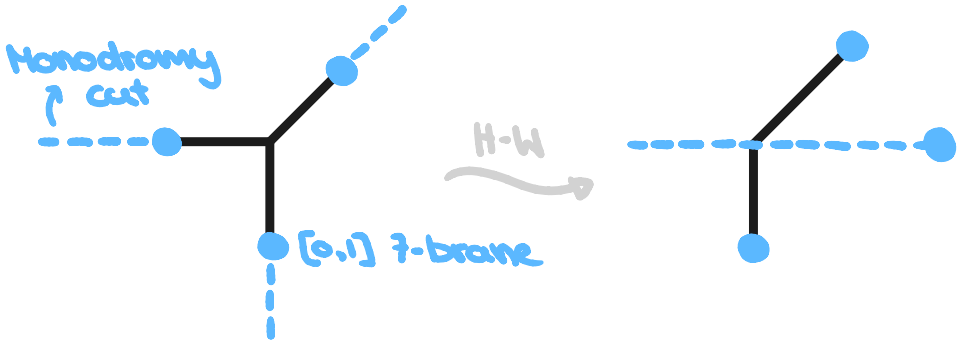

Figure 5.6: Inclusion of $[p, q]$ 7-branes (blue dots) on a simple vertex. After a Hanany-Witten transition of one of the 7-branes, the monodromy cut causes the upper-right 5-brane to tilt in the same way as before. We will usually not draw monodromy cuts if they are not relevant.

In [7], the authors found that you cannot have more than one D3 brane between a D5 and an NS5 brane without breaking supersymmetry. Something similar is true for brane webs, namely, you cannot have more than one D5 brane between a 7-brane and a brane with an NS-NS charge[1]. This phenomenon is usually referred to as the **generalised S-rule** [42].

Toric diagrams

A convenient and clean way to package the information of a 5-brane is via its dual diagram - often called the **grid** or **toric diagram**. It is constructed via the following rules:

(i) vertices of the web $\leftrightarrow$ polygons in the dual,

(ii) faces of the web $\leftrightarrow$ points in the dual,

(iii) edges of the web $\overset{\leftrightarrow}{\perp}$ lines in the dual,

The last item means that each edge in the brane web gets replaced by a line that is perpendicular to the original edge. The explicit construction can be seen in figure 5.7.

The toric diagram encodes most of the data from the original brane web in a very orderly manner, in particular, the non-perturbative data, but it loses all the size-related information, like coupling strengths or mass values.

While we use toric diagrams here as a convenient tool to encode brane webs, their more profound significance lies in geometric engineering. A toric diagram, which is convex, defines a specific toric Calabi-Yau threefold, and the low-energy limit of M-theory on $\mathbb{R}^{1,4} \times CY_3$ is equivalent to the $5d$ SCFT that emerges at the infinite coupling limit of the corresponding brane web [43].

The notion of toric diagrams can also be generalised to non-toric geometries, which allows for multiple 5-branes to end on a 7-brane. These are called generalised toric polygons [44]. This different

[1] If a given brane web breaks supersymmetry is, in general, an unsolved problem.

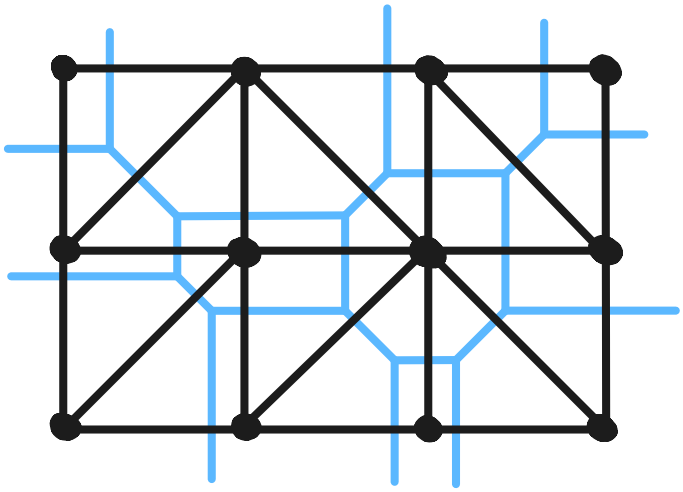

Figure 5.7: Toric diagram (black) and brane web (blue) of $SU(2) \times SU(2)$ with 4 flavours with some arbitrary tesselation.

boundary condition is encoded as a white point. So if multiple 5-branes end on the same 7-brane, the faces in between the edges of the web become white points. If the 5-branes end on separate 7-branes, the faces are the normal black points. See figure 5.8 for an illustration.

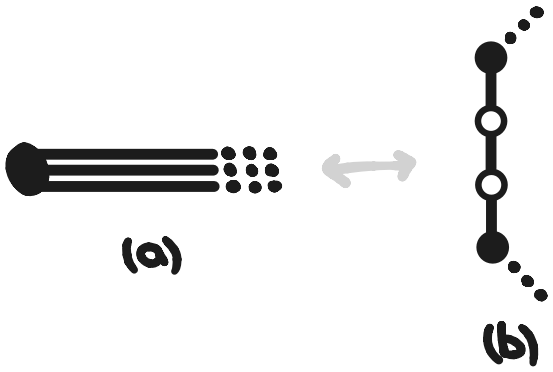

Figure 5.8: (a) Part of the brane web with multiple 5-branes ending on the same 7-brane. (b) Corresponding generalised toric diagram, where the boundary condition is encoded via the white points.

Chern-Simons level from web diagram

Recall from section 3.6 that we can have a Chern-Simons level which takes discrete values. For some general $SU(n)$ theory with n_+ flavours with positive mass and n_- flavours with negative mass, the low-energy theory will have a Chern-Simons level of

$$\kappa_{\text{eff}} = \kappa - \frac{n_+ - n_-}{2} \in \mathbb{Z}\,. \tag{5.6}$$

In [45], the author shows how the Chern-Simons level manifests itself in the brane web of an $SU(n)_\kappa$ theory with and without flavours. This is shown in figures 5.9 and 5.10. For the theory with flavours, we first have to integrate them out, that is, move them up/down such that they end up on the heavy legs and we get a low-energy theory for which we can use (5.6).

One can also immediately read all the relevant information from the toric diagram, see figure 5.11.

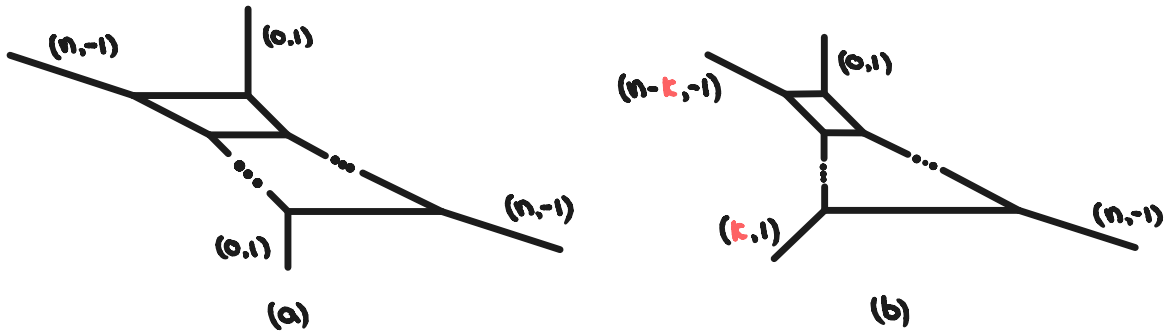

Figure 5.9: (a) $SU(n)_0$ with no flavours. (b) $SU(n)_\kappa$ with no flavours. The Chern-Simons level is introduced by changing the charges of some of the heavy branes.

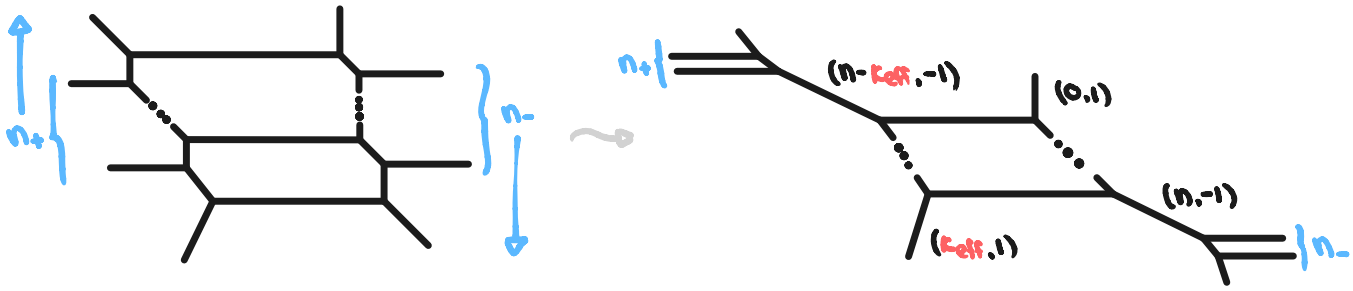

Figure 5.10: $SU(n)_\kappa$ with $n_+ + n_-$ flavours. To find the original Chern-Simons level κ, we integrate out the flavours by moving them onto the heavy branes, and then read off the effective Chern-Simons level from which one can compute the original Chern-Simons level.

5.2 Higgs branch and magnetic quivers

We can access the Higgs branch by shrinking all faces via local deformations and making the hypermultiplets massless; in essence, we are moving all the D5 branes to the same x^5 coordinate. The degrees of freedom associated with moving valid subwebs in and out of the page along the 7-branes parameterise the Higgs branch.

In figure 5.12 (a), we start with the brane web for an $SU(2)$ theory with 4 flavours. We make all hypermultiplets massless and shrink the faces to zero. In figure 5.12 (b), we recognise that there are now subwebs, which on their own satisfy all conditions for a valid brane web (conserving charges at vertices and not violating the S-rule). In addition, we may choose a decomposition which is maximal, meaning none of the subwebs can be further decomposed into other subwebs.

By conjecture 1, we know that there exists a $3d$ $\mathcal{N} = 4$ quiver whose Coulomb branch is the same as the Higgs branch of our $5d$ $\mathcal{N} = 1$ theory at hand. This quiver is called the **magnetic quiver** and can be read off the brane system. In figure 5.12 (c), we recognise four separate branes corresponding to $U(1)$ gauge group factors and one corresponding to a $U(2)$ factor. In this simple example, whether the subwebs cross/meet on the same 7-brane determines if we have an edge between the gauge nodes.

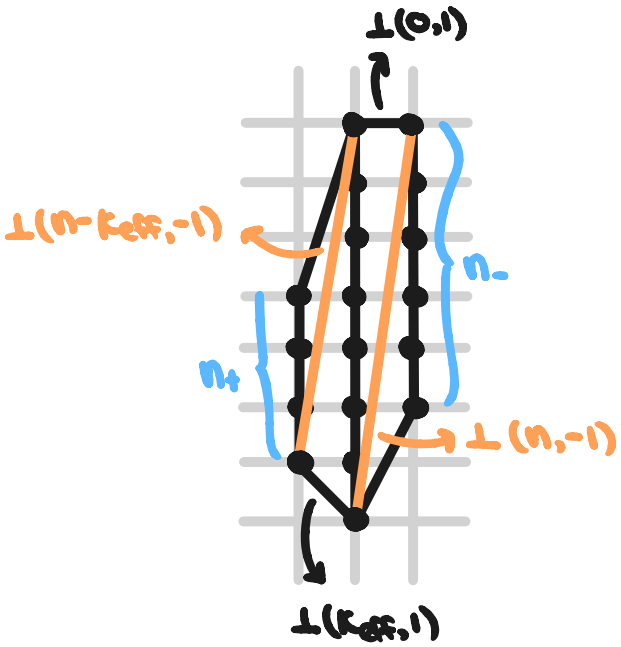

Figure 5.11: Toric diagram for $SU(n)_\kappa$ with $n_+ + n_-$ flavours. One can easily read off all the relevant information to compute the original Chern-Simons level.

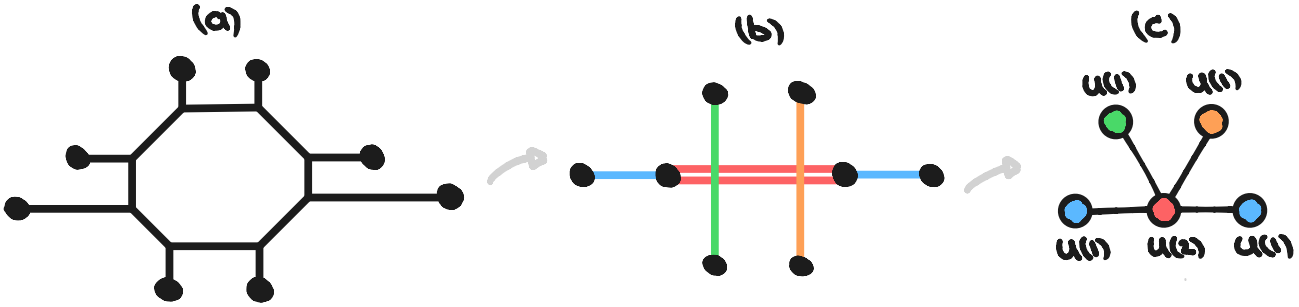

Figure 5.12: For $SU(2)$ with 4 flavours, we have: (a) A generic point on the Coulomb branch. (b) A point on the Higgs branch, coloured subwebs can be moved in and out of the page along the 7-branes. (c) Magnetic quiver from subweb decomposition.

Tropical geometry

There is some subtlety about the number of hypermultiplets transforming in the bifundamental representations of the gauge subgroups, that is, how many edges are between two given gauge nodes.

As it turns out, we can borrow the concept of a stable intersection from the literature on tropical geometry[2].

Definition 13. The **stable intersection** between two 5-brane subwebs is

$$\mathrm{SI} = \sum_{i<j} |\det \begin{pmatrix} p_i & q_i \\ p_j & q_j \end{pmatrix}| \,, \tag{5.7}$$

where (p_i, q_i) and (p_j, q_j) are the charges of the intersecting 5-branes in the respective subwebs.

The stable intersection is invariant under small movements of the corresponding subwebs. We may move two overlapping subwebs apart in any direction, without changing the value of the stable intersection. Another way to compute the stable intersection is from the toric diagram as the area of polygons with differently coloured edges, see figure 5.13.

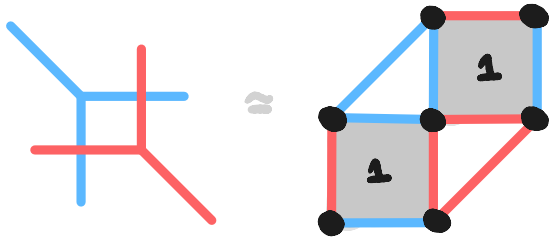

Figure 5.13: The stable intersection of the two subwebs is 2. This can be computed either via the definition of the stable intersection or by calculating the area of polygons with differently coloured edges in the toric diagram.

Contrary to the literature on tropical geometry, our curves (or 5-branes) end on 7-branes. And the stable intersection changes if we perform Hanany-Witten transitions. The answer to how we may generalise the stable intersection, and what the number of edges between two gauge nodes is, is the same.

Conjecture 2. *The number of edges between two gauge nodes is given by the following quantity between their respective subwebs*

$$E = SI + \sum_i X_i - \sum_i Y_i \,, \tag{5.8}$$

where SI is the stable intersection, X_i and Y_i are contributions from the 7-branes. X_i is the total number of pairs of two subwebs ending on the ith 7-brane - on the same side. Y_i is the total number of pairs of two subwebs ending on the ith 7-brane - on the opposite side.

[2]The adjective 'tropical' here is to honour the work by Imre Simon, whose Brazilian origin - according to French mathematicans - may be described as tropical.

As hinted at above, this quantity stays invariant, even after Hanany-Witten transitions and is the natural generalisation of the stable intersection in the case of curves that do not extend to infinity.

Example 10. For the brane system in figure 5.12 (b), we can now compute the various edge numbers explicitly.

Clearly, the green and orange subwebs will only have an edge number with the red subweb. This comes from the intersection only, as the different subwebs do not end on the same 7-branes. We compute it to be

$$E = |\det \begin{pmatrix} 0 & 1 \\ 2 & 0 \end{pmatrix}| = 2\,, \tag{5.9}$$

and since the red subweb corresponds to $U(2)$ with rank 2, there will be a single edge between the green/orange and red node.

Similarly, for one of the blue subwebs, it only has edges with the red subweb. But this time, it comes from the 7-brane contributions

$$E = 1 \times 2 - 0 = 2\,, \tag{5.10}$$

where a single blue brane may be paired with either of the two red branes on the other side of the 7-brane. Again, we have a single line between the nodes.

This does indeed reproduce the magnetic quiver we have in figure 5.12 (c).

5.3 Higgs branch at finite coupling - an example

Let us investigate the more involved example of $SU(3)$ with 4 flavours. At finite coupling, the Higgs branch is - as usual - parameterised by the massless hypermultiplets. At infinite coupling, we will additionally have massless instantons contribute to the Higgs branch. The analysis in both scenarios is very similar, and we will highlight the differences as they appear.

Figure 5.14 shows the toric diagram and corresponding brane web. At finite coupling, the Chern-Simons level does not matter, and here we choose the arbitrary value $\kappa = 0$. In figure 5.15 (a) and (b), we have two inequivalent maximal decompositions. This means that the Higgs branch is the union of two cones. In (c), we can inspect the decomposition that includes both of the maximal decompositions; this gives us another magnetic quiver corresponding to a non-trivial intersection of the cones. The two cones are called the **mesonic** $\mathcal{H}_M$ and the **baryonic cone** $\mathcal{H}_B$. Baryons have a charge under some $U(1)_B$, thus we expect this $U(1)_B$ factor to be present in the global symmetry of the cone. We will discuss how to find the global symmetry in section 6.3.

Crucially, because of conjecture 1, we can now use all of the tools developed for 3 dimensions on the magnetic quivers. As such, we may calculate their Hilbert series and match these to known

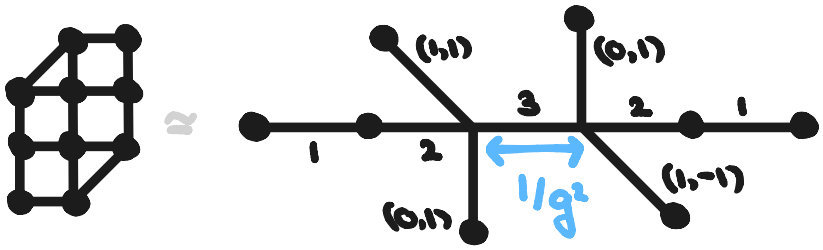

Figure 5.14: Toric diagram and brane web for $SU(3)_0$ with four flavours.

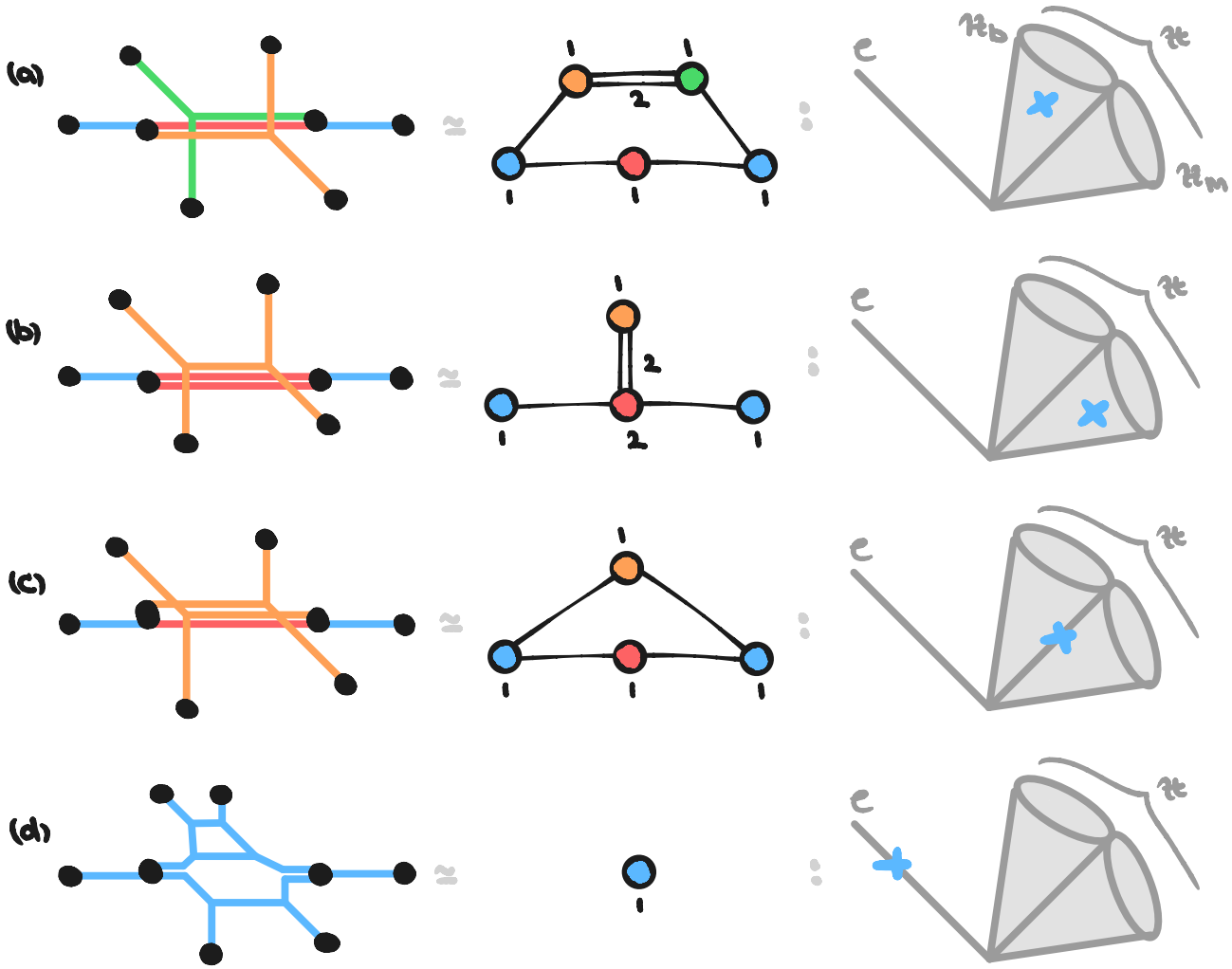

Figure 5.15: Phases of Higgs branch for $SU(3)_0$ with four flavours at finite coupling. (a) Baryonic cone of the Higgs branch. (b) Mesonic cone of the Higgs branch. (c) Intersection of the two cones, found by finding the decomposition that includes both the baryonic and mesonic parts. (d) Point on the Coulomb branch.

symplectic singularities or closures of nilpotent orbits from, for example, the catalogue in [46]. But since these quivers are well known in the literature, see [47], we just state the result:

$\mathcal{C}\Big($ 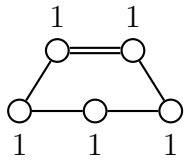 $\Big) =$ Baryonic extension of $\overline{min.A_3}$,

$\mathcal{C}\Big($ 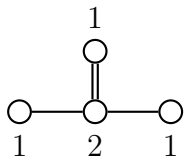 $\Big) = \overline{n.min.A_3}$, (5.11)

$\mathcal{C}\Big($ 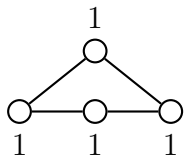 $\Big) = \overline{min.A_3}$.

5.4 Higgs branch at infinite coupling - an example

As alluded to in the introduction 0, much of the interest around 5-dimensional theories is centred around the infinite coupling limit where the theory can flow to an interacting SCFT at the UV fixed point. Due to the presence of massless instantons in this limit, the Higgs branch can open up new directions, and the global symmetry is enhanced.

At infinite coupling, we have to take the Chern-Simons level into account. This can complicate matters significantly, in particular, if we have a series of Hanany-Witten transitions to perform to reach a fixed point. A priori, it is not clear whether a fixed point even exists. For illustrative purposes, we have obviously chosen the Chern-Simons level such that we will not run into any of these issues here.

The analysis follows in the same way as for the finite coupling case, with the exception that the decomposition of the brane web changes. To reach the infinite coupling limit, we shrink the distance labelled $1/g^2$ in figure 5.14 to zero. The possible subweb decompositions and their intersection are shown in figure 5.16. The quiver for the baryonic cone stays the same, but the mesonic cone now has a new quiver associated with it.

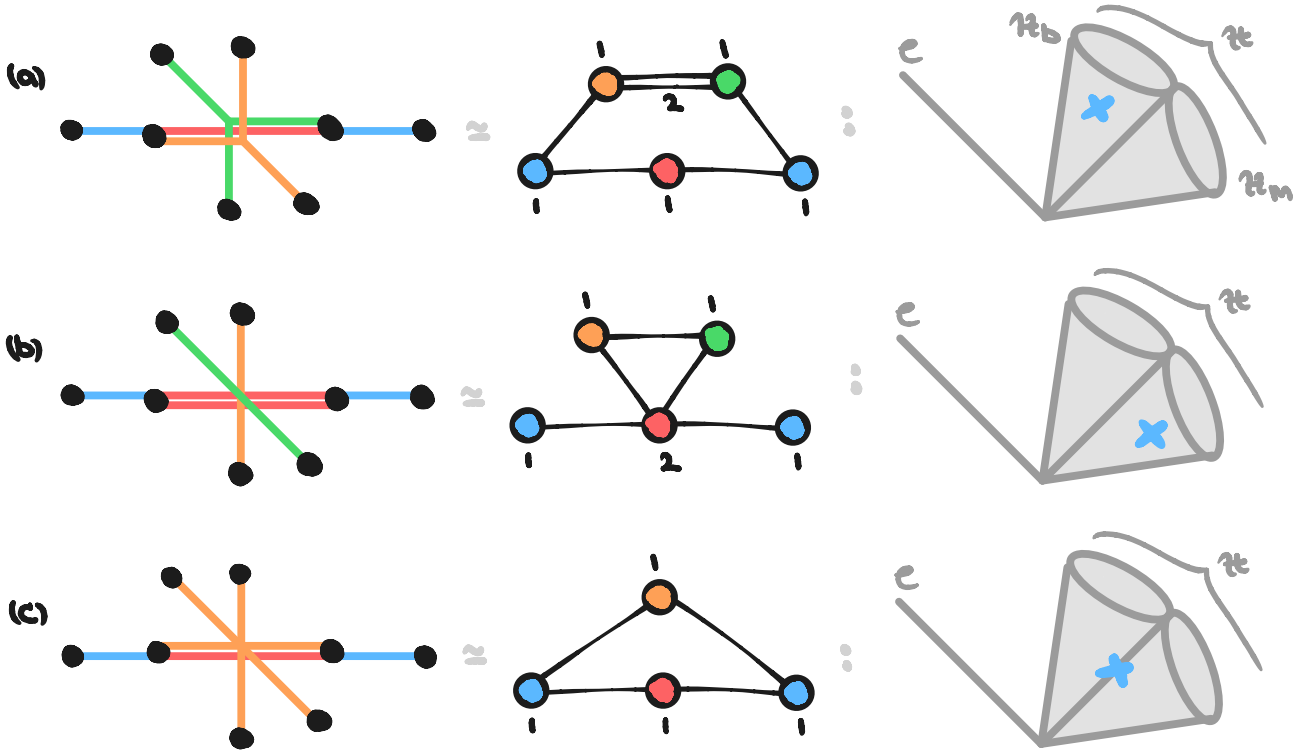

Figure 5.16: Phases of Higgs branch for $SU(3)_0$ with four flavours at infinite coupling. (a) Baryonic cone of the Higgs branch. (b) Mesonic cone of the Higgs branch, which enhances due to instanton contributions. (c) Intersection of the two cones.

6. More tools in quiver gauge theories

The purpose of this chapter is to introduce some more specific methods and tools that are commonly used. This ranges from tools like Hasse diagrams to encode the singularity structure of symplectic singularities, over a quiver subtraction algorithm to generate the Hasse diagrams [3], to a method to read off the global symmetry from a quiver without having to compute its Hilbert series [48].

6.1 Hasse diagrams

In supersymmetric gauge theories with 8 supercharges, the scalars that parameterise the Higgs branch, upon acquiring a vev, break the gauge group to some subgroup. This process is called the **Higgs mechanism**. For a theory with enough matter content, the gauge group breaks completely on a generic point on the Higgs branch. However, on certain special subspaces, some subgroups remain unbroken. This process of **partial Higgsing** gives us a rich and intricate structure. At any such subgroup, we may break the symmetry even further, but there may also be subgroups which are not immediately accessible, giving us a natural partial ordering.

To encode this partial ordering, we can use **Hasse diagrams**. A Hasse diagram is a graphical representation of a finite partially ordered set (poset). It captures the relation between two elements (dots) via the edges they have with each other. For example, consider the set $\{x, y\}$ with the partial ordering given by inclusion, meaning $A \leq B$ if set A is in set B. For the set $\{x, y\}$, we have

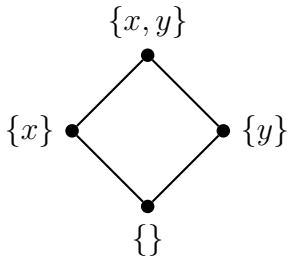

Geometrically, the Higgs branch is a symplectic singularity, which admits a natural stratification into symplectic leaves. The symplectic leaves are submanifolds which are partially ordered by the inclusion of their closures, see section 2.3. The key insight is captured in the following:

Conjecture 3. *The Hasse diagram describing the geometric stratification of the Higgs branch moduli space is identical to the one describing the pattern of partial Higgsing.*

A representation theory perspective

Let us begin with explicitly going through the representation theory of partial Higgsing. We will follow the example of $SU(3)$ with 6 flavours in [3]. The gauge group $SU(3)$ has the following possible subgroups: $SU(2) \times U(1)$, $SU(2)$, $U(1)^2$, $U(1)$, and the trivial subgroup $\{1\}$.

For $SU(3)$ breaking to $SU(2)$: We first look at how some basic representations reduce from A_2 to A_1

$$\begin{aligned} [10]_{A_2} \quad \text{or} \quad [01]_{A_2} \quad &\to \quad [1]_{A_1} + [0]_{A_1} \,, \\ [11]_{A_2} \quad &\to \quad [2]_{A_1} + \underbrace{2[1]_{A_1} + [0]_{A_1}}_{\text{acquire mass}} \,, \end{aligned} \tag{6.1}$$

where the vector of A_2 decomposes to the vector of A_1 together with some other representations, which will then acquire a mass. The hypermultiplet reduces to

$$6([10]_{A_2} + [01]_{A_2}) \quad \to \quad 12[1]_{A_1} + 12[0]_{A_1} \,. \tag{6.2}$$

The Higgs mechanism will now "eat" the components of the hypermultiplet that transform in the same representation as the one corresponding to the broken generators of the gauge group, i.e. the irreps that acquire a mass in the above. We are left with

$$\begin{aligned} 12[1] + 12[0] - 2(2[1] + [0]) &= 8[1] + 10[0] \\ &= \underbrace{4([1] + [1])}_{\text{4 hypermultiplets}} + \underbrace{5([0] + [0])}_{\text{scalars parameterising subgroup}} \,, \end{aligned} \tag{6.3}$$

where we have 4 hypermultiplets remaining. This gives us the theory $SU(2)$ with 4 flavours, and we have some scalars that parameterise the directions in the Higgs branch corresponding to the unbroken $SU(2)$ symmetry with dimension 5.

For $SU(3)$ breaking to $SU(2) \times U(1)$: Again the relevant representations reduce as

$$\begin{aligned} [10]_{A_2} \quad &\to \quad q^{-2}[1]_{A_1} + q^{1}[0]_{A_1} \,, \\ [01]_{A_2} \quad &\to \quad q^{-1}[0]_{A_1} + q^{2}[1]_{A_1} \,, \\ [11]_{A_2} \quad &\to \quad [2]_{A_1} + \underbrace{q^{3}[1]_{A_1} + q^{-3}[1]_{A_1} + [0]}_{\text{cannot acquire mass}} \,. \end{aligned} \tag{6.4}$$

For this case, there is no match between what the hypermultiplet (bifundamental representation) reduces to and what the vector multiplet (adjoint representation) reduces to. This means there are no Goldstone modes available and Higgsing is impossible. Similarly, breaking to $U(1)^2$ and $U(1)$ is impossible.

For $SU(2)$ breaking to $\{1\}$: Everything just maps to 1 so

$$\begin{aligned} [1]_{A_1} &\to 2\,, \\ [2]_{A_1} &\to 3\,. \end{aligned} \tag{6.5}$$

The four hypermultiplets $4([1]+[1])$ reduce to 16, and taking away twice the vector multiplet $2[2] \to 6$ gives us a 10-dimensional space.

We have thus found the Hasse diagram to be

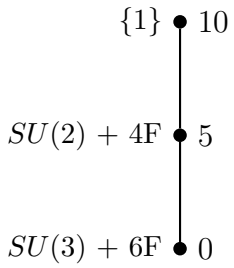

where we have denoted the theory it corresponds to on the left-hand side, and the dimension of the Higgs branch preserving the theory on the right-hand side.

A geometric perspective

For any symplectic singularity, there exists a stratification of symplectic leaves corresponding to the partial ordering

$$\mathcal{L}_i < \mathcal{L}_j \quad \text{if} \quad \mathcal{L}_i \subset \overline{\mathcal{L}}_j\,. \tag{6.6}$$

We may expand on example 3 in section 2.3 by giving its Hasse diagram and use this to illustrate a crucial point of this perspective:

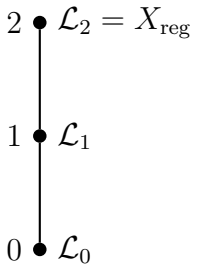

We associate the most singular point $\mathcal{L}_0$ with the full unbroken gauge theory, and we can see this more explicitly if we consider the transverse slice between this leaf and the top leaf

$$\begin{aligned} \mathcal{T}_0^2 &= \mathcal{T}_0 \cap \overline{\mathcal{L}}_2 \\ &= X \cap X = X\,, \end{aligned} \tag{6.7}$$

which is the moduli space - i.e. symplectic singularity - corresponding to full gauge theory. Hence, the transverse space of a symplectic leaf is the moduli space of the (partially) broken gauge theory. And for our representation theory example above, we can write this as

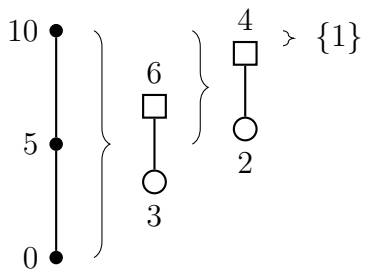

where the braces indicate the transverse slice between the two leaves at each end.

6.2 Quiver subtraction

To find the symplectic leaves and transverse slices in the symplectic singularity, we make use of an algorithm called **quiver subtraction**. The algorithm comes from translating operations on the brane system of a theory into the language of quivers.

Consider again the example of $SU(3)$ with 6 flavours. Beginning at a generic point on the Higgs branch, we write down the corresponding brane system, as shown on the left-hand side of figure 6.1. We then realign some of the light branes such that we may open up Coulomb branch directions of the moduli space. This corresponds to a **Kraft-Procesi transition** [49, 3] in 5-dimensions. And repeating this process, we find all brane systems corresponding to the symplectic leaves.

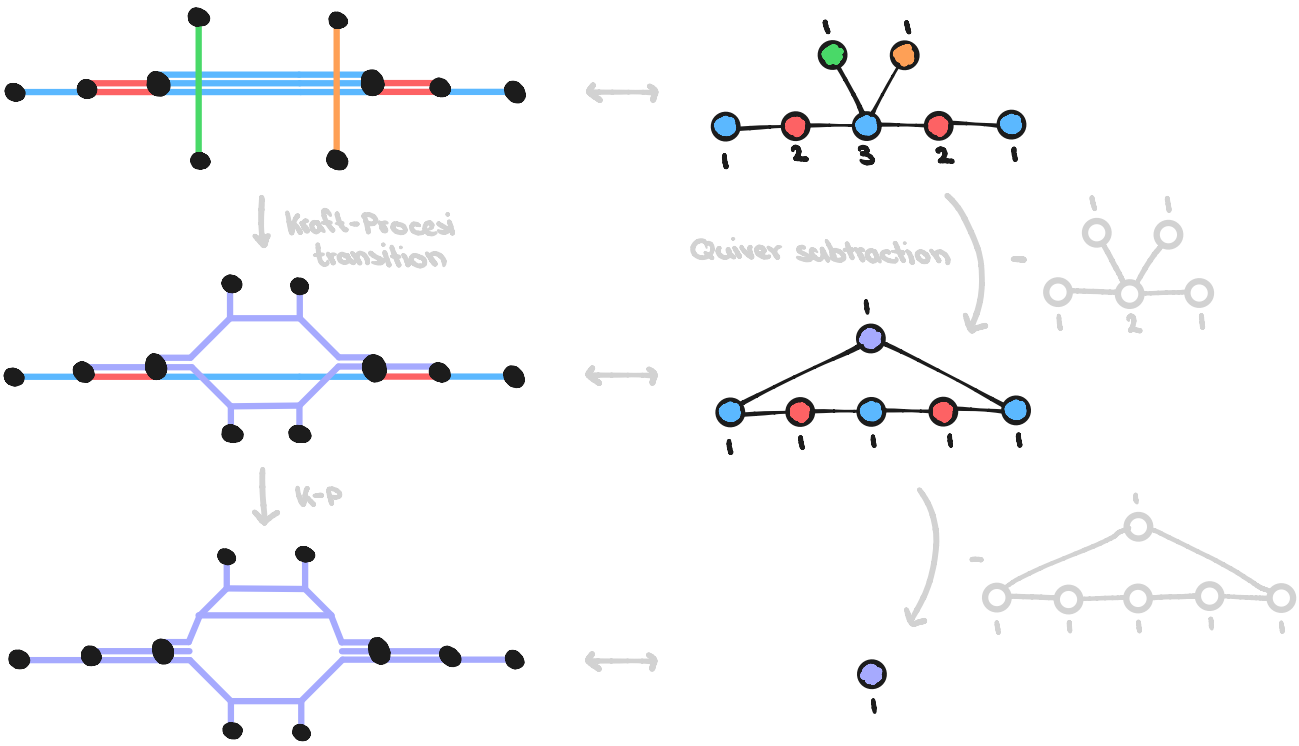

Figure 6.1: Kraft-Procesi transitions of 5-branes on the left-hand side and, equivalently, quiver subtraction on the right-hand side.

The conceptual idea of the quiver side, as shown on the right-hand side of figure 6.1, is that, starting from the relevant magnetic quiver, we can subtract a set of quivers, called **elementary**

slices, from the initial quiver to get the quiver corresponding to the next symplectic leaf, i.e. the brane system with a Coulomb branch direction opened up.

An important note is that this algorithm fails if we can subtract the same elementary slice twice in a row. In this case, we need to extend the formalism to include decorations of nodes in the quiver. This is explained in more detail in [50].

The algorithm

To make the above explanation more concrete, we present here the full algorithm, as developed in [3]. Suppose we have two symplectic leaves $\mathcal{L}$ and $\mathcal{L}'$ connected by a transverse slice in their Hasse diagram. Each of these pieces is represented by a magnetic quiver Q, Q' and D, respectively. To move from the higher leaf to the lower, we subtract the transverse slice quiver. Schematically we have

$$Q - D = Q' \,. \tag{6.8}$$

One last piece of information that we will need in the following is the idea of balance.

Definition 14. The **balance** b_i of the ith node in a quiver is defined as

$$b_i = \sum_j n_j \times e_j - 2n_i \,, \tag{6.9}$$

where j is over all the nodes connecting to the ith node, n_j is the node rank, and e_j is the number of edges connecting the jth node to the ith node.

The elementary slices are assumed to be either minimal nilpotent orbit closures or Kleinian singularities, see table 6.1. To subtract an elementary slice D from the quiver Q, we proceed as follows:

(i) Align quivers Q and D.

(ii) Subtract the node numbers of D from the ones in Q. If this yields a negative number, the subtraction of D is not possible.

(iii) If the balance of any of the nodes changes, add a single additional $U(1)$ node and connect it to all those nodes, possibly multiple times. The balances of Q and Q' should be the same after this.

Slice	Quiver	Dimension	Slice	Quiver	Dimension
a_n	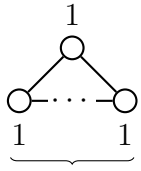	n	b_n	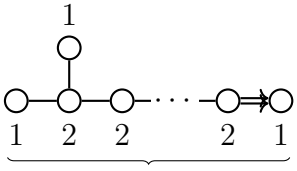	$2n-2$
c_n	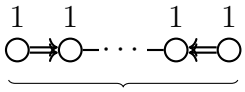	n	d_n	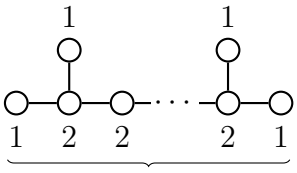	$2n-3$
e_6	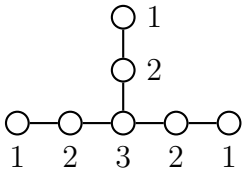	11	e_7	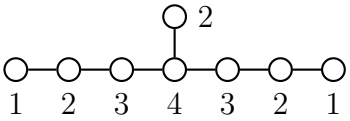	17
e_8	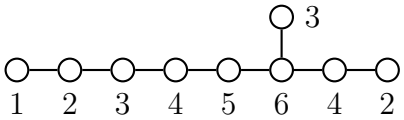	29	f_4	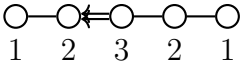	8
g_2	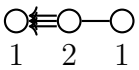	3	ac_n	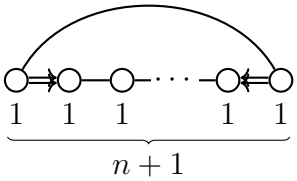	n
ag_2		2	cg_2	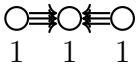	2
$h_{n,k}$	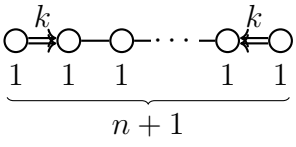	n	$\bar{h}_{n,k}$	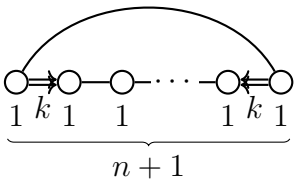	n
A_n	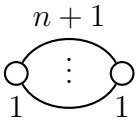	1			

Table 6.1: Elementary slices.

Let us illustrate this step-by-step in figure 6.2. By simply overlaying the quivers and subtracting the node numbers, we get a linear quiver with five $U(1)$ nodes. The nodes at the end, which were previously balanced, are now unbalanced. Thus, we add an additional node which we connect to both of the unbalanced nodes, restoring their original balance. An important note is that if the quiver was previously unbalanced, it needs to maintain the same unbalance in the new quiver after subtraction. Also, the newly added node may be unbalanced.

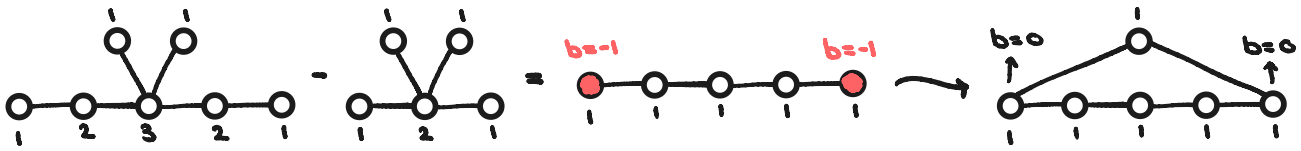

Figure 6.2: Illustration of quiver subtraction process. We overlay two quivers and subtract the node numbers, then to restore the original balance, we add an additional $U(1)$ node.

And finally, we just note the importance of edge multiplicities. Quivers can only be subtracted from one another if the edge multiplicities match identically. For example, the quiver

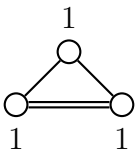

only has an a_1 slice and not an a_2 slice. Similarly, the quiver

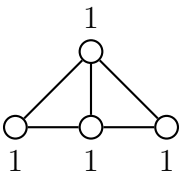

only has an a_2 slice and not an a_3 slice.

6.3 Global symmetry

The global symmetry can always be read from the t^2 term in the relevant Hilbert series. But since this can, at times, be tedious to compute, there is a neat method which also tells us the global symmetry of the Coulomb branch of a 3-dimensional theory (or, equivalently, the Higgs branch in dimensions 3 to 6). Unfortunately, this method is not entirely foolproof and sometimes will only reveal a subgroup of the global symmetry. This happens when, in the Hasse diagram, we can subtract the same slice twice in a row.

The algorithm as such is straightforward [48]:

Framed quiver: If the quiver comprises of s balanced sub-Dynkin diagrams D_i of the simple Lie groups G_i, and k unbalanced nodes, then the global symmetry is

$$\text{GS} = \prod_{i=1}^{s} G_i \times U(1)^k \,. \tag{6.10}$$

Unframed quiver: There are two possible cases:

(i) If all nodes are balanced, then the quiver is the (twisted) affine quiver for some simple Lie group G, see a_n to g_2 in table 6.1, and the global symmetry is simply

$$\text{GS} = G \tag{6.11}$$

(ii) If there are unbalanced nodes, for a quiver comprising s balanced sub-Dynkin diagrams D_i of the simple Lie groups G_i, and k unbalanced nodes, then the global symmetry is

$$\text{GS} = \prod_{i=1}^{s} G_i \times U(1)^{k-1} \,. \tag{6.12}$$

Example 11. Consider the quiver in figure 6.3. We have two unbalanced nodes and an A_3 Dynkin subdiagram. As it is an unframed quiver, the global symmetry is

$$\text{GS} = SU(4) \times U(1) \,. \tag{6.13}$$

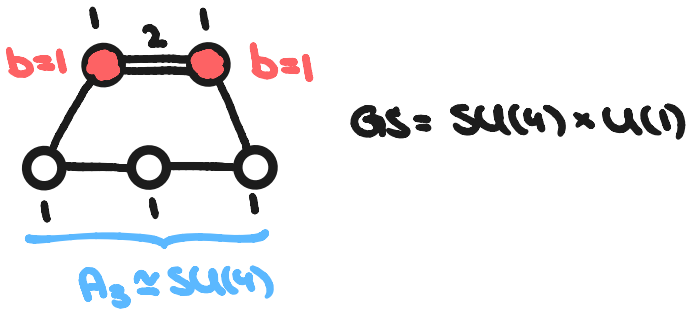

Figure 6.3: Global symmetry of unframed quiver with two unbalanced nodes (red) and an A_3 Dynkin subdiagram.

Part II

Calculations

7. A general pattern for a family of balanced quivers of type A_n

A general quiver theory of type A_n may be written as:

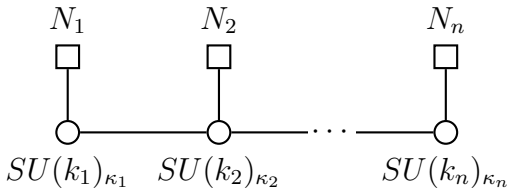

where for each gauge node we have three parameters: the rank of the gauge group $k_i - 1$, the number of flavours N_i, and the Chern-Simons level κ_i. This is, unfortunately, too large a parameter space to do any analysis on.

Instead, we decide to restrict the space in various ways to get exact insights. In this chapter, we focus on balanced quivers with zero Chern-Simons level with flavours only on the outside nodes. That is, quivers of the form:

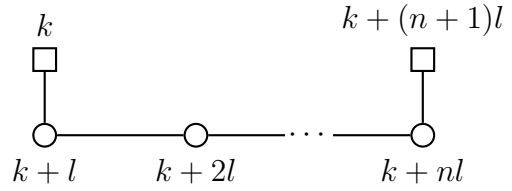

where we initially have $n + 2$ node numbers, but due to balance and the setup, it reduces to two independent variables k and l.

7.1 A bunch of examples

Before presenting the general pattern, it is illustrative to consider the first few examples of this family.

Theories of type A_1

This case has been extensively studied in the literature. See, for example, [15, 47]. Let us restate some of the results here. First, the A_1 quiver we are considering is

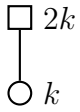

with classical global symmetry

$$U(2k) \times U(1)\,. \tag{7.1}$$

The toric diagram with zero Chern-Simons level is shown in figure 7.1. The corresponding brane webs, at finite and infinite coupling, are shown in figure 7.2.

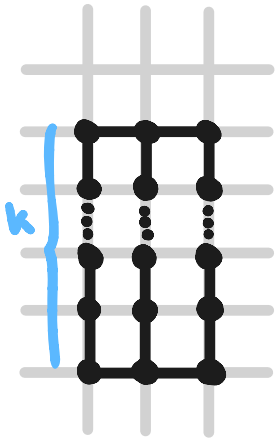

Figure 7.1: Toric diagram for balanced quiver of type A_1 with zero Chern-Simons level.

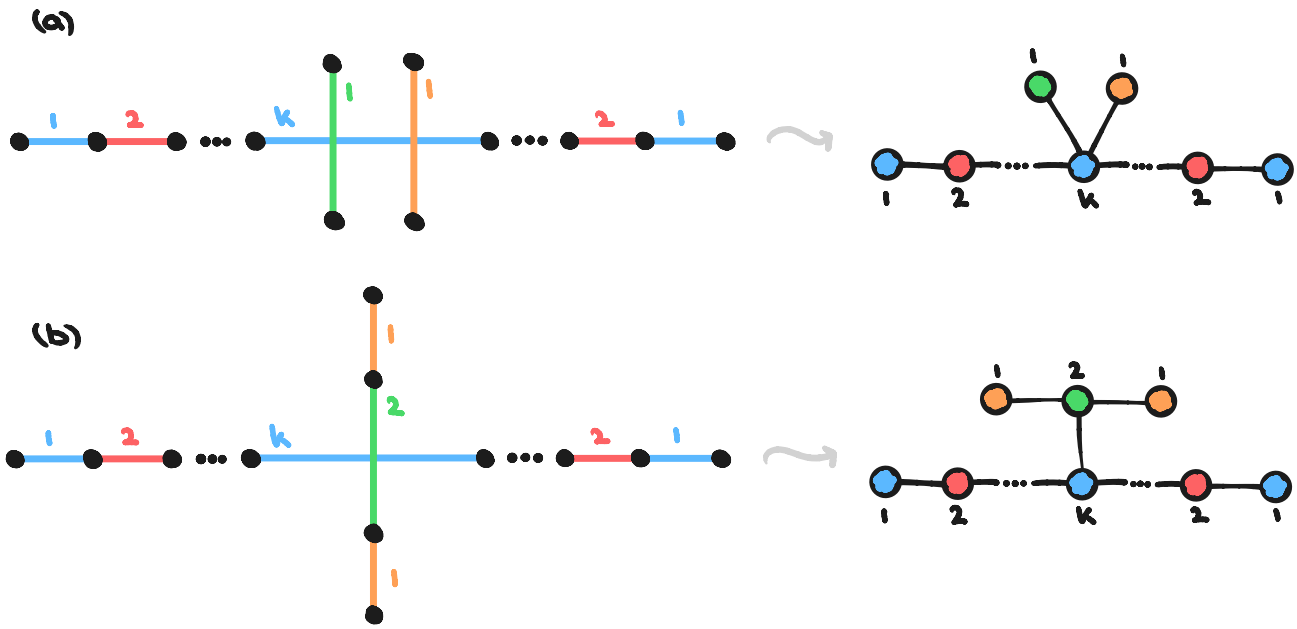

Figure 7.2: Brane system and magnetic quiver of balanced A_1 theory: (a) finite coupling and (b) infinite coupling. For branes where the angle, and thus the charge, is clear from the picture, we will only write the multiplicity.

At finite coupling, we have two separated vertical 5-branes that act as individual subwebs. This leads to a linear quiver going from 1 to k and back to 1 again, with 2 prongs for the vertical subwebs. The global symmetry is

$$\mathrm{GS}_{\text{finite}} = SU(2k) \times U(1)\,, \tag{7.2}$$

for $k \geq 3$. We note that due to quantising the theory, the global symmetry has changed as $U(2k) \times U(1) \to SU(2k) \times U(1)$.

For the infinite coupling case, we extend the length of one of the vertical branes such that the different 7-branes will not overlap before moving them together. This results in three vertical and independent subwebs with multiplicities 1, 1, and 2. And the magnetic quiver begins to exhibit a "forking" mechanism, where only one of the vertical nodes is connected to the main linear part of the quiver. The global symmetry changes to

$$\mathrm{GS}_{\text{infinite}} = SU(2k) \times SU(2)^2 \,, \tag{7.3}$$

for $k \geq 3$.

Theories of type A_2

Having dealt with the A_1 case, we can move on to quivers of type A_2. These are not as prevalent in the literature. They take the form:

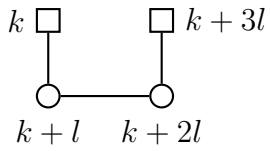

with classical global symmetry

$$U(k) \times U(k+3l) \times U(1)^3 \,. \tag{7.4}$$

The toric diagram with zero Chern-Simons level is shown in figure 7.3 and the brane systems and magnetic quivers for the various coupling phases are shown in figure 7.4. Crucially, the magnetic quivers again exhibit the "forking" mechanism already observed for A_1.

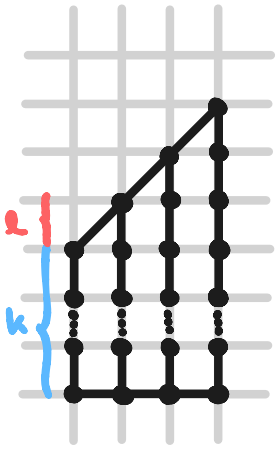

Figure 7.3: Toric diagram for balanced quiver of type A_2 with zero Chern-Simons level.

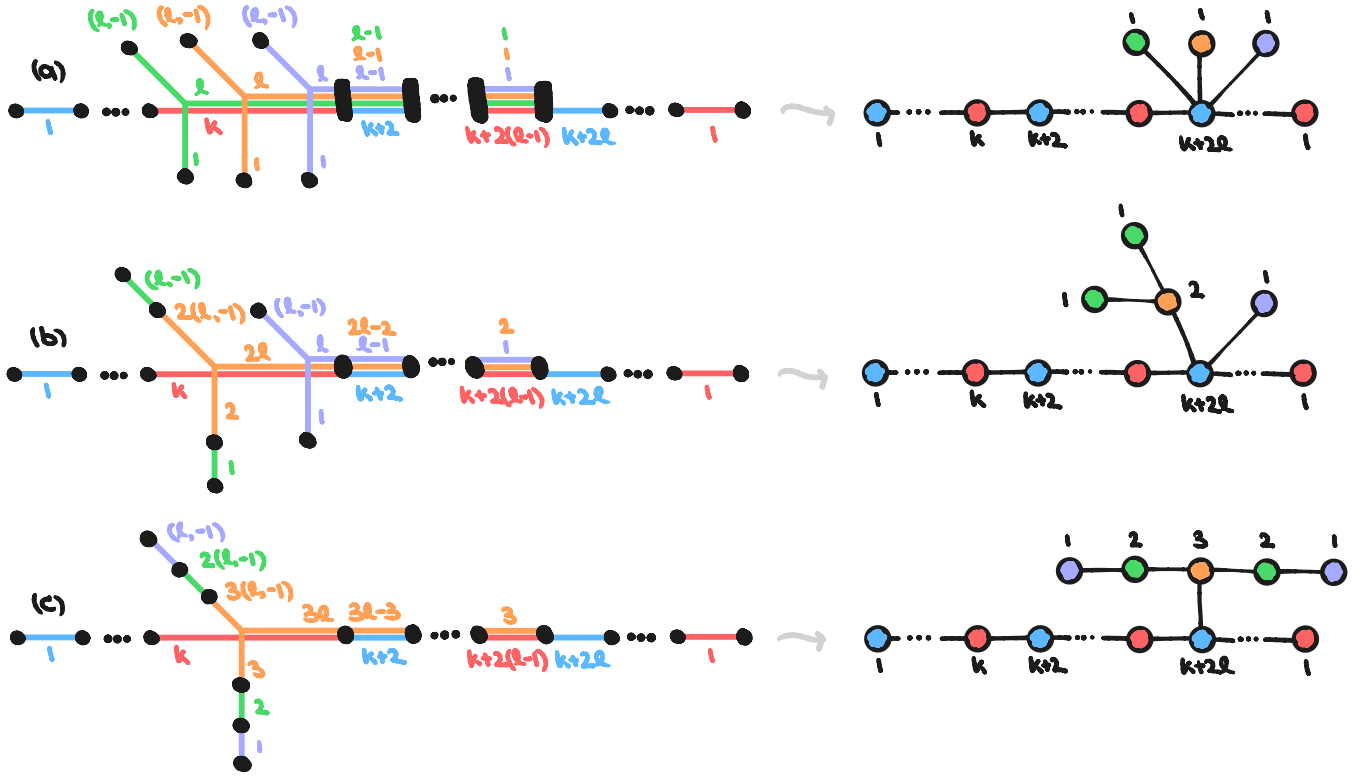

Figure 7.4: Brane systems and magnetic quivers for balanced quiver of type A_2 at: (a) finite-finite coupling, (b) finite-infinite coupling, and (c) infinite-infinite coupling. Note that because we have higher NS-NS charges of 2 and 3 for some of the subwebs in (b) and (c), the number of 5-branes allowed to end on 7-branes also increases to 2 and 3, respectively.

For $k + 2(l-1) \geq 1$, the global symmetries are

$$\begin{aligned} \text{GS}_{\text{fin. - fin.}} &= SU(k) \times SU(k+3l) \times U(1)^3 \,, \\ \text{GS}_{\text{inf. - inf.}} &= SU(k) \times SU(k+3l) \times SU(2)^2 \times U(1)^2 \,, \\ \text{GS}_{\text{inf. - inf.}} &= SU(k) \times SU(k+3l) \times SU(3)^2 \times U(1) \,. \end{aligned} \tag{7.5}$$

Theories of type A_3

For A_3, the quiver takes on the form:

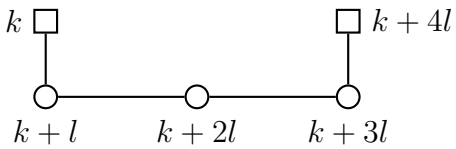

and the classical global symmetry is

$$U(k) \times U(k+4l) \times U(1)^4 \,. \tag{7.6}$$

The toric diagram takes on the usual form, as can be seen in figure 7.5. In figure 7.6, we can see the brane system for all coupling strengths being finite. Then, based on the coupling we sent to infinity,

we move the corresponding vertical branes together, obtaining the familiar forking mechanism of the arms of the magnetic quiver. The magnetic quivers are shown in figure 7.7.

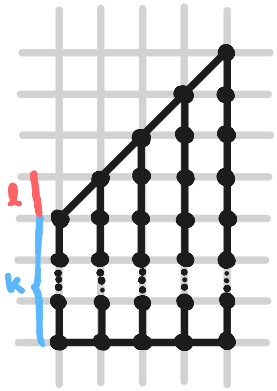

Figure 7.5: Toric diagram for balanced quiver of type A_3 with zero Chern-Simons level.

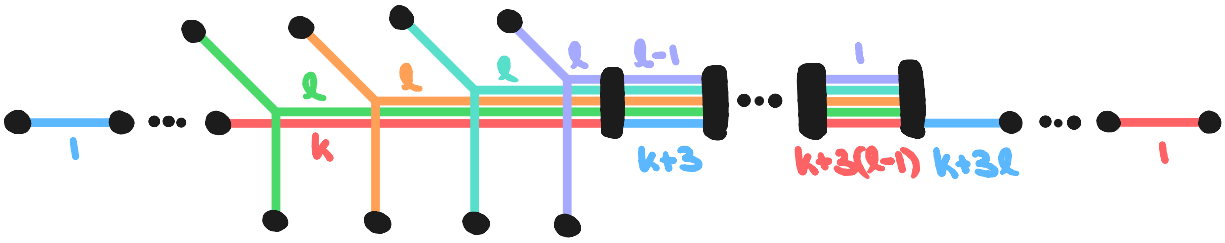

Figure 7.6: Brane system for balanced A_3 type quiver with all gauge couplings finite.

For $k+3l-2 \geq 1$, the global symmetries of the different phases are

$$\begin{aligned}
\text{GS}_{\text{fin. - fin. - fin.}} &= SU(k) \times SU(k+3l) \times U(1)^4\,, \\
\text{GS}_{\text{inf. - fin. - fin.}} &= SU(k) \times SU(k+3l) \times SU(2)^2 \times U(1)^3\,, \\
\text{GS}_{\text{inf. - fin. - inf.}} &= SU(k) \times SU(k+3l) \times SU(2)^4 \times U(1)^2\,, \\
\text{GS}_{\text{inf. - inf. - fin.}} &= SU(k) \times SU(k+3l) \times SU(3)^2 \times U(1)^2\,, \\
\text{GS}_{\text{inf. - inf. - inf.}} &= SU(k) \times SU(k+3l) \times SU(4)^4 \times U(1)\,.
\end{aligned} \tag{7.7}$$

7.2 The pattern in terms of partitions of $n+1$

For concreteness, let us focus on figure 7.7. The nodes connecting to the node with label $k+3l$ clearly form partitions of 4. Furthermore, if they have a value of 2 or greater, there are two arms with nodes decreasing in value by 1 connected to that node. The case of all coupling strengths being infinite corresponds to the highest partition, (4) in this case, and the case of all coupling strengths being finite corresponds to the lowest, (1^4).

Let us now formalise this a little more. Any integer partition of $n+1$ can be written in its normal notation

$$(\lambda_1, \ldots, \lambda_r)\,, \tag{7.8}$$

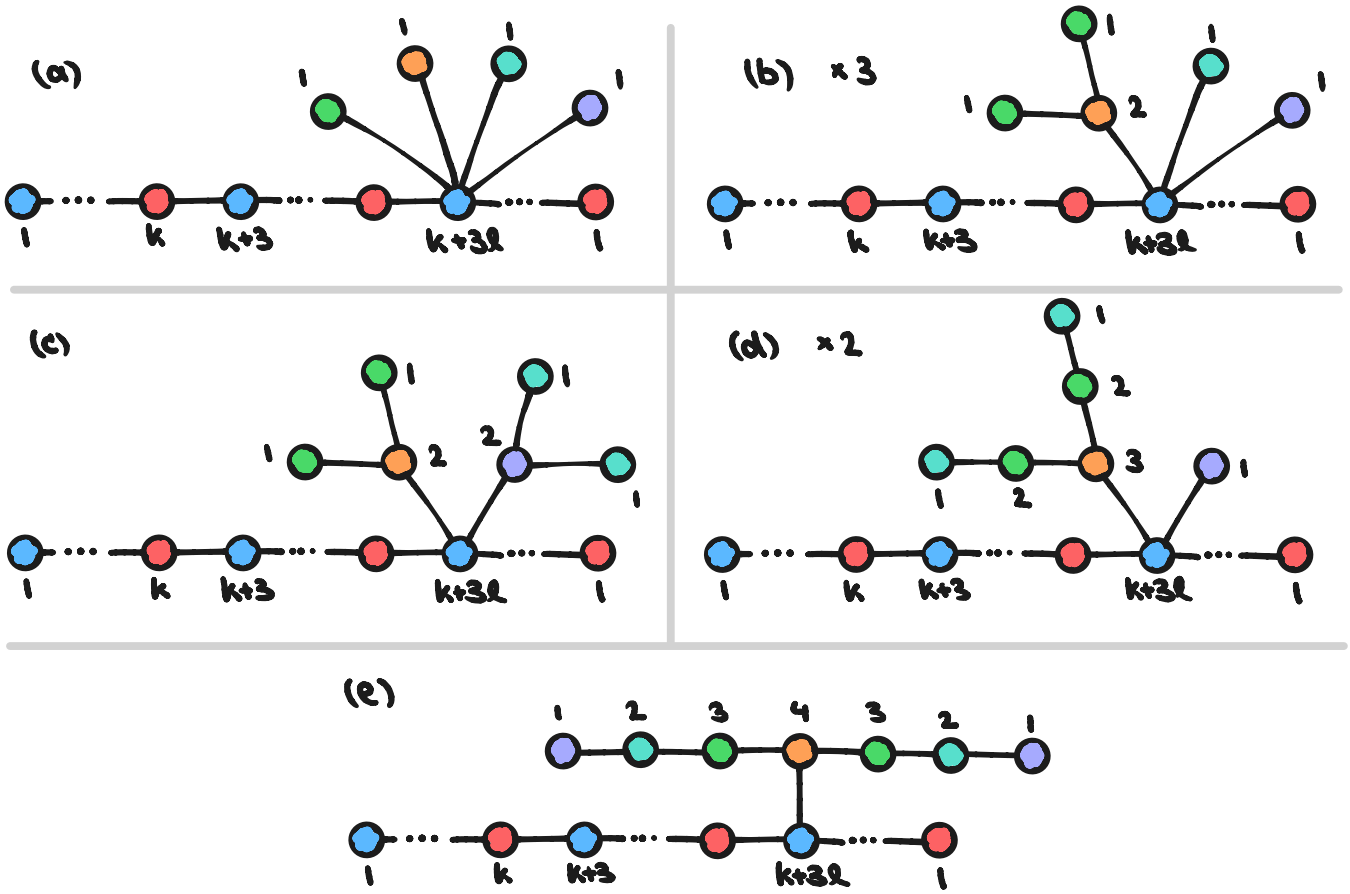

Figure 7.7: Magnetic quivers of balanced A_3 type quiver at different coupling phases.

with $\lambda_1 \geq \cdots \geq \lambda_r$, such that $\lambda_1 + \cdots + \lambda_r = n + 1$. Or, in its fully simplified form, where an exponent indicates repeated elements

$$(\mu_1^{a_1}, \ldots, \mu_s^{a_s}) \,, \tag{7.9}$$

with $\mu_1 > \cdots > \mu_s$.

From a given structure of finite and infinite gauge coupling strengths, we can translate to an integer partition using the following rules:

(i) Every finite coupling corresponds to 2 consecutive elements in the partition. If there are only finite couplings, this means we will have $n + 1$ factors of 1.

(ii) For every row of m consecutive infinite gauge couplings, we get a factor of $m + 1$ in the partition.

This is equivalent to simply starting with $n + 1$ factors of 1, and then iteratively, for each new infinite coupling, merging adjacent factors. Let us briefly give some examples. For the coupling phase infinite-infinite-finite, the partition is $(3, 1)$. And for the phase infinite-finite-infinite, we have $(2, 2)$.

Conjecture 4. *We have that:*

(i) The set of partitions $\mathcal{P}(n + 1)$ is in one-to-one correspondence with the different coupling

phases of balanced A_n theories with flavours only on the outside gauge nodes. Some phases can be realised in multiple ways, leading to multiplicities which are given by

$$\frac{r!}{(a_1!)\dots(a_s!)}\,, \tag{7.10}$$

where r corresponds to the r in $(\lambda_1,\dots,\lambda_r)\in\mathcal{P}(n+1)$ and the a_i correspond to the a_i in $(\mu_{a_1},\dots,\mu_{a_s})\in\mathcal{P}(n+1)$.

(ii) The magnetic quiver of the coupling phase encoded by the partition $(\lambda_1,\dots,\lambda_r)$ is given by figure 7.8.

(iii) The global symmetry of the magnetic quiver with coupling phase $(\mu_1^{a_1},\dots,\mu_s^{a_s})=(\lambda_1,\dots,\lambda_r)$, and $n\geq 2$, is

$$SU(k)\times SU(k+(n+1)l)\times SU(\mu_1)^{2a_1}\times\dots\times SU(\mu_s)^{2a_s}\times U(1)^r\,. \tag{7.11}$$

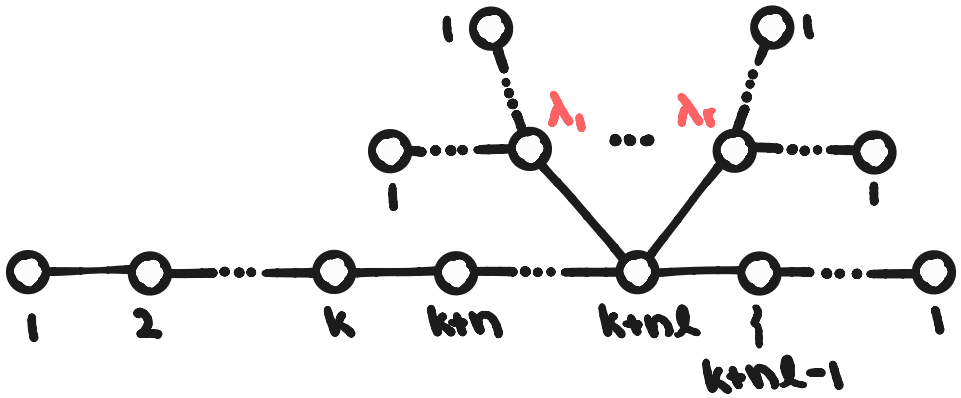

Figure 7.8: Magnetic quiver for balanced A_n type quiver in the coupling phase corresponding to the partition $(\lambda_1,\dots,\lambda_r)\in\mathcal{P}(n+1)$. If any of the λ_i is larger than 1, the node will have two arms going down in decrements of 1.

8. The finite coupling case of arbitrary quivers of type A_2

We take inspiration from the analysis in [47], and extend the analysis to some cases of a completely general quiver of type A_2 at finite coupling.

8.1 The setup and all possible cases

At finite coupling, the Chern-Simons level does not impact our theory. From a brane perspective, this can be explained by noting that one can always adjust the lengths of the external branes such to avoid any crossing. From the field theory point of view, the Chern-Simons terms only affect the vector multiplet, which we set to zero. Only once we have instantons contributing at infinite coupling, we have to consider the impact of the Chern-Simons level.

This means that our toric diagram does not need to be convex anymore, and we may move parts of it around to simplify our calculations. A general quiver of type A_2 is of the form:

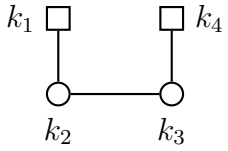

and for its toric diagram we choose to maintain a flat bottom such that we will only get $(0, 1)$ 5-branes on the bottom half of the brane web, see figure 8.1.

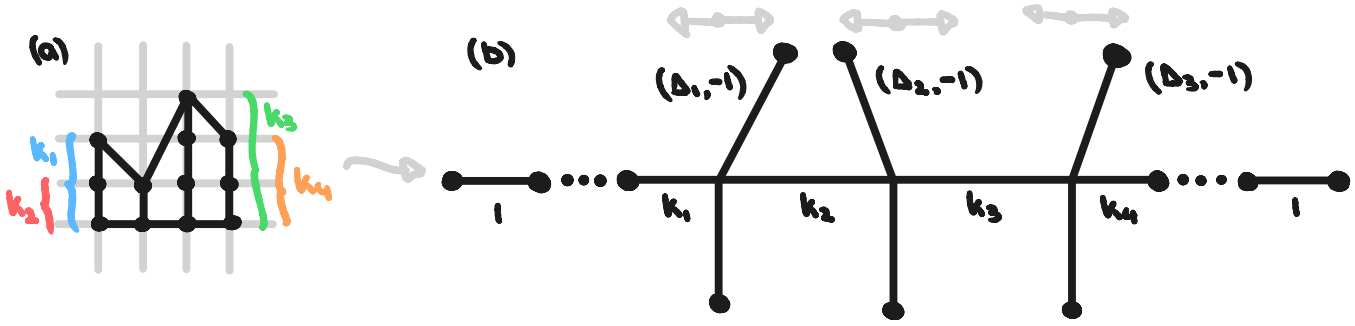

Figure 8.1: (a) Toric diagram for general quiver of type A_2. (b) Corresponding brane web, where we have defined $\Delta_1 = k_2 - k_1$, $\Delta_2 = k_3 - k2$, and $\Delta_3 = k_4 - k_3$.

It will be useful to redefine some quantities:

$$\Delta_1 = k_2 - k_1\,, \quad \Delta_2 = k_3 - k_2\,, \quad \Delta_3 = k_4 - k_3\,. \tag{8.1}$$

Then, depending on the value of the Δ_i, subwebs extend to the left or right side of the corresponding vertical brane. This can be seen more clearly in figure 8.2. Thus, a priori, we have the following cases

$$\Delta_1 \begin{cases} > 0 \\ = 0 \\ < 0 \end{cases} \quad \text{and} \quad \Delta_2 \begin{cases} > 0 \\ = 0 \end{cases} \quad \text{and} \quad \Delta_3 \begin{cases} > 0 \\ = 0 \\ < 0 \end{cases} \tag{8.2}$$

where Δ_2 has one less case because the quiver is symmetric. This gives us a total of 18 cases, but as it will turn out, there are actually more than this due to additional conditions of subweb formations that we will run into later.

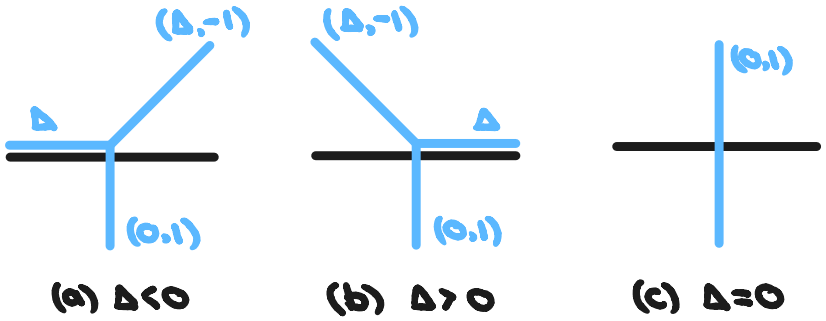

Figure 8.2: Subweb formation based on value of Δ: (a) $\Delta < 0$, (b) $\Delta > 0$, and (c) $\Delta = 0$.

8.2 The case $k_1 \leq k_2 \leq k_3 \leq k_4$

The first 8 cases can be dealt with together. Let us first assume $k_1 < k_2 < k_3 < k_4$, and then consider what would happen if we have an equality. As a consistency condition, we can check that our analysis here replicates the magnetic quiver we have found in the previous section for a balanced quiver of type A_2.

In figure 8.3, we have shown the subweb decomposition as well as the magnetic quiver. In particular, we assumed that $\Delta_3 < \Delta_2 < \Delta_1$ for illustrative purposes, but the same pattern is true for any other arrangement with the modification that the purple, yellow, and green nodes would change places accordingly. The edge number between these nodes will always be of the form $\Delta_{\text{larger}} - \Delta_{\text{smaller}}$.

The balanced quiver from section 7.1 manifests itself in this picture as $\Delta_1 = \Delta_2 = \Delta_3$. This evidently reproduces the result from the previous section, as the purple, yellow, and green nodes now connect to the node with label $k_1 + 2\Delta_3$ and there are no edges between them.

Lastly, we can consider the case when, say, $\Delta_2 = 0$ or $k_2 = k_3$. This is shown in figure 8.4. The orange node now connects immediately to the node with label k_1, and as it still crosses the

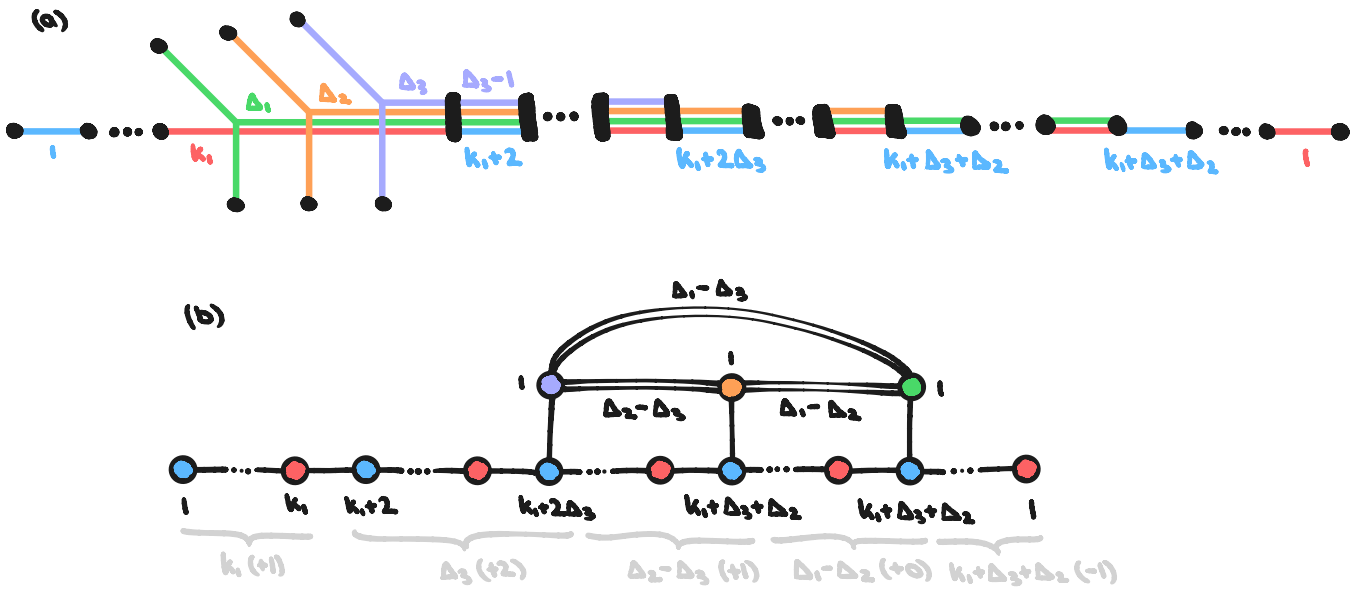

Figure 8.3: The case of $k_1 < k_2 < k_3 < k_4$: (a) brane system and (b) magnetic quiver.

green brane, also maintains its connection with it. But as the orange and purple lines do not cross anymore, there will not be any edges between these nodes. With these patterns in hand, one could now immediately write down the 8 separate cases.

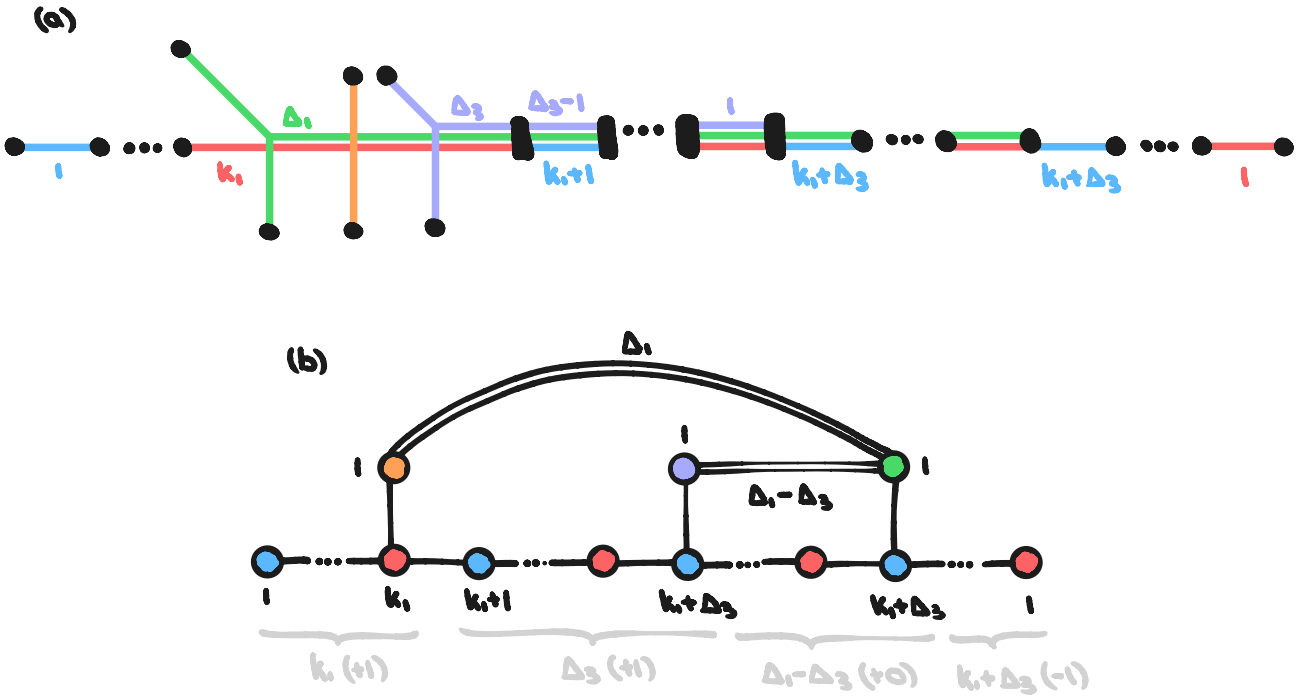

Figure 8.4: The case of $k_1 < k_2 = k_3 < k_4$: (a) brane system and (b) magnetic quiver.

8.3 The case $k_1 < k_2 < k_3 > k_4$

The situation, unfortunately, quickly escalates in complexity. In figure 8.5, we can see that for the case of $k_1 < k_2 < k_3 > k_4$, we get different decompositions based on whether

$$k_1 - \Delta_3 \begin{cases} \geq 0 \\ < 0 \end{cases} . \tag{8.3}$$

If $k_1 - \Delta_3 < 0$, then the purple brane has to combine and form a subweb with either the orange or green subwebs. Adding to our misery, this means that again we have various new cases based on the values of $\Delta_2 - \Delta_3$ and $\Delta_1 - \Delta_3$. We will not investigate this case any further.

The magnetic quiver for the brane web in figure 8.5 (a) is shown in figure 8.6. Where now the edges between the nodes associated with the vertical branes are of the form $\Delta_i + \Delta_j$ rather than $\Delta_i - \Delta_j$. The structure of the bottom linear part of the quiver also changes.

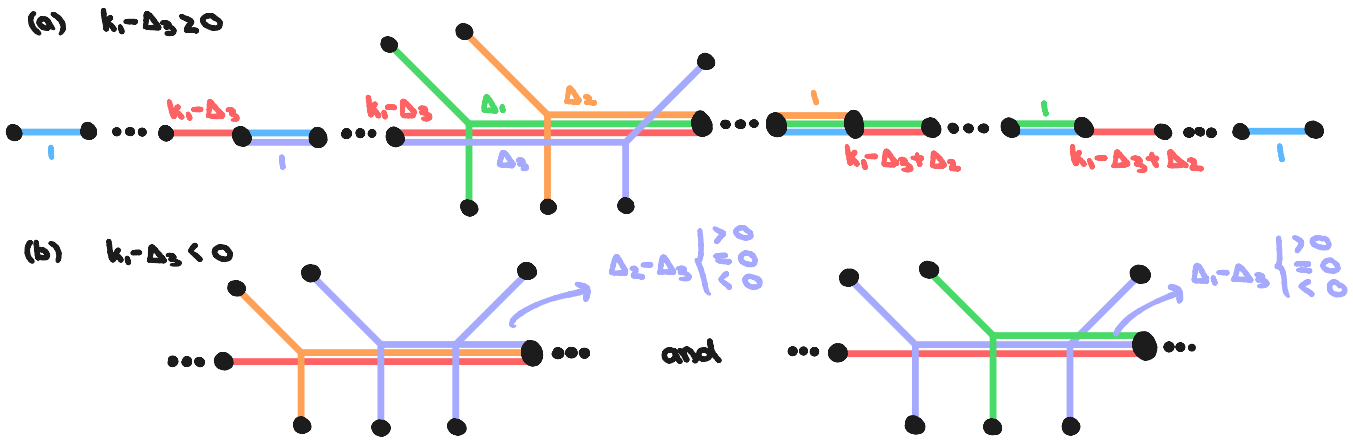

Figure 8.5: (a) Brane web for the case of $k_1 - \Delta_3 \geq 0$. (b) Brane web for the case of $k_1 - \Delta_3 < 0$. The latter quickly deteriorates into a cascade of different cases.

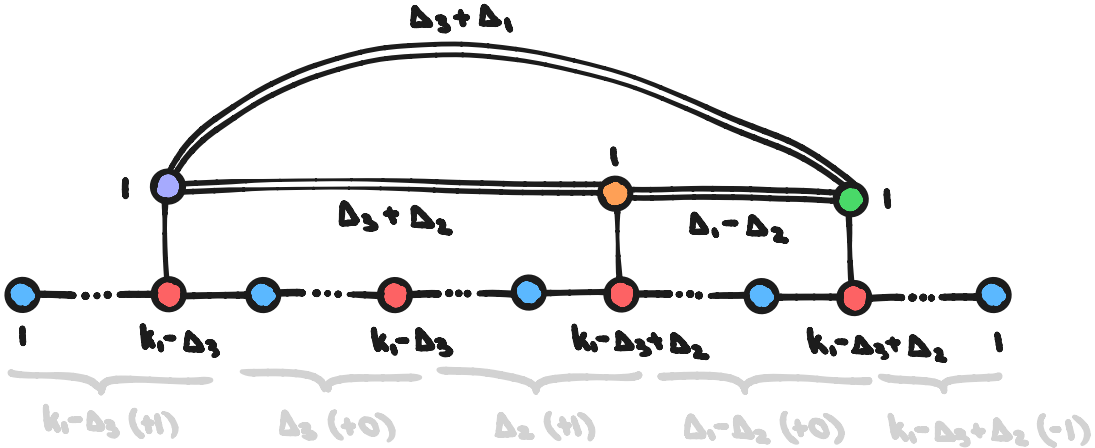

Figure 8.6: Magnetic quiver for the case of $k_1 - \Delta_3 \geq 0$.

9. Aside: A computational tool for magnetic quivers

In the next chapter, we want to analyse theories of type A_2, whose toric diagram is convex, at infinite coupling. While the convexity condition does simplify the analysis, we are still dealing with 6 variables: 2 flavour nodes, 2 gauge nodes, and 2 Chern-Simons levels. To make sense of all these different possibilities which result in different magnetic quivers, we have developed a Python library[1]. Given a certain brane web, it automatically finds the possible maximal subweb decompositions respecting both charge conservation and the S-rule. Once the decompositions have been found, it computes the corresponding magnetic quiver. Optionally, it can also compute the Hasse diagram of the magnetic quiver via quiver subtraction, though the functionality of this is more limited as it does not deal with decorations. Other algorithms using fission and decay may be better suited for this use case, see [51]. Yet, our algorithm immediately shows transitions, dimensions and the quivers corresponding to different nodes in the Hasse diagram, something which the fission and decay algorithm does not do.

9.1 Brane web to magnetic quiver

We will very briefly outline how the algorithm works. The brane webs are stored as graphs, where we broadly have three types of objects: edges corresponding to 5-branes, nodes corresponding to either junctions of 5-branes or individual 7-branes. The number of allowed junctions is currently limited to one, which is the case of all coupling strengths being infinite.

Once a brane web has been initialised, the following steps are executed to find the magnetic quiver:

(i) Find the possible subwebs over the junction and between the first set of 7-branes using charge conservation only. All subwebs, which are the combination of two or more other subwebs, are also removed, making our subwebs minimal and thus the decompositions maximal.

(ii) Identify the subwebs that violate the S-rule and, if possible, extend them across 7-branes such that the number of 5-branes ending on any 7-branes is not more than the NS5 charge. If this is not possible, we disregard the subweb.

[1]The complete source code is available at: github.com/ccmfb/magnetic_quivers

(iii) Subtract our subwebs from the initial brane web in such a way as to find decompositions.

(iv) Read off magnetic quiver node content from decompositions.

(v) Find edge number between nodes/subwebs by spatially offsetting one subweb and calculating the intersection number, plus additional 7-brane contributions. This results in the full magnetic quiver.

Let us slightly expand on some of the points. Consider, for example, the brane web in figure 9.1, step (i) would identify the blue and red subwebs. The combination of both of them is not a minimal subweb and thus would be removed by the algorithm. Also, the red subweb satisfies the S-rule, whereas the blue one does not. To remedy this point, step (ii) checks if there are sufficient 5-branes on the other side of the 7-brane on which the 2 blue 5-branes end. In this case, the blue subweb can be extended to include an additional 5-brane, see figure 9.2. A slightly technical point here is that when the NS5 charge is computed for any 5-brane between junction and 7-brane, we first find the $SL(2,\mathbb{Z})$ transformation that turns the (p,q) 5-brane into a $(1,0)$ 5-brane. And after applying this transformation to the whole brane web, we can calculate the NS5 charge for all possible branes, not just ones which are already D5 branes. While step (iii) might seem trivial here, if we have multiple vertical branes, there can be various different ways to match up subwebs, and the algorithm systematically investigates the possibilities by subtracting the found subwebs. The steps (iv) and (v) find the magnetic quiver.

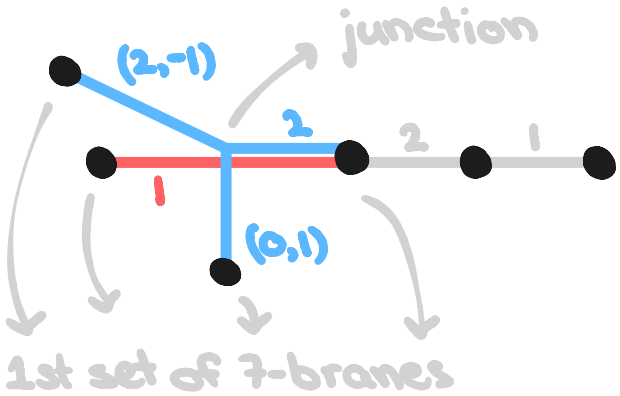

Figure 9.1: Some arbitrary brane web. The blue and red subwebs are the ones found across the junction in step (i).

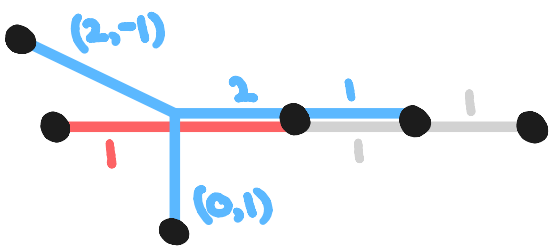

Figure 9.2: Some arbitrary brane web. The blue and red subwebs are the ones found after the extension across the 7-brane in step (ii).

9.2 Magnetic quiver to Hasse diagram

The step from magnetic quiver to Hasse diagram is a straightforward implementation of the existing algorithm in [3]. Again, we store quivers as graphs. Once a quiver is inputted, we can calculate the dimension of its Coulomb branch and thus load a set of minimal transitions with dimension less than or equal to the dimension of the whole magnetic quiver. Then we can subtract the minimal transitions to determine the Hasse diagram.

There is some added functionality in our method over the decay and fission algorithm. We are able to not only display the exact transition between points in the Hasse diagram, but if you hover over any node, it will also show the corresponding magnetic quiver, see figure 9.3 and 9.4.

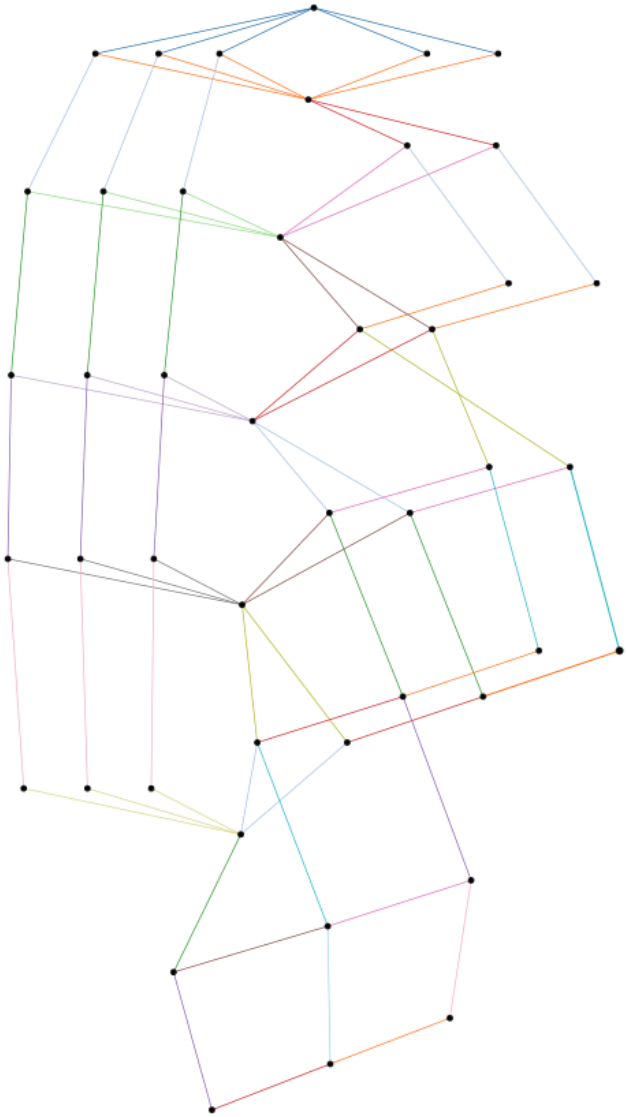

Figure 9.3: Complete Hasse diagram for balanced $SU(6) \times SU(8)$ theory.

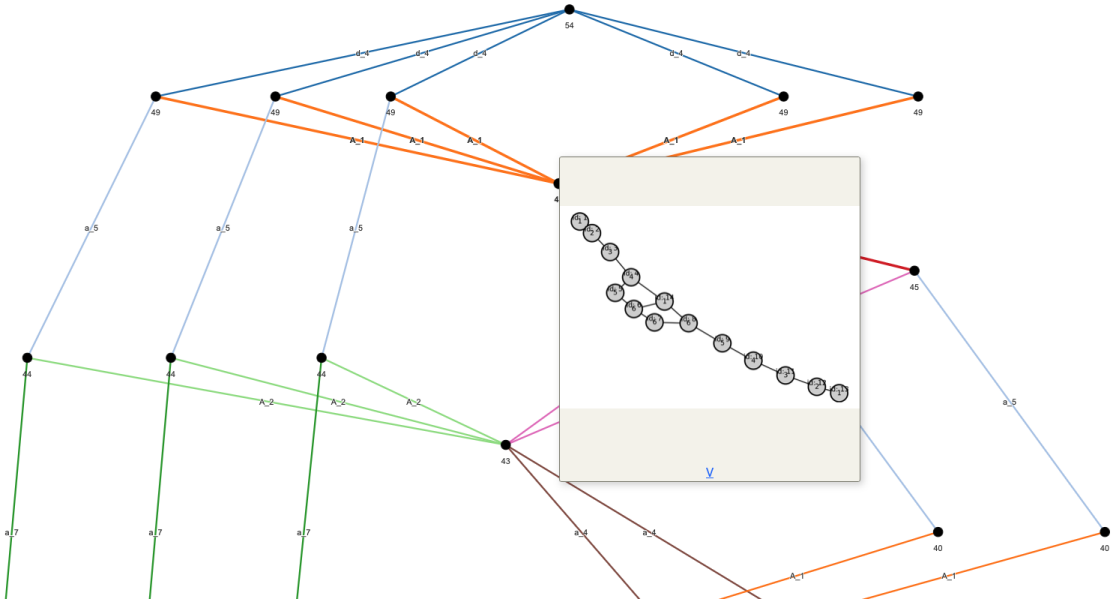

Figure 9.4: Zoomed in view of Hasse diagram for balanced $SU(6) \times SU(8)$ theory. Transitions and dimensions are shown, as well as the magnetic quiver corresponding to the hovered-over node.

10. The infinite coupling case for toric quivers of type A_2

Previously, we analysed an arbitrary quiver of type A_2 at finite coupling. This was possible because we could always avoid brane crossings by simply adjusting the length of the heavy branes. At infinite coupling, this is not quite as easy. To avoid having to consider Hanany-Witten transitions, we need to be more restrictive in the types of quivers we consider. Hence, we will only consider those quivers whose toric diagram is convex.

10.1 Example for $k_2, k_3 \leq 4$

In figure 10.1, we can see a convex toric diagram, where we may, for simplicity, choose that there is a horizontal line at the bottom between the two vertical lines corresponding to the gauge nodes. For this to be convex, we require

$$\begin{aligned} p \geq 0 \quad &\text{and} \quad k_2 - (k_1 + p) \geq k_3 - k_2 \,, \\ q \geq 0 \quad &\text{and} \quad (k_4 + q) - k_3 \leq k_3 - k_2 \,. \end{aligned} \tag{10.1}$$

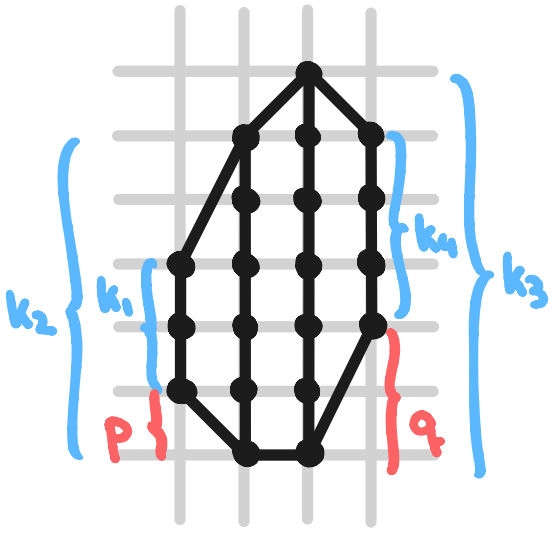

Figure 10.1: Toric diagram for some general convex A_2 theory.

The main idea of this chapter is that we can use the Python library discussed in chapter 9 to

generate any quiver of this form. The bounding case in (10.2) warrants a different brane system setup in the Python script, and to be able to automate the process of generating many magnetic quivers, we thus restrict the values we will consider a little more to

$$\begin{aligned} p > 0 \quad &\text{and} \quad k_2 - (k_1 + p) > k_3 - k_2 \,, \\ q > 0 \quad &\text{and} \quad (k_4 + q) - k_3 < k_3 - k_2 \,. \end{aligned} \tag{10.2}$$

It should be emphasised that we only do this for the automatic generation of many cases; the Python code itself works for any convex brane web at infinite coupling.

We proceed by generating all possible brane webs for $k_2, k_3 \leq 4$ that satisfy the conditions in (10.2), and list them by their magnetic quiver in table 10.1.

Magnetic Quiver	Electric theories defined by $k_2 - k_3 - k_1 - k_2 - p - q$
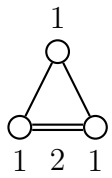	2-2-0-0-1-1, 3-3-0-0-1-2, 3-3-0-0-2-1, 3-3-0-1-1-1, 3-3-0-1-2-1, 3-3-1-0-1-1, 3-3-1-0-1-2, 3-3-1-1-1-1, 3-3-1-1-1-1, 3-4-0-1-1-2, 3-4-0-2-1-1, 3-4-0-2-1-2, 3-4-0-3-1-1, 4-4-0-0-1-3, 4-4-0-0-2-2, 4-4-0-0-3-1, 4-4-0-1-1-2, 4-4-0-1-2-1, 4-4-0-1-2-2, 4-4-0-1-3-1, 4-4-0-2-1-1, 4-4-0-2-1-1, 4-4-0-2-3-1, 4-4-0-2-3-1, 4-4-1-0-1-2, 4-4-1-0-1-3, 4-4-1-0-2-1, 4-4-1-0-2-2, 4-4-1-1-1-1, 4-4-1-1-1-1, 4-4-1-1-1-2, 4-4-1-1-2-1, 4-4-1-1-2-2, 4-4-1-1-2-2, 4-4-1-2-1-1, 4-4-1-2-2-1, 4-4-2-0-1-1, 4-4-2-0-1-1, 4-4-2-0-1-3, 4-4-2-0-1-3, 4-4-2-1-1-1, 4-4-2-1-1-2, 4-4-2-2-1-1
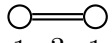	3-3-0-0-1-1, 3-3-0-0-2-2, 3-3-0-1-1-1, 3-3-0-1-2-1, 3-3-1-0-1-1, 3-3-1-0-1-2, 3-4-0-0-1-1, 3-4-0-0-1-2, 3-4-0-0-1-3, 3-4-0-0-1-4, 3-4-0-1-1-1, 3-4-0-1-1-1, 3-4-0-1-1-1, 3-4-0-1-1-3, 3-4-0-1-1-3, 3-4-0-1-1-3, 3-4-0-2-1-1, 3-4-0-2-1-2, 4-4-0-0-1-1, 4-4-0-0-1-2, 4-4-0-0-2-1, 4-4-0-0-2-3, 4-4-0-0-3-2, 4-4-0-0-3-3, 4-4-0-1-1-1, 4-4-0-1-1-1, 4-4-0-1-1-2, 4-4-0-1-3-1, 4-4-0-1-3-2, 4-4-0-1-3-2, 4-4-0-2-2-1, 4-4-0-2-2-1, 4-4-1-0-1-1, 4-4-1-0-1-1, 4-4-1-0-1-3, 4-4-1-0-2-1, 4-4-1-0-2-3, 4-4-1-0-2-3, 4-4-1-1-1-1, 4-4-1-1-1-1, 4-4-1-1-2-2, 4-4-1-1-2-2, 4-4-2-0-1-2, 4-4-2-0-1-2
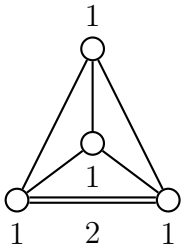	3-3-1-1-1-1, 4-4-1-1-1-2, 4-4-1-1-2-1
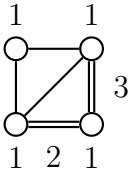	3-4-0-2-1-1, 3-4-0-2-1-2, 4-4-0-2-2-1, 4-4-1-2-1-1, 4-4-1-2-2-1, 4-4-2-0-1-2
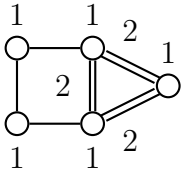	3-4-0-3-1-1, 3-4-0-3-1-1

Continued on next page

Magnetic Quiver	Electric theories defined by $k_2 - k_3 - k_1 - k_2 - p - q$
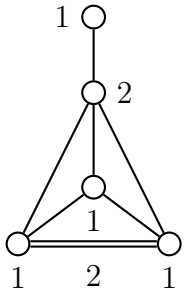	3-4-0-3-1-1
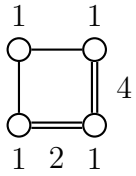	4-4-1-2-1-1, 4-4-1-2-2-1, 4-4-2-1-1-1, 4-4-2-1-1-2
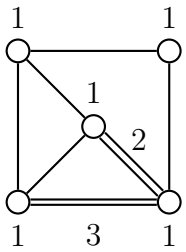	4-4-1-2-1-1, 4-4-1-2-2-1, 4-4-2-1-1-1, 4-4-2-1-1-2
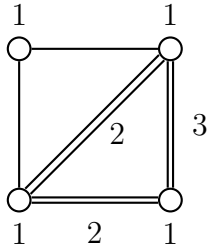	4-4-2-1-1-1, 4-4-2-1-1-2, 4-4-2-2-1-1, 4-4-2-2-1-1
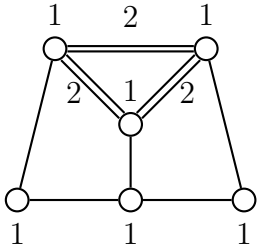	4-4-2-2-1-1, 4-4-2-2-1-1
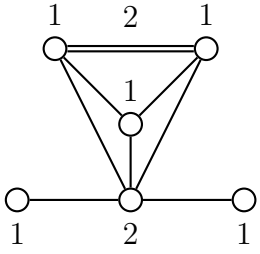	4-4-2-2-1-1

Table 10.1: Magnetic quivers and their corresponding electric theories for $k_2, k_3 \leq 4$. If an electric theory occurs for multiple magnetic quivers, then its Higgs branch splits into multiple branches, each represented by a corresponding magnetic quiver.

11. Conclusion

This dissertation aimed to provide a comprehensive introduction to theories with 8 supercharges and to extend the analysis of magnetic quivers to new families of $5d$ $\mathcal{N} = 1$ theories. By applying the various tools, such as brane webs and toric diagrams, we successfully identified previously unknown patterns and structures.

Summary and interpretation Our first contribution is the identification of a pattern for balanced quivers of type A_n with flavour nodes restricted to the outside gauge nodes. We demonstrated that the coupling phases of these theories, corresponding to arrangements of finite or infinite gauge couplings, are elegantly classified by integer partitions of $n + 1$. This means that once a coupling structure is known, it can be mapped to a partition, which in turn defines a magnetic quiver as well as the global symmetry. This connection between integer partitions and magnetic quivers seems to suggest that, at least in part, one can find patterns for large families of electric quivers.

Secondly, our analysis of arbitrary quivers of type A_2 at finite coupling revealed significant complexity driven by the relative ranks of the flavour and gauge nodes. We showed that the structure of the magnetic quiver is highly sensitive to the signs of the differences in $\Delta_i = k_{i+1} - k_i$. While for some configuration $k_1 \leq k_2 \leq k_3 \leq k_4$, a reasonably simple magnetic quiver classification was found. For cases such as $k_1 < k_2 < k_3 > k_4$, the formation of subwebs becomes much more dependent on various conditions.

Finally, to tackle the problem of quivers of type A_2, whose toric diagram is convex, at infinite coupling, we developed a Python library to automate the computation of magnetic quivers from brane webs. This computational tool is a completely new approach to tackling the problem of identifying magnetic quivers for families of theories. This library allowed us to generate an extensive catalogue of electric theories and their corresponding magnetic quivers, an excerpt of which was provided in this dissertation.

Limitations and future directions Despite the advances made, there are certain limitations, as well as future directions which could be pursued further:

(i) The clear pattern found for a specific fixed balance suggests that exploring other fixed balancing schemes could reveal similar structures.

(ii) Our analysis of A_2 quivers at finite coupling was limited by their complexity, and as such, we

only explored a subset of possible cases. To further investigate the remaining cases, one could expand the Python library to deal with multiple junctions. This would allow for a systematic exploration.

(iii) The catalogue of magnetic quivers generated for A_2 quiver theories at infinite coupling represents a rich dataset. A more detailed study of this data might reveal some patterns or classifications which are not immediately obvious.

Bibliography

[1] N. Seiberg and E. Witten, *Electric - magnetic duality, monopole condensation, and confinement in N=2 supersymmetric Yang-Mills theory*, *Nucl. Phys. B* **426** (1994) 19 [hep-th/9407087].

[2] N. Seiberg and E. Witten, *Monopoles, duality and chiral symmetry breaking in N=2 supersymmetric QCD*, *Nucl. Phys. B* **431** (1994) 484 [hep-th/9408099].

[3] A. Bourget, S. Cabrera, J.F. Grimminger, A. Hanany, M. Sperling, A. Zajac et al., *The Higgs mechanism — Hasse diagrams for symplectic singularities*, *JHEP* **01** (2020) 157 [1908.04245].

[4] S. Cremonesi, A. Hanany and A. Zaffaroni, *Monopole operators and Hilbert series of Coulomb branches of* $3d$ $\mathcal{N} = 4$ *gauge theories*, *JHEP* **01** (2014) 005 [1309.2657].

[5] M.R. Douglas and G.W. Moore, *D-branes, quivers, and ALE instantons*, hep-th/9603167.

[6] S.H. Katz, A. Klemm and C. Vafa, *Geometric engineering of quantum field theories*, *Nucl. Phys. B* **497** (1997) 173 [hep-th/9609239].

[7] A. Hanany and E. Witten, *Type iib superstrings, bps monopoles, and three-dimensional gauge dynamics*, *Nuclear Physics B* **492** (1997) 152–190 [9611230].

[8] E. Witten, *Solutions of four-dimensional field theories via M-theory*, *Nucl. Phys. B* **500** (1997) 3 [hep-th/9703166].

[9] O. Aharony and A. Hanany, *Branes, superpotentials and superconformal fixed points*, *Nucl. Phys. B* **504** (1997) 239 [hep-th/9704170].

[10] O. Aharony, A. Hanany and B. Kol, *Webs of (p,q) five-branes, five-dimensional field theories and grid diagrams*, *JHEP* **01** (1998) 002 [hep-th/9710116].

[11] A. Hanany and A. Zaffaroni, *Branes and six-dimensional supersymmetric theories*, *Nucl. Phys. B* **529** (1998) 180 [hep-th/9712145].

[12] N. Seiberg, *Five-dimensional SUSY field theories, nontrivial fixed points and string dynamics*, *Phys. Lett. B* **388** (1996) 753 [hep-th/9608111].

[13] K.A. Intriligator, D.R. Morrison and N. Seiberg, *Five-dimensional supersymmetric gauge theories and degenerations of Calabi-Yau spaces*, *Nucl. Phys. B* **497** (1997) 56 [hep-th/9702198].

[14] D.R. Morrison and N. Seiberg, *Extremal transitions and five-dimensional supersymmetric field theories*, *Nucl. Phys. B* **483** (1997) 229 [hep-th/9609070].

[15] S. Cabrera, A. Hanany and F. Yagi, *Tropical Geometry and Five Dimensional Higgs Branches at Infinite Coupling*, *JHEP* **01** (2019) 068 [1810.01379].

[16] C. Bouchard, "String theory lecture notes." https://ccmfb.github.io, June, 2025.

[17] B. Hall, *Lie Groups, Lie Algebras, and Representations: An Elementary Introduction*, Graduate Texts in Mathematics, Springer (2003).

[18] W. Fulton and J. Harris, *Representation Theory: A First Course*, Graduate texts in mathematics, Springer (1991).

[19] J. Grimminger, *SQFT - branes - moduli, symplectic singularities in physics*, Ph.D. thesis, Imperial Coll., London, 2023. 10.25560/109907.

[20] J. Harris, *Algebraic Geometry: A First Course*, Graduate Texts in Mathematics, Springer (1992).

[21] R. Hartshorne, *Algebraic Geometry*, Graduate Texts in Mathematics, Springer (1977).

[22] A. Hanany and R. Kalveks, *Highest Weight Generating Functions for Hilbert Series*, *JHEP* **10** (2014) 152 [1408.4690].

[23] B. Feng, A. Hanany and Y.-H. He, *Counting gauge invariants: The Plethystic program*, *JHEP* **03** (2007) 090 [hep-th/0701063].

[24] S. Benvenuti, B. Feng, A. Hanany and Y.-H. He, *Counting BPS Operators in Gauge Theories: Quivers, Syzygies and Plethystics*, *JHEP* **11** (2007) 050 [hep-th/0608050].

[25] J. Grimminger, "Stratified hyper-kähler moduli spaces and physics." https://scgp.stonybrook.edu/video_portal/video.php?id=6082, Sept., 2023.

[26] B. Fu, *A survey on symplectic singularities and resolutions*, 2005. math/0510346.

[27] G. Bellamy, "Symplectic singularities and their quantizations." https://sites.google.com/view/gwynbellamy, September, 2018.

[28] A. Beauville, *Symplectic singularities*, *Invent. Math.* **139** (2000) 541 [math/9903070].

[29] D. Kaledin, *Symplectic singularities from the poisson point of view*, 2006. math/0310186.

[30] S.C. Marquez, *Branes and the Vacuum Structure of Supersymmetric Gauge Theories*, Ph.D. thesis, Imperial College London, 2019.

[31] D. Collingwood and W. McGovern, *Nilpotent Orbits In Semisimple Lie Algebra: An Introduction*, Mathematics series, Taylor & Francis (1993).

[32] Y. Namikawa, *A characterization of nilpotent orbit closures among symplectic singularities*, *arXiv e-prints* (2016) arXiv:1603.06105 [1603.06105].

[33] D. Tong, "Supersymmetric field theory." https://www.damtp.cam.ac.uk/user/tong/susy.html.

[34] D. Bailin and A. Love, *Supersymmetric Gauge Field Theory and String Theory*, Graduate Student Series in Physics, CRC Press (1994).

[35] A. Hanany, N. Mekareeya and G. Torri, *The Hilbert Series of Adjoint SQCD*, *Nucl. Phys. B* **825** (2010) 52 [0812.2315].

[36] D. Gaiotto and E. Witten, *S-Duality of Boundary Conditions In N=4 Super Yang-Mills Theory*, *Adv. Theor. Math. Phys.* **13** (2009) 721 [0807.3720].

[37] L. Alvarez-Gaume and S.F. Hassan, *Introduction to S duality in N=2 supersymmetric gauge theories: A Pedagogical review of the work of Seiberg and Witten*, *Fortsch. Phys.* **45** (1997) 159 [hep-th/9701069].

[38] H. Hayashi, S.-S. Kim, K. Lee and F. Yagi, *Complete prepotential for 5d $\mathcal{N} = 1$ superconformal field theories*, *JHEP* **02** (2020) 074 [1912.10301].

[39] B. Feng and A. Hanany, *Mirror symmetry by O3 planes*, *JHEP* **11** (2000) 033 [hep-th/0004092].

[40] K.A. Intriligator and N. Seiberg, *Mirror symmetry in three-dimensional gauge theories*, *Phys. Lett. B* **387** (1996) 513 [hep-th/9607207].

[41] O. DeWolfe, A. Hanany, A. Iqbal and E. Katz, *Five-branes, seven-branes and five-dimensional E(n) field theories*, *JHEP* **03** (1999) 006 [hep-th/9902179].

[42] F. Benini, S. Benvenuti and Y. Tachikawa, *Webs of five-branes and N=2 superconformal field theories*, *JHEP* **09** (2009) 052 [0906.0359].

[43] N.C. Leung and C. Vafa, *Branes and toric geometry*, *Adv. Theor. Math. Phys.* **2** (1998) 91 [hep-th/9711013].

[44] A. Bourget, A. Collinucci and S. Schafer-Nameki, *Generalized Toric Polygons, T-branes, and 5d SCFTs*, *SciPost Phys.* **18** (2025) 079 [2301.05239].

[45] G. Zafrir, *Duality and enhancement of symmetry in 5d gauge theories*, *JHEP* **12** (2014) 116 [1408.4040].

[46] A. Hanany and R. Kalveks, *Quiver Theories for Moduli Spaces of Classical Group Nilpotent Orbits*, *JHEP* **06** (2016) 130 [1601.04020].

[47] A. Bourget, S. Cabrera, J.F. Grimminger, A. Hanany and Z. Zhong, *Brane Webs and Magnetic Quivers for SQCD*, *JHEP* **03** (2020) 176 [1909.00667].

[48] K. Gledhill and A. Hanany, *Coulomb branch global symmetry and quiver addition*, *JHEP* **12** (2021) 127 [2109.07237].

[49] S. Cabrera and A. Hanany, *Branes and the Kraft-Procesi Transition*, *JHEP* **11** (2016) 175 [1609.07798].

[50] A. Bourget, J.F. Grimminger, A. Hanany and Z. Zhong, *The Hasse diagram of the moduli space of instantons*, *JHEP* **08** (2022) 283 [2202.01218].

[51] A. Bourget, M. Sperling and Z. Zhong, *Higgs branch RG flows via decay and fission*, *Phys. Rev. D* **109** (2024) 126013 [2401.08757].